REPORT NO. P67-303
HAC REFERENCE NO. A8232

[redacted]

FINAL ENGINEERING REPORT
VOLUME I (JANUARY 1966 – APRIL 1969)

HIGH-GAIN SELF-STEERING MICROWAVE REPEATER

Contract No. : NAS 5-10101

Prepared by

R. A. Birgenheier
W. H. Kummer
Antenna Department, Aerospace Group
Hughes Aircraft Company
Culver City, California

FOR

GODDARD SPACE FLIGHT CENTER
CODE 733
GREENBELT, MARYLAND
Louis J. Ippolito, Technical Officer 733

Report No. P67-303
HAC Reference No. A8232

FINAL ENGINEERING REPORT
VOLUME I (JANUARY 1966 — APRIL 1969)

HIGH-GAIN SELF-STEERING MICROWAVE REPEATER

Contract No.: NAS5-10101

Prepared by

R. A. Birgenheier
W. H. Kummer
Antenna Department, Aerospace Group
Hughes Aircraft Company
Culver City, California

for Vol. II - N. I.

GODDARD SPACE FLIGHT CENTER
CODE 733
GREENBELT, MARYLAND
Louis J. Ippolito, Technical Office

SUMMARY

A study of advanced self-steering techniques that could be applied to satellite communication links was conducted and is reported in a two-volume final report. During the study, an engineering model of a high-gain self-steering microwave transponder and associated attitude readout circuitry was designed, fabricated, and tested. In addition, the application of a specific type of self-steering repeater to a Data Relay Satellite System was explored, and a possible configuration for such a system was evolved. A unique module-coupling technique was invented for the elimination of beam-pointing errors that arise when a single channel is used for duplex operation.

Volume I of the final report contains a discussion of the various types of self-steering arrays, brief descriptions of breadboard models of two different arrays built at the Hughes Aircraft Company, the general design considerations that applied for the engineering model and attitude readout, and a detailed description of the engineering model with the results of tests and measurements made of the antenna system. Volume I also contains the discussion of the specific application of a self-steering array.

Volume II of the final report contains the results of extensive system tests and the conclusions and recommendations of the program.

CONTENTS

ILLUSTRATIONS

TABLES

ACKNOWLEDGMENTS

The successful completion of this program resulted through the participation and cooperation of many members of the Research and Development Division. Of these, the most notable are M. C. Behnke, T. S. Fong, B. J. Forman, J. E. Howard, L. A. Kaye, C. Lew, F. A. Meyer, and O. C. L. Witte. M. T. Delzell is acknowledged for editing of the technical reports.

In addition, acknowledgment is also made of the continued interest and encouragement of A. Kampinsky and L. Ippolito, Goddard Space Flight Center, NASA, during the course of this program.

1.0 INTRODUCTION

1.1 SCOPE AND PURPOSE

During the past several years, considerable effort has been devoted to the study and development of antenna techniques such as phased arrays and self-steering arrays to increase present-day communication capabilities. A two-phase survey of spacecraft antenna systems was performed by the Hughes Aircraft Company from October 1963 to January 1966.* The first phase included a literature search, a field survey, and a critical analysis of many possible scanning and steering techniques. Several were chosen as being particularly applicable to spacecraft communication, and two specific configurations, a multiple-beam transdirective concept and a self-phasing retrodirective concept, were recommended for further study and implementation. During the second phase of the study these two systems were breadboarded and tested.

The present program is the outgrowth of this work and has as its purpose the design, fabrication, testing, and evaluation of an engineering model of a high-gain self-steering microwave transponder. The program was started in January of 1966 with the system scheduled for delivery late in 1967; because several components of the transmitting section lie at the limits of current technology, final assembly was delayed into 1968.

The final report is divided into two volumes of which this document is the first. Volume I contains the design considerations and general approach selected for the transponder and the attitude readout circuits, a detailed description of operation of the engineering model, and the results of tests and measurements. This volume also contains a general survey of the types of self-steering array systems and a description of a system that would be suitable for a specific application, in this instance, a Data Relay Satellite System.

---

*Kummer and Villeneuve, 1965; Kummer and Birgenheier, 1966.

1.2 BACKGROUND

Some of the requirements for spacecraft communications that have arisen suggest the use of self-steering antenna systems with significant advantages over conventional antennas now employed. One such application is the Delay Relay Satellite System (DRSS) that is being proposed. A system concept for the DRSS is shown schematically in Figure 1. It would be composed of low orbiting user vehicles from which communications are maintained to a central earth terminal by relaying signals through a microwave repeater at synchronous altitude. Typically, the user vehicles might be Apollo spacecraft in earth orbit, Nimbus weather satellites, or aircraft. The communication systems on these vehicles are very modest in terms of antenna gain and transmitting power.

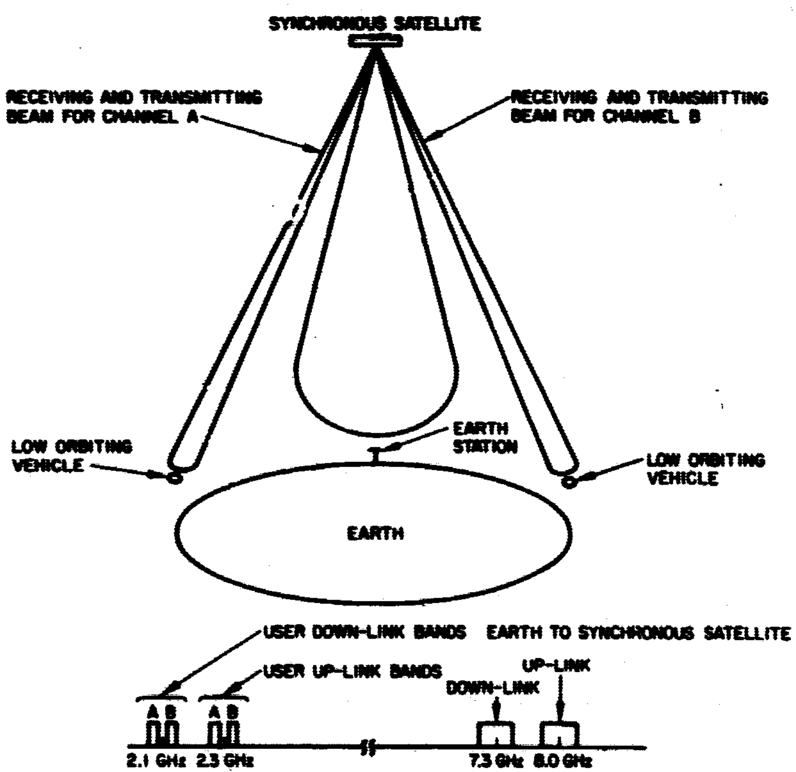

Figure 1. Data Relay Satellite System concept.

To obtain the required signal-to-noise ratios with reasonable data rates, the repeater system on the synchronous satellite must have a very high antenna gain and high effective radiated power (ERP). These requirements dictate that the beamwidth of the DRSS repeater must be much narrower than the beamwidth subtended by the earth. Narrower beamwidths, in turn, add the requirement that the beams must be steered to point in the direction of the user. Since there may be many users and, thus, many beams, mechanical or electrical positioning of the repeater system may be physically impossible unless more than one antenna is used. In addition, the exact orientation of the synchronous satellite and the location of the users must be known if antenna positioning by command is to be performed.

Because of the difficult requirements and constraints imposed by the DRSS system, a self-steering microwave repeater seems to be a natural solution for the synchronously orbiting system. It would form beams automatically in the direction of the low orbiting users regardless of their relative positions or velocities. It would not need either search or acquisition modes but, instead, would be continuously looking over its coverage angle. When it receives a signal from a user, it forms a high-gain beam in that direction. Another desirable feature is its capability to form multiple, independent beams without undue complications.

A possible configuration for a self-steering repeater for the DRSS is discussed in this volume of the Final Report. The system takes the form of an array of 100 clusters of doubly wound spiral radiators. The self-steering technique employed uses phase inversion by mixing. A unique module-coupling scheme was derived to eliminate beam-pointing errors due to the frequency separation between transmitter and receiver. An exploration of microelectronic techniques for possible application to the front-ends of self-steering systems indicates a combination of microstrip and stripline components would be achievable at the present state of the art. Possible configurations for front-end modules are discussed.

For the DRSS antenna system presented, frequencies of 2.1 and 2.3 GHz were chosen, but the techniques can be scaled to 1.6 and 2.3 GHz. At significantly different microwave frequencies, however, such as 7 and 8 GHz, the microwave components would be different.

1.3 ORGANIZATION OF FINAL REPORT

Self-steering principles are reviewed in Section 2.0 of this volume of the final report. The review includes a discussion of the two self-steering breadboards fabricated by Hughes and some of the more pertinent data obtained. This section is followed in Section 3.0 by a discussion of the engineering model which is being built by Hughes Aircraft Company and the preliminary data that have been obtained. This section also includes a discussion of an attitude readout similar to that which could be employed on the DRSS if necessary. Section 4.0 presents a discussion of a self-steering system that may be proposed for DRSS application; tables presenting system characteristics and estimates of weight and power consumption are included. Section 5.0, New Technology, presents a new steering technique that could be used to eliminate the beam-pointing error problem when a single array is used for duplex communications. It also presents a discussion of design and packaging techniques that could be employed in the design of an integrated r-f module. The work presented on the r-f module and on the new beam-steering technique was augmented by the contractor's independent research and development programs.

2.0 SELF-STEERING ANTENNA TECHNIQUES

Self-steering antenna techniques applicable to satellite communication links may be divided conveniently into four classifications: (1) switched multiple-beam antennas, (2) Van Atta arrays, (3) self-phasing arrays, and (4) adaptive arrays. In multiple-beam antennas, the proper beam to be retransmitted is selected by switching and control circuitry, either in response to a command from a transmitting station or as indicated by a pilot signal from the receiving station. In the Van Atta array the incident radiation is simply redirected back to the source; in active Van Atta systems, information may be obtained from some other source and modulated onto the redirected signal. In the self-phasing arrays, conformal elements with separate electronic circuitry are automatically phased by a mixing technique to produce a beam in the required direction. In the adaptive arrays, a phase-locked loop at each element adjusts the element phases appropriately across the antenna aperture in response to an incoming signal. The last three groups all operate on similar principles but are implemented in different ways. The switched multiple-beam antennas are distinct from the others. The operation and characteristics of each group are discussed in the following subsections.

2.1 SWITCHED MULTIPLE-BEAM ANTENNAS

Switched multiple-beam antennas that are used in self-steering applications utilize appropriate switching and control circuits to select the proper beam automatically when a pilot signal is received from that beam-pointing direction (Kummer and Villeneuve, 1965; Belfi, 1964). The selection is made through the use of logic circuitry that selects the antenna beam output by some means, such as the strongest pilot signal, and connects it to a receiver. The signal is then amplified and may be retransmitted in a second direction. This second direction is also selected by logic circuitry which compares the strength of a pilot signal from that direction as it appears at the various antenna beam outputs. The transmitter is then connected to that beam which receives the strongest pilot signal, and transmission in the desired direction results. When the pilot signal arrives from a direction intermediate among a number of adjacent beams, a fairly elaborate power division technique is required to prevent large gain reductions near beam crossover points.

Several configurations in this type of self-steering antenna are possible. These include multiple feed reflectors, lenses, and beam-forming matrices (Kummer and Villeneuve, 1965; Butler and Lowe, 1961). The reflectors with multiple feeds may be shown to suffer from problems of spillover and/or aperture blockage effects. Thin lenses may also suffer spillover problems unless rather complex feeding techniques are employed to shape the primary feed patterns. Many reflectors and lenses also suffer beam deterioration with off-axis scanning and do not appear too desirable. Spherical or cylindrical Luneberg lenses do not exhibit either spillover effects or beam degradation with scan angle; however, systems that utilize these lenses and reflectors require a large volume since their depth (from feed to aperture) must be essentially equal to or greater than the aperture itself (Kummer and Villeneuve, 1965). Planar arrays using beam-forming matrices overcome the latter problem to some extent but become lossy and very complex when large arrays are used.

An experimental antenna breadboard system of the multiple-beam type using planar arrays and beam-forming matrices was constructed by the Hughes Aircraft Company Antenna Department for the Goddard Space Flight Center on Contract No. NAS 5-3545 (Kummer and Birgenheier, 1966). The system, shown in block diagram in Figure 2, used two planar arrays of helical radiators, arranged in four rows of four elements each. The arrays were designed to cover a 50-degree conical region from a gravity-gradient stabilized vehicle in a 6000 nautical mile orbit, and elements and their spacing were

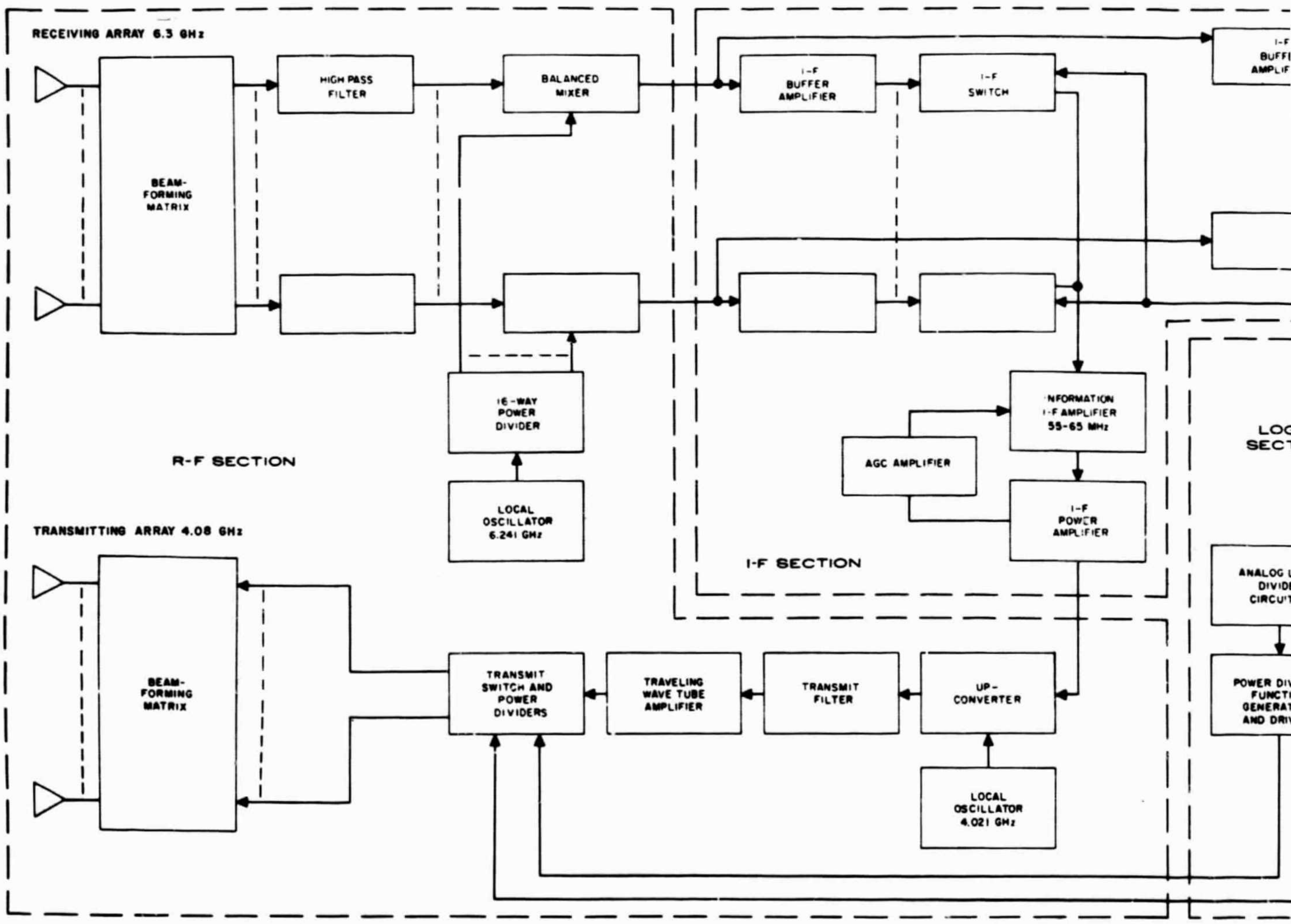

FOLDOUT FRAME 1

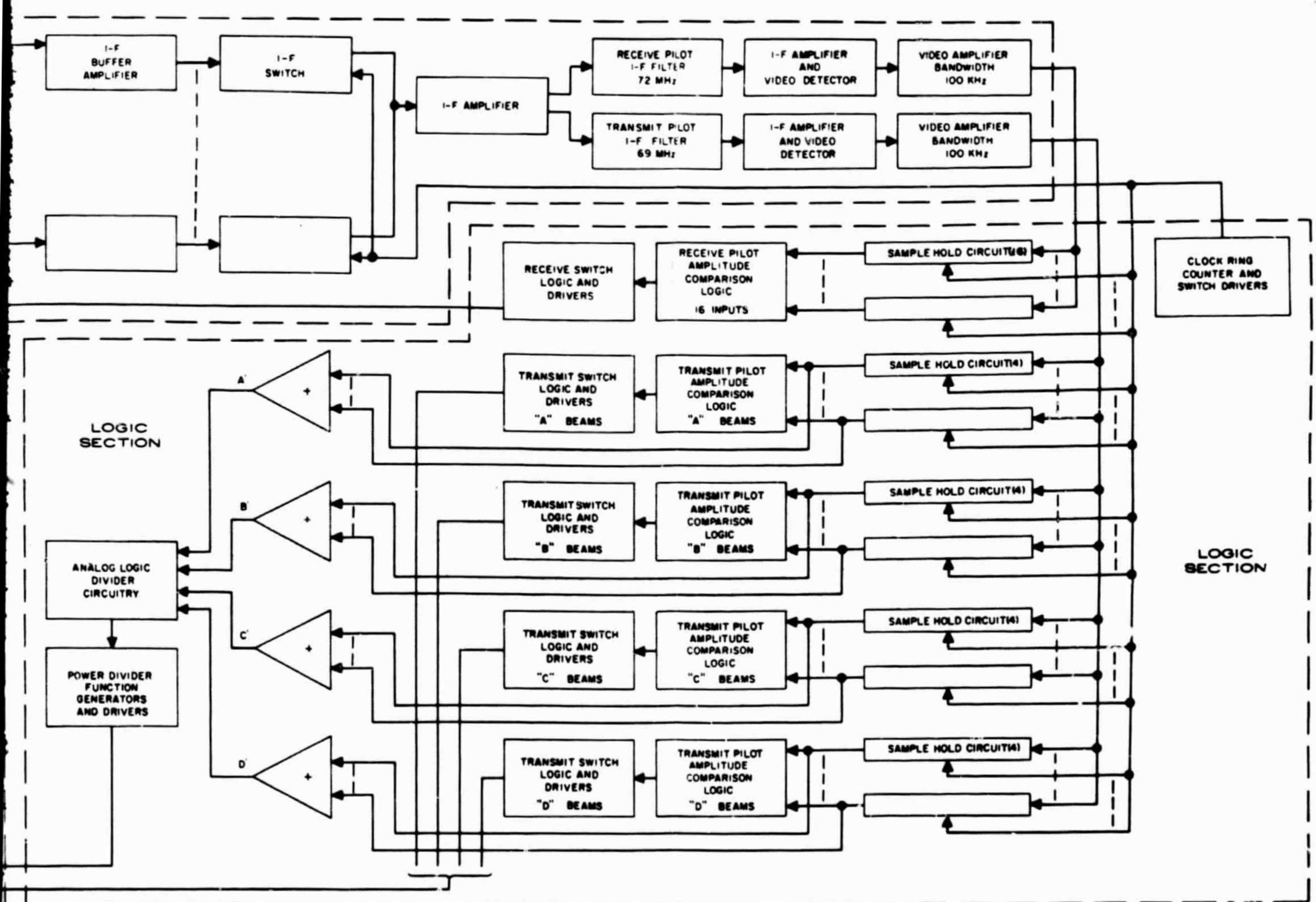

Figure 2. Hughes multiple-beam antenna breadboard schematic.

FOLDOUT FRAME 2

selected for that purpose. Each array was connected to its own 4-by-4 beam-forming matrix. The receiving array operated at 6.3 GHz, while the transmitting array operated at 4.081 GHz and was a scaled version of the 6.3 GHz array.

In operation, a pilot signal at 6.310 GHz directed the receiving beam, and a second pilot at 6.312 GHz directed the transmitting beam. To receive, the logic selected the highest pilot level and connected the corresponding receiving beam to the receiving amplifier. The signal was amplified and limited to remove the effects of signal variations as the angle of arrival moved from beam peak to beam crossover. To transmit, the transmitting logic selected the four adjacent beams that had the highest transmit pilot level, compared them, and distributed the transmitted power among the corresponding transmitting beams through electronically variable power dividers. This arrangement minimized power level variations as the transmitting direction moved from beam peaks to beam crossover points.

Some typical operating characteristics of the array are shown in Figures 3 and 4. Figure 3 shows a typical transmitting element pattern. Figure 4 shows the received level of the retransmitted signal at 4.081 GHz as the array was rotated. The level is substantially as predicted by theory and essentially follows the envelope of the adjacent beams. It contains some ripples as the angle passed from beam peaks through crossover points.

The system illustrated the basic feasibility of this self-steering technique. However, for even moderately sized two-dimensional arrays, the required logic circuitry and power division controls are quite extensive and complex. In addition, the beam-forming matrix becomes extremely complicated with any increase in size and can occupy considerable volume. Element phase and amplitude tolerances become more difficult to control for larger, complicated matrices. The losses in the matrix also increase rapidly with size and appear to make two-dimensional arrays of this type somewhat impractical when they become large in terms of wavelength.

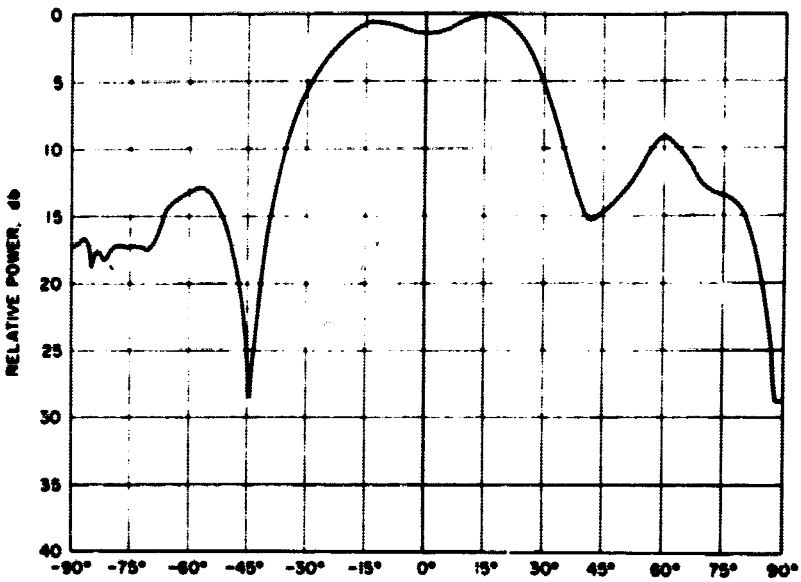

Figure 3. Representative pattern of helix element in multiple-beam array.

Some of the more important properties of multiple-beam antennas are summarized below.

Advantages

(1) No variable phase shifters are required to scan the beam.

(2) These arrays are applicable to both nonsynchronous and synchronous gravity-gradient stabilized orbits for earth-to-satellite, aircraft-to-satellite, and satellite-to-earth systems.

(3) No earth sensor and no preprogrammed controls are required.

(4) Inherently reliable r-f components (matrix or lens) are utilized.

Disadvantages

(1) Large numbers of couplers or hybrids are required in arrays that utilize a matrix.

(2) A pilot signal must be generated and transmitted at the receiving location.

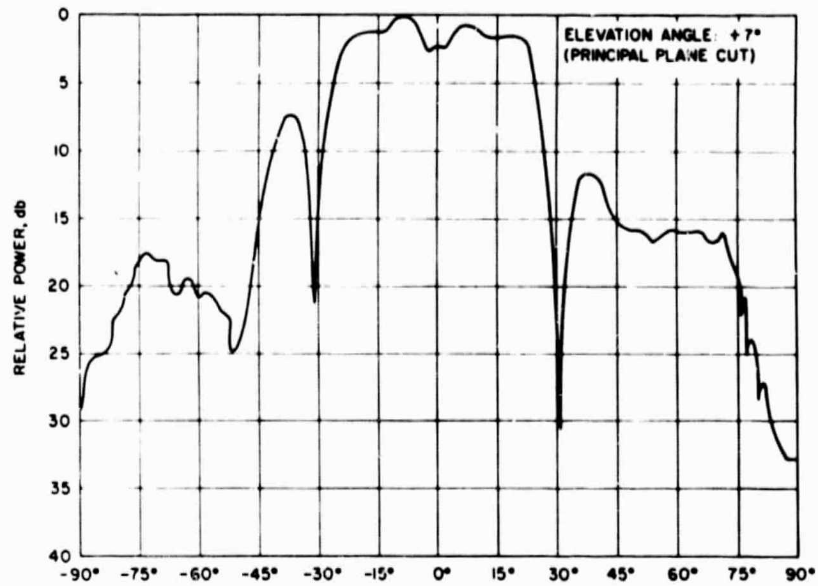

Transmitting pattern with system lock-on transmitting pilot signal.

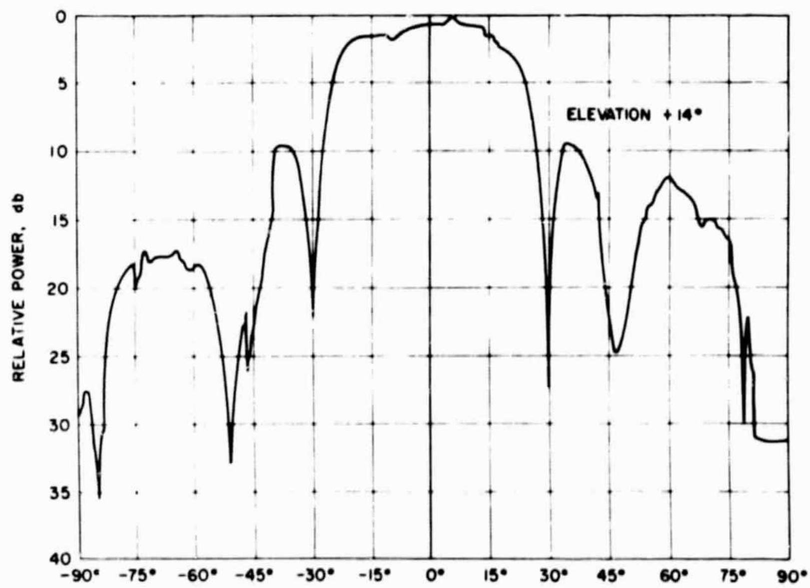

Closed-loop pattern with system locked-on both receiving and transmitting pilot signals.

Figure 4. Multiple-beam antenna patterns.

(3) A multiple-beam array may be too heavy, depending on the configuration: for example, when a lens is used.

(4) Electronically controlled r-f switches and switch control circuitry are needed.

(5) Additional r-f and control circuitry are needed to provide smooth transfer of the signal between beams.

(6) Phase compensation over the incident wavefront cannot be provided.

(7) Failure may be catastrophic, depending on the circumstances.

2.2 VAN ATTA ARRAYS

Perhaps the simplest type of retrodirective system is the Van Atta array (Van Atta, 1959) which has been proposed for use in several communications satellites (Ryerson, 1960; Hansen, 1961a; Andre, 1963). This type of array may be active or passive and directs incident radiation back in the direction of the source. The basic array is illustrated in Figure 5. The lines interconnecting pairs of elements all have the same electrical length. Ideally in the absence of mismatch and mutual coupling effects, a wave incident at an angle θ with the array axis is redirected with full array gain back toward the source of the incident radiation. Strictly speaking, for proper operation the

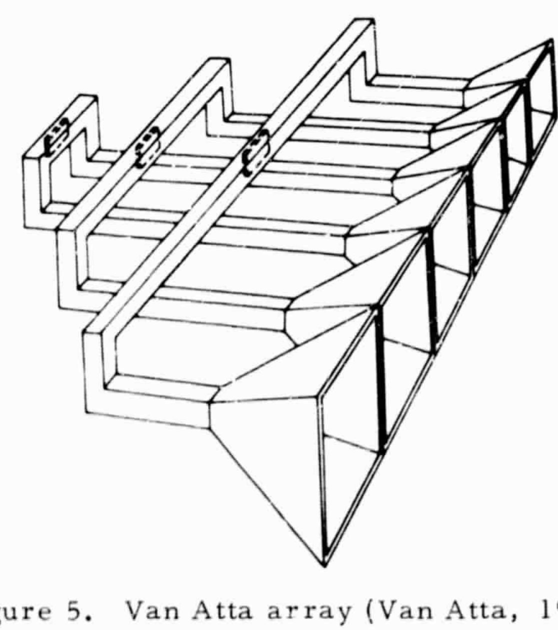

Figure 5. Van Atta array (Van Atta, 1959).

Van Atta array is confined to planar array configurations (Hansen, 1961b). It is therefore the least general of the retrodirective arrays considered since the others can lie on arbitrary surfaces.

If amplification is inserted in the transmission lines between pairs of elements, the system becomes active. In accordance with the discussion of Hansen, because of the changes in effective element impedances, bilateral amplifiers are not desirable and back-to-back unilateral amplifiers are more attractive. Circulators would be used to couple into and out of the amplifiers. Additional isolation can be obtained through frequency shifts between received and retransmitted signals. The same type of beam-pointing errors that occur for other redirective and retrodirective arrays would result from the frequency translation, however. This source of error could be reduced by the use of two arrays of different sizes scaled to the two frequencies, one for reception and one for transmission. When scaled arrays are used, circulators or bilateral amplifiers are not necessary. The systems in general fail gracefully and, in addition, have the advantage of preserving doppler frequencies.

An experimental model of a Van Atta array system was built and tested by Andre and Leonard, (1964). The system consisted of two interleaved arrays of nine orthogonally oriented printed dipoles and employed tunnel-diode amplifiers and mixers (Figure 6). The nominal

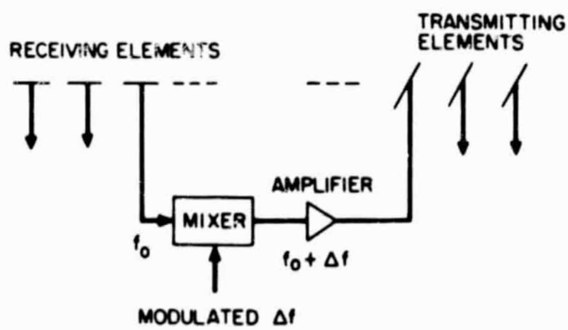

Figure 6. Active Van Atta system with separate arrays for reception and retransmission.

receiving frequency was 2.0 GHz and the transmitting frequency, 2.15 GHz; the r-f bandwidth was approximately 120 MHz. The two arrays were not scaled in size to offset the effect of frequency shift, but the orthogonal orientation of the elements in the two arrays provided isolation between received and retransmitted signals. The information signal, which was obtained from some other source, was impressed on the reradiated signal by introducing it on the local oscillator signal at frequency Δf. The antenna system was operated under conditions of both single and multiple access. Its measured gain was reported to be 14 db.

A second experimental version of the Van Atta array has been described briefly by Gruenberg and Johnson (1964). It consists of a 25-element Van Atta array in which 24 conjugate elements are pulse code modulated by on-off switches. The switching modulates the reradiated signal. The modulation comes from a signal received by the 25th (center) element. This receiving element accepts the modulated signal from a distant transmitter. A separate receiving station then beams an unmodulated signal to the array. This signal is modulated by the array switches and directed back to the receiving station.

2.3 SELF-PHASED ARRAYS

A third form of self-steering arrays consists of those that use phase inversion by mixing to obtain the required aperture phase progression.* The systems used to accomplish the phase inversion may have a variety of forms, each with particular advantages in a given situation. One of the simplest configurations (Sichelstiel et al., 1963; Pon, 1964) is shown in Figure 7. The basic operating principle may be seen from the figure: the phase of the incoming pilot signal is inverted at each element by the circuitry to create the condition

---

*Kummer and Villeneuve, 1965; Cutler et al., 1963; Sichelstiel et al., 1963; Pon, 1964; Rutz-Phillip, 1964.

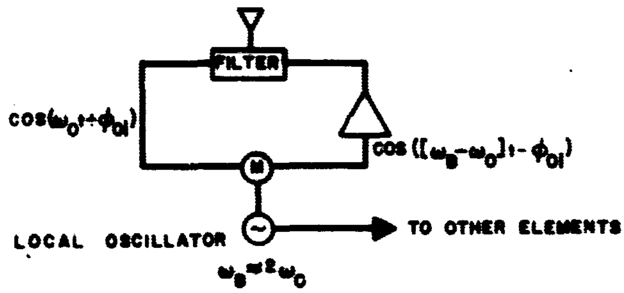

Figure 7. Elementary array module.

necessary for retransmission of a signal back in the direction from which the pilot came. Information may be modulated on the local oscillator signal to be sent back in the desired direction.

In actual practice it is simpler to obtain large amplifier gains and to perform some of the filtering functions at intermediate frequencies. A breadboard array of this type built by the Hughes Antenna Department (Kummer and Birgenheier, 1966) is shown in the diagram of Figure 8. A single 6.301 GHz receiving helix is used on the information up-link. The signal is amplified in a 60-MHz i-f strip and up-converted to 4.021 GHz where it is further amplified by a traveling-wave tube and distributed to each element in a 16-element square array of 4-GHz helices. A pilot at 4.159 GHz is converted to 60 MHz, amplified and up-converted to 4.081 GHz by mixing the 60-MHz pilot with the 4.021-GHz information signal, and is then reradiated. The mixing of the 60-MHz pilot i-f and the 4.021 GHz information signal impresses the correct phase on the signal to cause a beam to be reradiated in the direction of the incoming pilot signal.

Both this array and the Hughes switched multiple-beam array were designed to simulate the operating characteristics of gravity gradient stabilized systems on a satellite in a 6,000 nautical mile orbit. The desired coverage region was an angular cone of approximately ±25

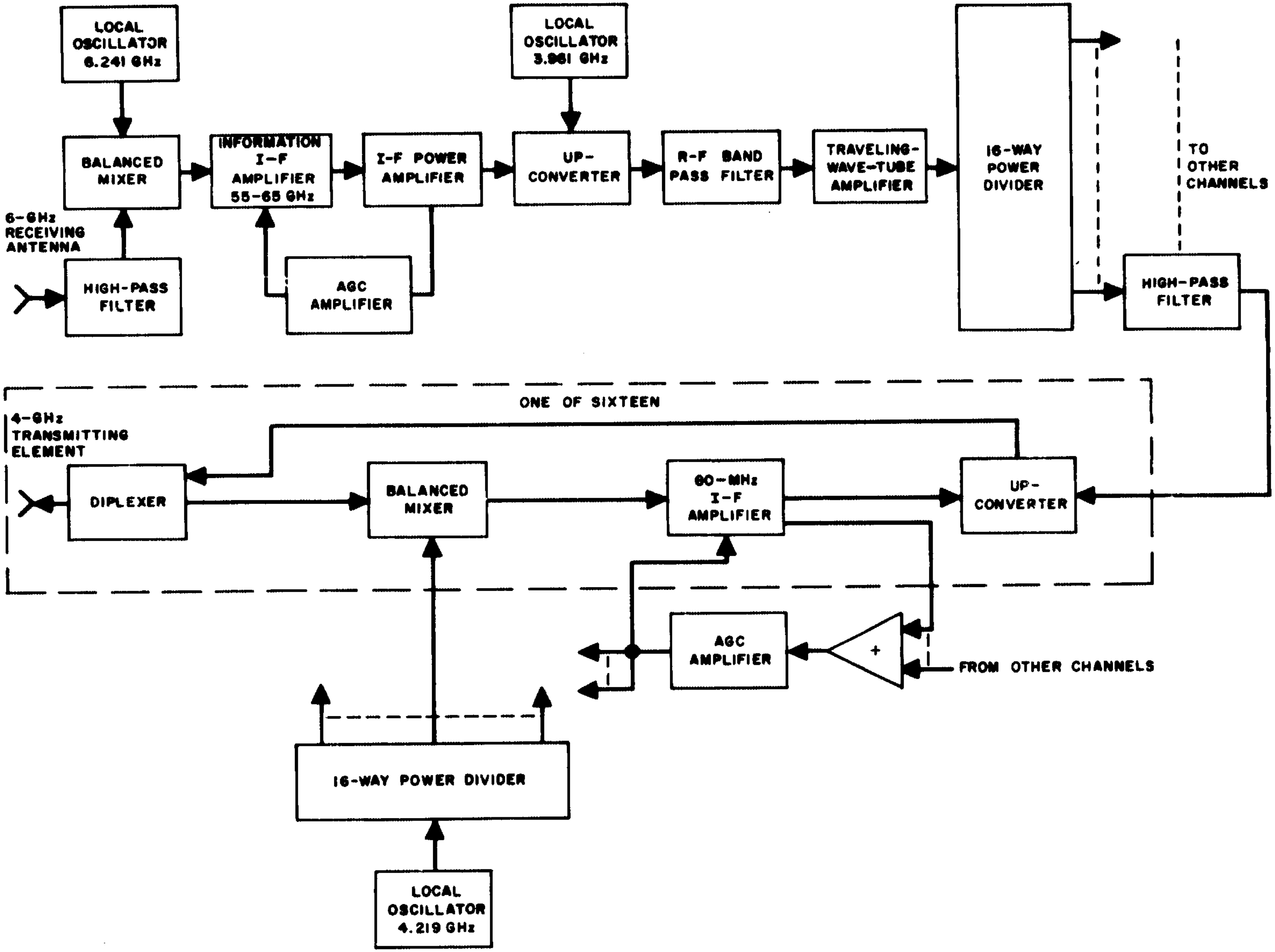

Figure 8. Hughes self-phasing antenna system schematic.

degrees. The elements used in the transmitting array were the same as those used in the transmitting array of the switched multiple-beam breadboard system. Figure 9 shows the relative retransmitted signal levels for two representative elevation angles as received at the pilot signal location as the retrodirective array was rotated. It is evident that the desired coverage was obtained. It is also evident that the coverage with this array is smoother than that obtained with the multiple-beam array (cf. Figure 4).

More sophisticated forms of arrays of the type just discussed may be devised using mixing techniques. These arrays can be designed to act as self-steering receiving arrays as well as retrodirective arrays or redirected arrays. Figure 10 illustrates a possible configuration of the latter type of array. The total incoming signal at the n^{th} element consists of a narrow-band pilot signal (ω_p) that is offset from a broad information band (ω_m). The signals are subtracted from a suitable offset frequency (ω_1) and the difference frequencies are filtered, separately amplified, and mixed once more. The signal at the last difference frequency ($\omega_m - \omega_p$), which is independent of the incoming phase, is summed with all similar outputs from the other elements. At the output of the summer, the array gain is realized. As the signal is processed, spectral splitting due to differential doppler shifts resulting from rotational motion of the vehicle is removed, and the apparent doppler shift is reduced.

Various types of arrays whose beams are steered automatically by the use of the interelement phase shift of an incident pilot signal have certain advantages and disadvantages in common.

<u>Advantages</u>

(1) The failure of one channel or more is not catastrophic since each channel is independent.

(2) Controlled phase shifters are not required to steer the beam.

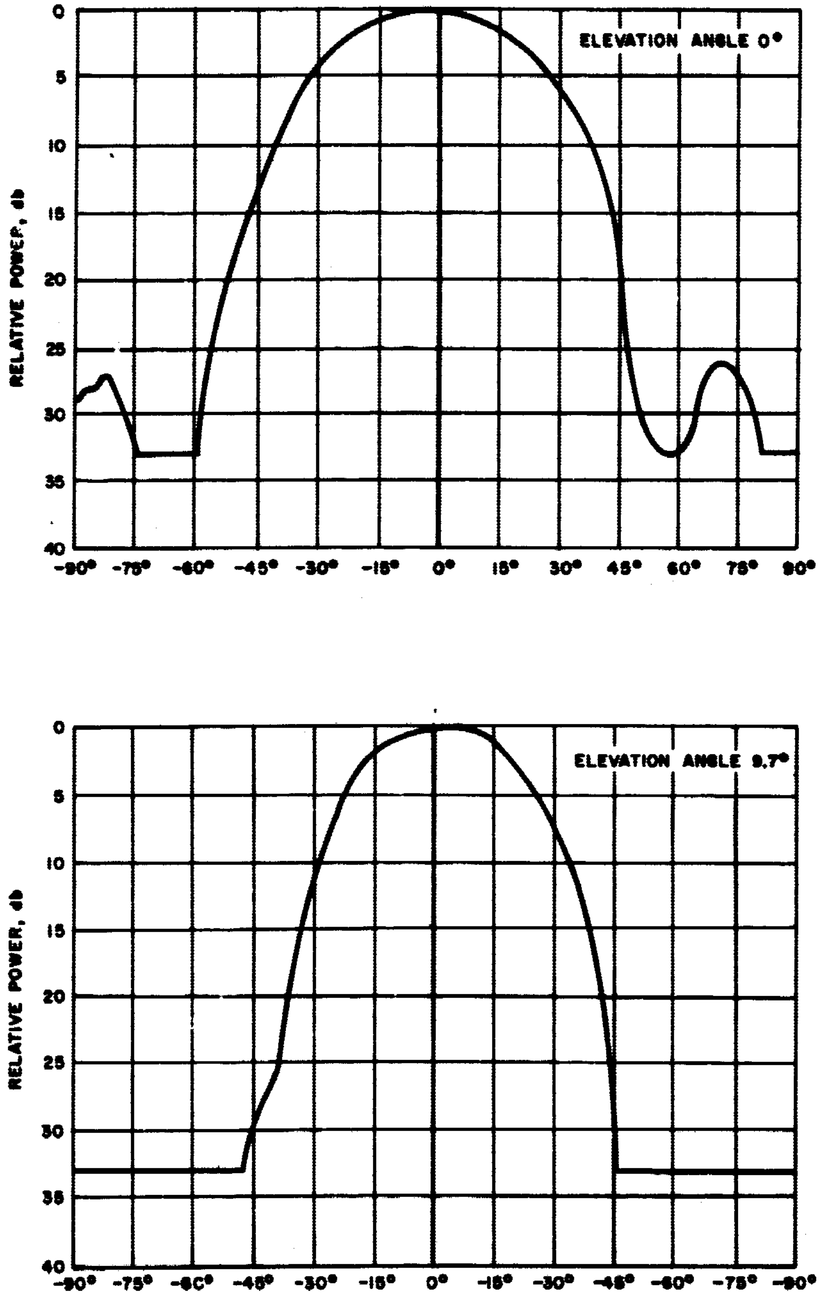

Figure 9. Round-trip patterns of self-phased array.

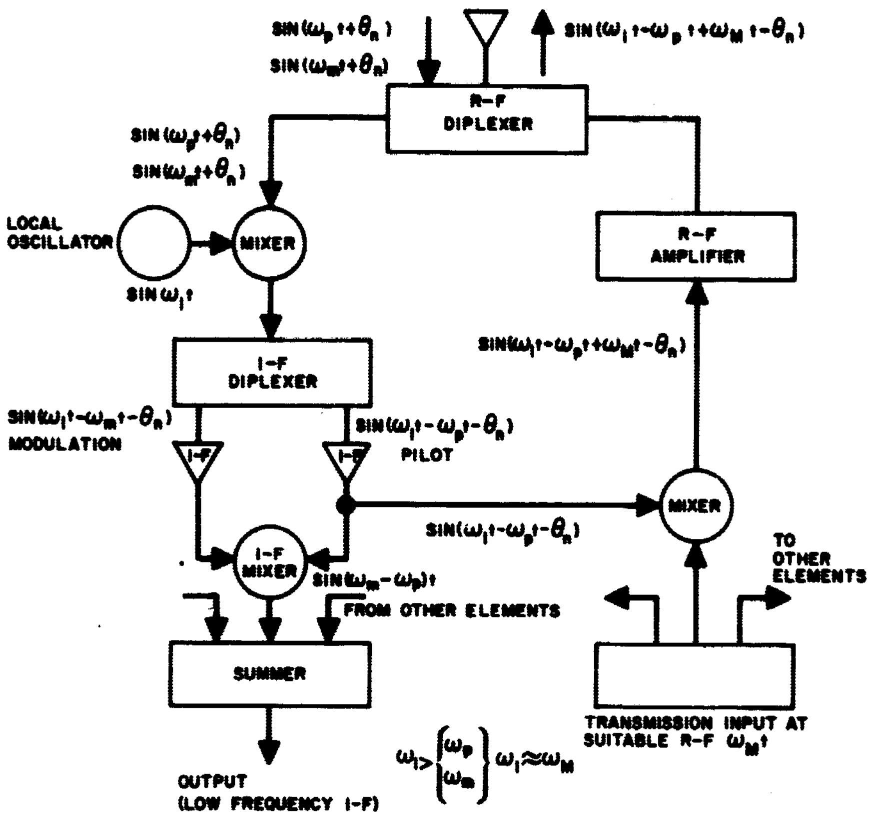

Figure 10. Self-phasing redirective array.

(3) Self-phasing arrays can be applied to nonsynchronous, synchronous, stabilized, or unstablized systems.

(4) These arrays may be used for aircraft-aircraft, aircraft-satellite, or satellite-earth systems.

(5) Neither an earth sensor nor preprogrammed controls are required.

(6) These arrays have growth potential.

(7) Switches and switch controls are not required.

(8) Phase nonuniformities over the incident wavefront are compensated.

(9) Radiating elements can be positioned on any conformal surface.

(10) Doppler frequencies are preserved internally.

(11) The transmitting signal is offset so that two-way links have zero doppler shift.

Disadvantages

(1) Some components are utilized that need further development into flight-qualified, lightweight form, as is true of some components of most self-steering systems.

(2) Generation and transmission of a pilot signal is required at the receiving location.

(3) N phase-matched channels are required for an N-element array.

(4) A complete receiver and transmitter is required for each channel.

(5) If pilot signals are noisy, performance tends to be degraded.

2.4 ADAPTIVE SYSTEMS

Adaptive arrays are self-steering systems that employ phase-locked loops. These circuits have been finding increasing application in recent years as phase synchronizing devices for an arbitrary distribution of radiating elements. The phase-locked loops automatically adjust the signals received by each element of the array to be in phase so that they can be coherently combined. In this way the full gain of the array may be obtained when the array is receiving. The signals in the phase-locked loops also may be used to steer a transmitted signal back in the direction from which energy is received. In this section an array is described briefly that uses phase-locked loops, and the important characteristics of phase-locked loops are discussed in considerable detail so that the important parameters that must be considered in the design of an adaptive antenna system can be pointed out.

2.4.1 System Operation

An element of a self-steering array and its associated circuitry are shown in Figure 11. The element shown in the figure is receiving at a frequency ω_i. The total phase of the incoming signal is $\omega_i t + \varphi_i$ where φ_i may be arbitrary. For purposes of convenience in implementing the phase-locked loop, the signal is converted in the first mixer to an intermediate frequency $(\omega_i - \omega_0)$ with a phase angle $\varphi_i - \varphi_0$. The signal from the voltage-controlled oscillator is mixed with the intermediate frequency signal, and the sum frequency out of the mixer is compared in the phase detector with the signal from the reference oscillator which is operating at ω_1 with phase φ_1. The frequency of the

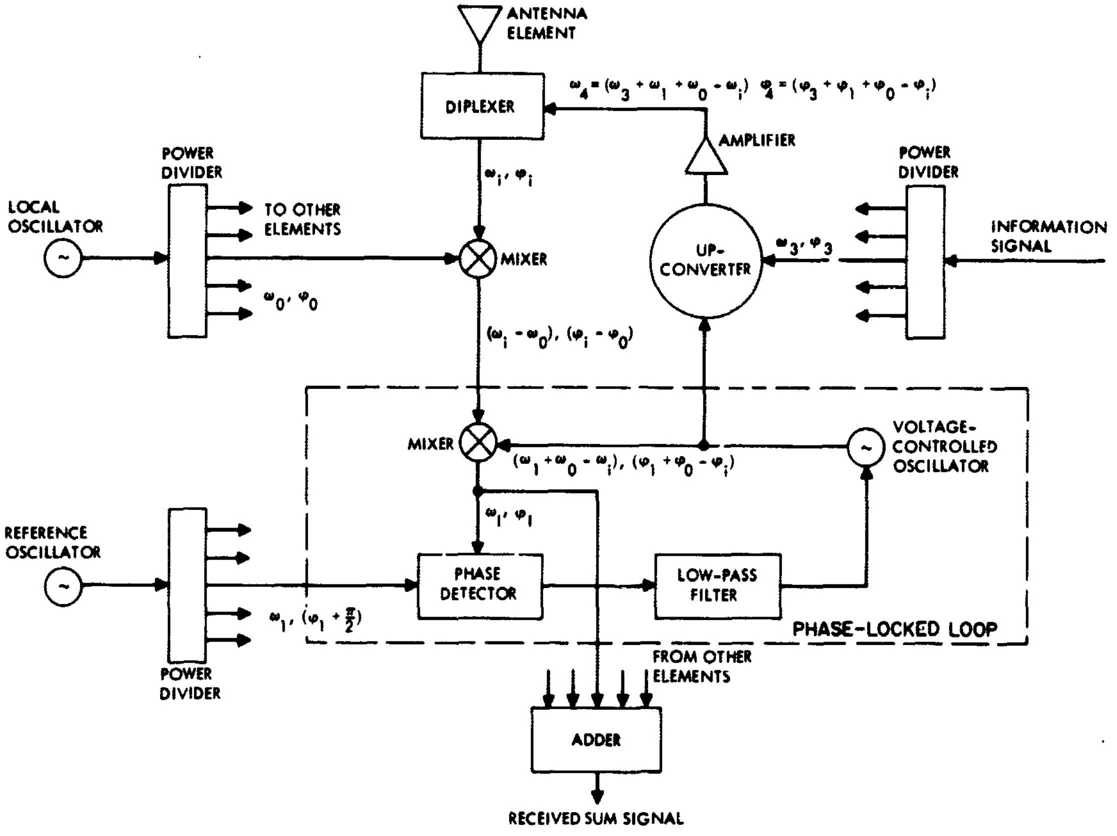

Figure 11. Retrodirective antenna that uses a phase-locked loop.

voltage-controlled oscillator is automatically adjusted to minimize the output of the phase detector. This output is minimized when the voltage-controlled oscillator operates at frequency $\omega_2 = \omega_1 + \omega_0 - \omega_i$ and has a phase given by $\varphi_2 = \varphi_1 + \varphi_0 - \varphi_i$. Consequently, the phase of the signal from the second mixer is locked to that of the reference oscillator. Since the signals from all elements are locked to the same reference signal, they are in phase with each other and may be added directly. The gain of the array is thereby achieved for reception.

The phase-locked loop is an automatic phase control system. Its major components are a multiplier, a time invariant linear filter, and a voltage-controlled oscillator (VCO). Figure 12 illustrates a schematic of a basic phase-locked loop showing the signals at pertinent points. The input signal consists of a desired term plus a noise term and is given by

$$\sqrt{2}\, A \sin \left[\omega_0 t + \theta_1 (t)\right] + n(t) \qquad (2-1)$$

where n(t) is the noise term and $\theta_1(t)$ is the phase of the input signal. The noise is assumed to be flat, narrow-band, stationary, and gaussian with two-sided spectral density $N_0/2$ over the frequency ranges of interest. It may be written in the following form

$$n(t) = \sqrt{2} \left[n_1(t) \sin \omega_0 t + n_2(t) \cos \omega_0 t\right] \qquad (2-2)$$

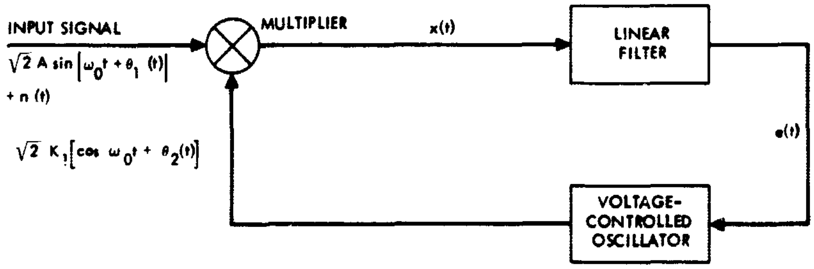

Figure 12. Phase-locked loop schematic.

where A is the rms amplitude of the input signal and $n_1(t)$ and $n_2(t)$ are independent gaussian processes with zero mean and with spectral densities identical to that of n(t) except centered about zero frequency. The signal from the VCO may be written as

$$\sqrt{2}\, K_1 \cos\left[\omega_0 t + \theta_2(t)\right] \tag{2-3}$$

where ω_0 is the frequncy of the VCO when its control signal e(t) is zero and $\theta_2(t)$ is the phase angle of the VCO. The frequency of the VCO is linearly dependent on the control voltage so that

$$\frac{d\theta_2}{dt} = K_2\, e(t) \tag{2-4}$$

where K_2 is a proportionality constant. Consequently, θ_2 is given by

$$\theta_2(t) = K_2 \int_0^t e(u)\, du + \theta_2(0) \tag{2-5}$$

where $\theta_2(0)$ is the value of θ_2 at $t = 0$.

The output of the multiplier consists of low frequency terms and terms centered at $2\omega_0$. The latter terms are filtered out by the loop so that the terms of interest are

$$x(t) = A K_1 \sin\left[\theta_1(t) - \theta_2(t)\right] - K_1 n_1(t) \sin\theta_2(t) + K_1 n_2(t) \cos\theta_2(t) \tag{2-6}$$

On defining

$$\varphi(t) = \theta_1(t) - \theta_2(t) \tag{2-7}$$

and

$$n'(t) = -n_1(t) \sin\theta_2(t) + n_2(t) \cos\theta_2(t) \tag{2-8}$$

Equation (2-6) may be rewritten as

$$x(t) = A K_1 \sin \varphi(t) + K_1 n'(t) \tag{2-9}$$

If the impulse response of the filter is denoted f(t), then the output e(t) of the filter due to an input x(t) is given by

$$e(t) = e_0(t) + \int_0^t x(u) f(t-u)\, du \tag{2-10a}$$

$$e(t) = e_0(t) + K_1 \int_0^t \left[A \sin \varphi(u) + n'(u)\right] f(t-u)\, du \tag{2-10b}$$

where $e_0(t)$ is the output resulting from initial conditions in the filter. When Equation (2-10b) and Equation (2-7) are substituted into Equation (2-4), the following equation results;

$$\frac{d\varphi}{dt} = \frac{d\theta_1}{dt} - K_2\, e_0(t) - K \int_0^t \left[A \sin \varphi(u) + n'(u)\right] f(t-u)\, du \tag{2-11}$$

where $K \equiv K_1 K_2$ is the loop gain. When the filter is initially quiescent, $e_0(t) \equiv 0$, and the equation for loop operation in the presence of additive noise is

$$\frac{d\varphi}{dt} = \frac{d\theta_1(t)}{dt} - K \int_0^t \left[A \sin \varphi(u) + n'(u)\right] f(t-u)\, du \tag{2-12}$$

It can be shown (Viterbi, 1966) that as far as the loop operation is concerned, the noise term n'(t) may be treated as a "white" gaussian process of flat spectral density $N_0/2$. Equations (2-11) and (2-12) may be considered as representing the phase-locked loop model shown in Figure 13. Since the noise term n'(t) is a random process, there is no way of determining an exact solution of Equation (2-12). All that can be determined are the statistics of $\varphi(t)$, and in general, these are difficult to obtain.

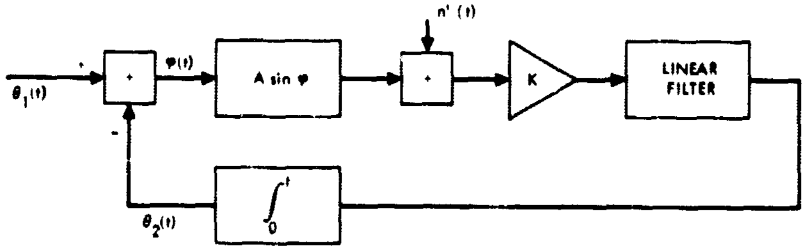

Figure 13. Model of phase-locked loop.

2.4.2 Approximate Loop Performance Analyses

When the signal-to-noise ratio in the input is large, several approximate analyses may be carried out.

a. Operation of Phase-Locked Loops in Absence of Noise. - In one approximation the noise is neglected and a deterministic solution for φ may be obtained when $\theta_1(t)$ is known. The equation governing the loop operation is just Equation (2-12) with n' set equal to zero. The resulting equation is

$$\frac{d\varphi}{dt} = \frac{d\theta_1(t)}{dt} - K A \int_0^t \sin \varphi(u) f(t - u) du \qquad (2\text{-}13)$$

Use of this approximation permits determination of the response of the loop to various input forms for $\theta_1(t)$. This equation is nonlinear in φ and generally is not easily solved. However, it readily leads to the value of the steady-state phase error that results, provided that $d\varphi/dt$ approaches zero for large t. If this condition is satisfied, Equation (2-13) becomes for large t

$$\int_0^t \sin \varphi(u) f(t - u) du = \frac{1}{KA} \frac{d\theta_1}{dt} \qquad (2\text{-}14)$$

which by the convolution theorem for Laplace transforms may be transformed to

$$\mathcal{L}\left[\sin \varphi(t)\right] = \frac{s\Theta_1(s)}{K\ A\ F(s)} \tag{2-14}$$

where $\mathcal{L}$ denotes the operation of taking the Laplace transform, s is the transform variable, F(s) is the transfer function of the filte and $\Theta_1(s)$ is the Laplace transform of $\theta_1(t)$. The value of $\sin \varphi(t)$ a $t \to \infty$ is given by the final value theorem as

$$\lim_{t \to \infty} \sin \varphi(t) = \lim_{s \to 0} s\,\mathcal{L}\left[\sin \varphi(t)\right] = \lim_{s \to 0} \frac{s^2\ \Theta_1(s)}{K\ A\ F(s)} \tag{2-15}$$

The steady state value of $\sin \varphi$ then depends on the nature of $\theta_1(t)$ and on the filter characteristics. There are four filter characteristics that are commonly considered. The corresponding loops are termed first order, second order, imperfect second order, and third order. The corresponding transfer functions are

1. First order (no filter)

$$F(s) = 1 \tag{2-16}$$

2. Second (perfect integrator with gain a in parallel with direct path)

$$F(s) = 1 + \frac{a}{s} \tag{2-17}$$

3. Imperfect second order

$$F(s) = \frac{s + a}{s + \epsilon} \tag{2-18}$$

4. Third order

$$F(s) = 1 + \frac{a}{s} + \frac{b}{s^2} \tag{2-19}$$

A possible implementation of the filter for an imperfect second-order loop is shown in Figure 14. The steady-state phase errors for several variations of the input signal phase $\theta_1(t)$ are shown in Table 1. For this configuration

$$a = 1/R_2C \tag{2-20a}$$

$$\epsilon = 1/(R_1 + R_2)C \tag{2-20b}$$

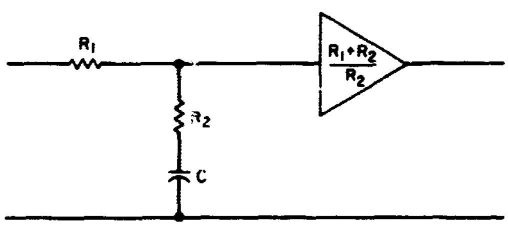

Figure 14. Configuration of filter for imperfect second-order loop.

b. Linearized Loop Analysis. — Another approximation that can be used to analyze loop performance for high input signal-to-noise ratios and small phase errors is the linear approximation. In this approximation, $\sin \varphi$ is approximated by φ and Equation (2-12) becomes

Phase of Input Signal, $\theta_1(t)$	Order of Loop	Transfer Function of Filter, F(s)	Steady-state Phase-Error, $\lim_{t \to \infty} \varphi(t)$
$(\omega - \omega_0) t + \theta_0$ fixed doppler	first	1	$\frac{(\omega - \omega_0)}{AK}$
$(\omega - \omega_0) t + \theta_0$	second	$1 + \frac{a}{s}$	0
$(\omega - \omega_0) t + \theta_0$	imperfect second	$\frac{s + a}{s + \epsilon}$	$\frac{\epsilon}{a}\left(\frac{\omega - \omega_0}{AK}\right)$
$\frac{1}{2} Rt^2 + (\omega - \omega_0) t + \theta_0$	second	$1 + \frac{a}{s}$	$\frac{R}{aAK}$
$\frac{1}{2} Rt^2 + (\omega - \omega_0) t + \theta_0$	third	$1 + \frac{a}{s} + \frac{b}{s^2}$	0

Table 1. Tracking errors of loops of various orders for the noiseless case.

$$\frac{d\varphi}{dt} + KA \int_0^t \varphi(u)\, f(t - u)\, du = \frac{d\theta_1}{dt} - KA \int_0^t n'(u)\, f(t - u)\, du \quad (2\text{-}21)$$

Since the equation is linear in φ, the solution may be separated into two portions, φ_1 and φ_2, φ_1 resulting from the driving function $d\theta_1/dt$ and φ_2 resulting from the noise term. The solution for φ_1 may be carried out as in the noiseless case in the previous subsection with the added simplification that the equation has been linearized. The solution for φ_2 cannot be carried out explicitly because $n'(t)$ is a random process. However, if the noise is stationary, the response to the noise will, in the steady state, be stationary with zero mean (Viterbi, 1966). Then $S_\varphi(\omega)$, the spectral density of the phase error, is related to $S_n(\omega)$, the spectral density of the noise, by

$$S_\varphi(\omega) = \left| \frac{KF(j\omega)/j\omega}{1 + AKF(j\omega)/j\omega} \right|^2 S_n(\omega) \qquad (2\text{-}22)$$

If the noise is white with a two-sided spectral density, $S_n(\omega) = N_0/2$. When the closed loop transfer function, H(s), is defined as

$$H(s) = \frac{AKF(s)/s}{1 + AKF(s)/s} \qquad (2\text{-}23)$$

then Equation (2-23) becomes

$$S_\varphi(\omega) = \frac{N_0}{2A^2} \left| H(j\omega) \right|^2 \qquad (2\text{-}24)$$

The variance of the phase error due to noise is then given by

$$\sigma_\varphi^{\ 2} = \frac{1}{2\pi} \int_{-\infty}^{\infty} S_\varphi(\omega)\, d\omega = \frac{N_0}{A^2 4\pi j} \int_{-j\infty}^{j\infty} H(s)\, H(-s)\, ds \qquad (2\text{-}25)$$

If the loop noise bandwidth is defined as

$$B_L = \frac{1}{4\pi j} \int_{-j\infty}^{j\infty} H(s)\, H(-s)\, ds \qquad (2\text{-}26)$$

the phase error variance, in the steady state, becomes

$$\sigma_\varphi^{\ 2} = \frac{N_0}{A^2} B_L \qquad (2\text{-}27)$$

Thus, the noise bandwidth of the loop is the bandwidth in hertz of an ideal low-pass filter whose output variance is $\sigma_\varphi^{\ 2}$ when the input is a white process of one-sided density N_0/A^2.

The loop noise bandwidths and $\sigma_\varphi^{\ 2}$ of the first-order through third-order loops are given in Table 2. It is evident that, for a fixed

Order of Loop	Closed-loop Transfer Function, H(s)	Loop Noise Bandwidth, B_L	Phase Error Variances, ^{2}
First	$\frac{AK}{s + AK}$	$\frac{AK}{4}$	$\frac{N_0 K}{4A}$
Second	$\frac{AK (s + a)}{s^2 + AKs + AKa}$	$\frac{AK + a}{4}$	$\frac{N_0 (AK + a)}{4A^2}$
Imperfect second	$\frac{AK (s + a)}{s^2 + (AK + \epsilon)s + AKa}$	$\frac{AK (AK + a)}{4(AK + \epsilon)}$	$\frac{N_0 K(AK + a)}{4A (AK + \epsilon)}$
Third	$\frac{AK (s^2 + as + b)}{s^3 + AKs^2 + aAKs + bAK}$	$\frac{AK (aAK + a^2 - b)}{4(aAK - b)}$	$\frac{N_0 K(aAK + a^2 - b)}{4A(aAK - b)}$

Table 2. Noise bandwidths and phase error variances for various phase-locked loops.

loop gain K, the loop bandwidth increases as the amplitude of the input signal increases, and the rapidity of the phase fluctuations can therefore increase. However, the variance of the phase error decreases as the amplitude of the input signal increases, indicating that the excursions about the mean value of phase error become smaller. Comparison of Tables 1 and 2 shows that increasing the loop gain, K, decreases the steady-state mean phase errors but increases both the rapidity and the variance of phase error fluctuation due to noise. Increasing the signal amplitude, A, simultaneously decreases both the steady-state phase error and the variance of the fluctuation due to noise.

2.4.3 Effect of Band-pass Limiter

In some applications of phase-locked loops, the signal level might vary over large dynamic ranges and cause loop operation to depart significantly from the desired operating characteristics. Operation might possibly even exceed the dynamic range of the loop components.

To alleviate this problem, the loop can be preceded by a band-pass limiter. The ideal unit of this kind consists of a hard limiter followed by a band-pass filter. The limiter output is +1 when the input is positive and -1 when the input is negative. The filter eliminates harmonics of the carrier frequency that are introduced by the limiter. Davenport (1953) considered an input process of a band-pass limiter that has the form

$$z(t) = 2A \sin (\omega_0 t + \theta) + n(t) \tag{2-28}$$

where n(t) is zero mean gaussian noise of total power N_{in} and is wide-band but restricted to a frequency range about $\pm\omega_0$. He showed that the signal-to-noise ratio at the output of this band-pass limiter is

$$\frac{S_{out}}{N_{out}} = k \frac{A^2}{N_{in}} \tag{2-29}$$

where S_{out} is the undistorted signal portion of the output and N_{out} is the remaining output power. The factor k varies between $\pi/4$ for very low input signal-to-noise ratios and 2 for very high signal-to-noise ratios. Equation (2-29) is only approximately true for phase-modulated signals and then only if the rate of change of the phase modulation is much less than ω_0, the carrier frequency. If, in addition, the modulation and noise bandwidths are relatively narrow compared with ω_0, then the output power of the limiter is a constant, independent of the input power:

$$S_{out} + N_{out} = A_0^2 \tag{2-30}$$

When Equations (2-29) and (2-30) are combined, the following expression results for the <u>signal</u> amplitude into the phase-locked loop;

$$\sqrt{\frac{1}{1 + \left(N_{in}/kA^2\right)}}\ A_0 = \xi A_0$$

where ξ is the limiter suppression factor. Thus, the band-pass limiter provides an automatic gain and bandwidth control feature that is advantageous in practical systems (Jaffe and Rechtin, 1955).

Since the band-pass limiter is a nonlinear device, the statistics of the output noise are not gaussian and some of the results obtained previously that depend on the gaussian noise input to the phase-locked loop do not hold exactly. However, as the ratio of the bandwidth of the band-pass filter to the bandwidth of the input noise becomes very small, the statistics of the output noise of the band-pass limiter approach those of gaussian noise. An additional consideration arises from the bandwidth assumption made in the earlier analysis of the loop operation. That assumption was that the bandwidth of the loop input noise was wide compared with that of the loop. Consequently, although the bandwidth of the band-pass filter should be narrow compared with that of the input noise, it should still be wide compared with the loop bandwidth. One last condition must be met: to satisfy the assumption of constant output power from the band-pass limiter, its input process, as pointed out previously, should have a narrow band compared with ω_0.

2.4.4 General Behavior of Phase-locked Loops

The steady-state phase error of first-, second-, and third-order phase-locked loops has already been considered, and the equations of operation and the variance of the steady-state phase error have been derived for the linearized loop approximation. Other quantities of interest include the time required for the loop to lock-on, the conditions under which the lock-on will occur without cycle slipping, and the time required to achieve frequency-lock. These quantities may be determined through the use of graphical phase-plane analysis in which $d\varphi/dt$ is plotted as a function of φ. From analyses of this type, coupled with analytical approximations, the general properties of the loop may be estimated. Several specific cases are discussed.

a. <u>First-Order Loop with a Constant Frequency Input.</u> — The exact behavior of $\varphi(t)$ for a constant frequency input at ω is given by the integral

$$\varphi(t) = \int_{\varphi(0)}^{\varphi} \frac{d\varphi'}{\left[(\omega - \omega_0) - AK \sin \varphi'\right]} \tag{2-31}$$

The steady-state value of the phase error must be one of the points given by

$$\lim_{t \to \infty} \varphi(t) = \sin^{-1} \frac{(\omega - \omega_0)}{AK} \pm 2n\pi \tag{2-32}$$

where n is an integer. It is evident that if

$$\frac{\omega - \omega_0}{AK} > 1 \tag{2-33}$$

the loop will not lock-on.

b. <u>Second-Order Loop with a Constant Frequency Input.</u> — For a second-order loop with a constant frequency input, acquisition will always occur, though if the initial frequency offset exceeds a certain value, cycle slipping will occur before frequency lock is obtained. The approximate frequency-error decay per cycle of φ is given by

$$\delta\left(\frac{d\varphi}{dt}\right) \approx \frac{-(AK)^2 \pi}{\left(\left.\frac{d\varphi}{dt}\right|_0\right)^2 - AK} \tag{2-34}$$

The time required to achieve frequency lock (pull-in time) is given approximately by

$$t \sim \frac{1}{a}\left(\frac{\omega - \omega_0}{AK} - \theta_0\right)^2 \tag{2-35}$$

where θ_0 is the initial phase of the incident signal. This expression assumes that $\theta_2(0) = 0$, i. e., that the VCO is initially at its quiescent frequency ω_0.

The parameters of the second-order loop are commonly expressed in terms of a natural frequency ω_n and a damping factor ζ where

$$\left.\begin{aligned} \omega_n^2 &= aAK \\ \zeta &= \frac{1}{2\sqrt{a/AK}} \end{aligned}\right\} \tag{2-36}$$

A value of ζ that is commonly used in loop design as a compromise between stability and speed of response is $1/\sqrt{2}$.

c. Second-Order Loop with Linearly Varying Input Frequency.— When the range between transmitter and receiver changes with a uniform acceleration, the phase of the input signal has a quadratic term that is interpreted as a changing doppler shift. The phase may be expressed as

$$\theta_1(t) = \frac{1}{2} Rt^2 + (\omega - \omega_0) t + \theta_0 \tag{2-37}$$

It may be shown that if $R > aAK$, the loop can never achieve lock or, if the loop is initially in lock, application of the signal will cause it to lose lock. When $R < aAK$, phase-lock may be achieved, and the steady-state phase error is given by

$$\lim_{t \to \infty} \varphi(t) = \sin^{-1} (R/aAK) \tag{2-38}$$

However, phase-plane analyses show that a second-order loop (perfect) can acquire a noise-free signal with linearly varying doppler shift with certainty only if $R < aAK/2$, and that once lock-on is achieved, the loop can track the signal only when $R < aAK$.

The results for a linearly varying input frequency can be applied to a situation in which the input frequency is fixed, but to shorten acquisition time, the VCO is linearly swept over the frequency range of interest. If R is the rate of change of the frequency of the VCO, the system equations are unchanged. The result is that if

$$R > .(4B_L - a) \tag{2-39}$$

lock-on will never be achieved, and that if

$$R < \frac{1}{2}a(4B_L - a) \tag{2-40}$$

lock-on will always be achieved. For values of R intermediate between the above limits, lock may or may not be achieved, depending on initial values of θ_1 and $d\varphi/dt$.

d. <u>Second-Order Loop with Imperfect Integrator.</u> — If the second-order loop integrator is not perfect, the loop will not track a linearly varying frequency. In addition, it will not acquire a constant frequency offset signal if

$$\omega - \omega_0 > \frac{a\,AK}{\epsilon} \tag{2-41}$$

Even when $\omega - \omega_0 < aAK/\epsilon$, the loop may not achieve lock. By approximate analytical methods, it may be shown, however, that when the loop is initially quiescent, lock-on will always occur if

$$\frac{\omega - \omega_0}{AK} < 2\left[\frac{a}{AK}\left(1 + \frac{AK}{2\epsilon}\right)\right]^{1/2} \tag{2-42}$$

e. <u>Noise Behavior of Phase-Locked Loops.</u> — The presence of noise in the input to the phase-locked loop modifies its operation from the ideal noise-free case. The effect is to make the phase error φ a random process, and in the steady state, φ is described by its probability density function that tells how it is distributed about its mean value. Consequently, even though tracking is predicted for the noiseless case, the density function for φ will include values that correspond to loss of lock, and only probabilities of lock or loss of lock can be predicted in any given system. The method used to determine the probability density function of φ requires the application of Fokker-Planck techniques and is quite involved. Only results are quoted here.

(1) First-order loop — constant frequency signal (Viter i, 1966). The probability density function of φ is given by

$$P(\varphi) = C \exp(\alpha \cos\varphi + \beta\varphi)\left[1 + D\int_{-\pi}^{\varphi} \exp(-\alpha\cos x - \beta x)\,dx\right]$$

$$-\pi \le \varphi < \pi \tag{2-43}$$

where

$$D = \frac{\exp[-2\beta\pi] - 1}{\int_{-\pi}^{\pi} \exp[-(\alpha\cos x + \beta x)]\,dx} \tag{2-44}$$

and C is determined from the requirement that

$$\int_{-\pi}^{\pi} P(\varphi)\,d\varphi = 1 \tag{2-45}$$

The terms α and β are given by

$$\alpha = \frac{4A}{KN_0} = \frac{A^2}{N_0 B_L} \tag{2-46}$$

$$\beta = \frac{4(\omega - \omega_0)}{K^2 N_0} \qquad (2\text{-}47)$$

If $\beta = 0$, i. e., if $\omega = \omega_0$, tnen

$$P(\varphi) = \frac{\exp\left[\alpha \cos \varphi\right]}{2\pi I_0(\alpha)} \qquad -\pi < \varphi > \pi \qquad (2\text{-}48)$$

(2) Second-order loop — constant frequency signal (Viterbi, 1966). When the signal-to-noise ratio is sufficiently large, the probability density function of φ may be approximated for large α' by

$$P(\varphi) = \frac{\exp\left[\alpha' \cos \varphi\right]}{2\pi I_0(\alpha')} \qquad -\pi < \varphi < \pi \qquad (2\text{-}49)$$

where

$$\alpha' = \frac{A^2}{N_0 (AK + a)/4} = \frac{A^2}{N_0 B_L} \qquad (2\text{-}50)$$

These expressions can be used to determine the probability that φ exceeds a prescribed limiting value beyond which the loop is considered to be no longer in lock.

PRECEDING PAGE BLANK NOT FILMED.

3.0 HIGH-GAIN SELF-STEERING TRANSPONDER ENGINEERING MODEL

An engineering model of a self-steering transponder (shown in Figure 15) for satellite-to-earth communications was designed and fabricated at the Hughes Aircraft Company for the Goddard Space Flight Center. The system was designed as a relay station between any two pairs of ground stations that lie within a 30-degree cone of coverage. The satellite vehicle was assumed to be in a synchronous orbit and to be gravity-gradient stabilized. The description of operation and design considerations of the transponder are presented in this section. Also presented are the design goals for the system and the results of the system tests that were performed.

3.1 OPERATION OF ENGINEERING MODEL

The engineering model is designed to serve as a communications relay for two independent communications channels, each with an instantaneous bandwidth of 125 MHz. The receiver and transmitter frequencies are centered about 8.0 GHz and 7.3 GHz respectively. The frequency bands and beam designations for reception and transmission are shown in Figure 16. The transponder will steer four independent, high-gain beams (two for receiving and two for transmitting) along arbitrary directions within a ±15-degree coverage angle. The positions of the beams are controlled by the phase information obtained from c-w pilot signals generated by the communicating ground stations. Since operation of the two channels of the system is identical, only channel A is described, with the aid of the block diagram in Figure 17.

3.1.1 Initial Reception

The receiver front end of the engineering model is designed to accept signals in a 350-MHz band; it receives the 125-MHz band for channels A and B and the 100-MHz guardband between them. Contained at the center of this guard band are the four pilot signals

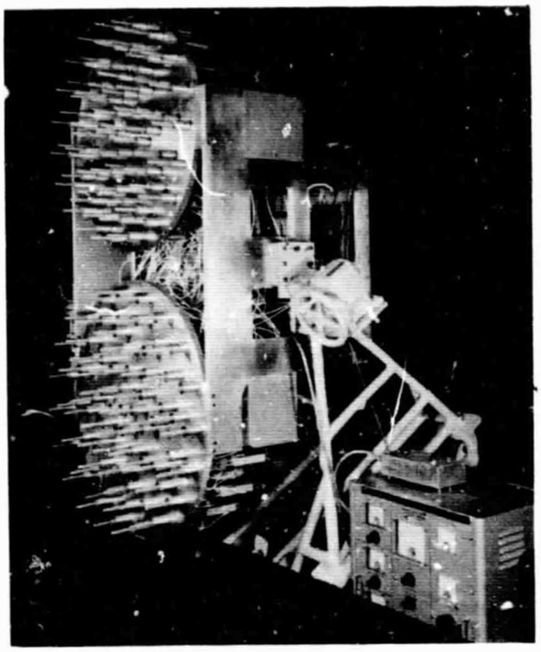

Figure 15. Engineering model of the high-gain, self-steering transponder. (HAC Photo No. 4R03268)

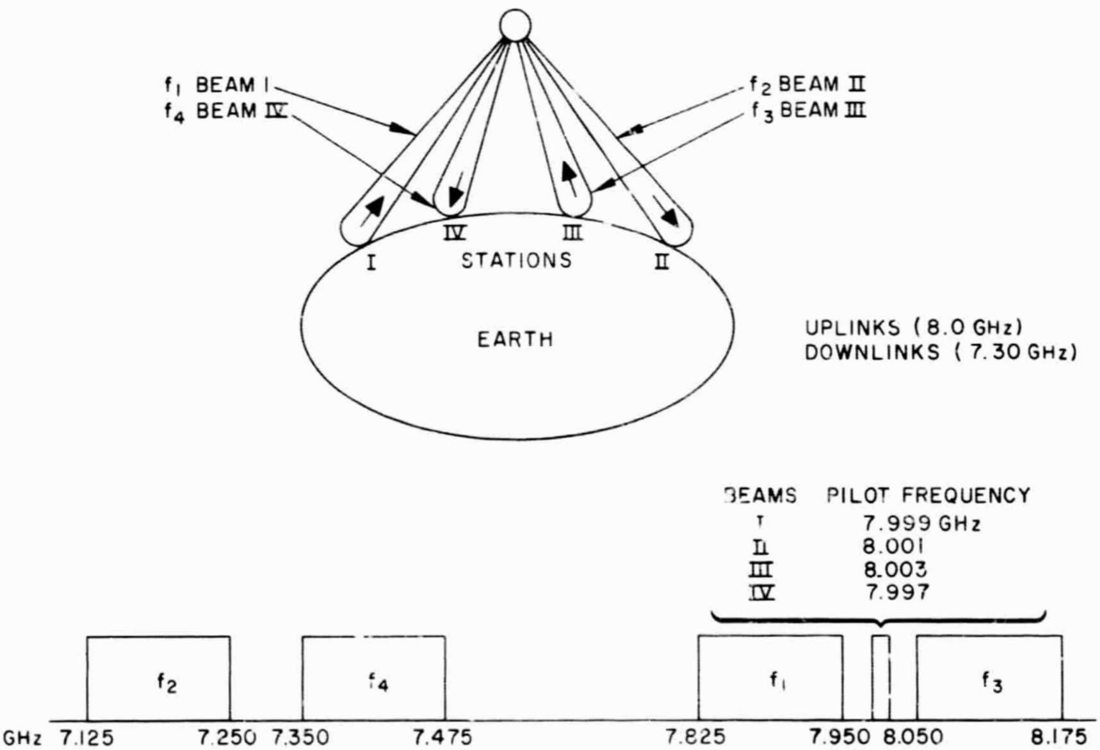

Figure 16. Beam designations and frequency bands utilized by the self-steering transponder.

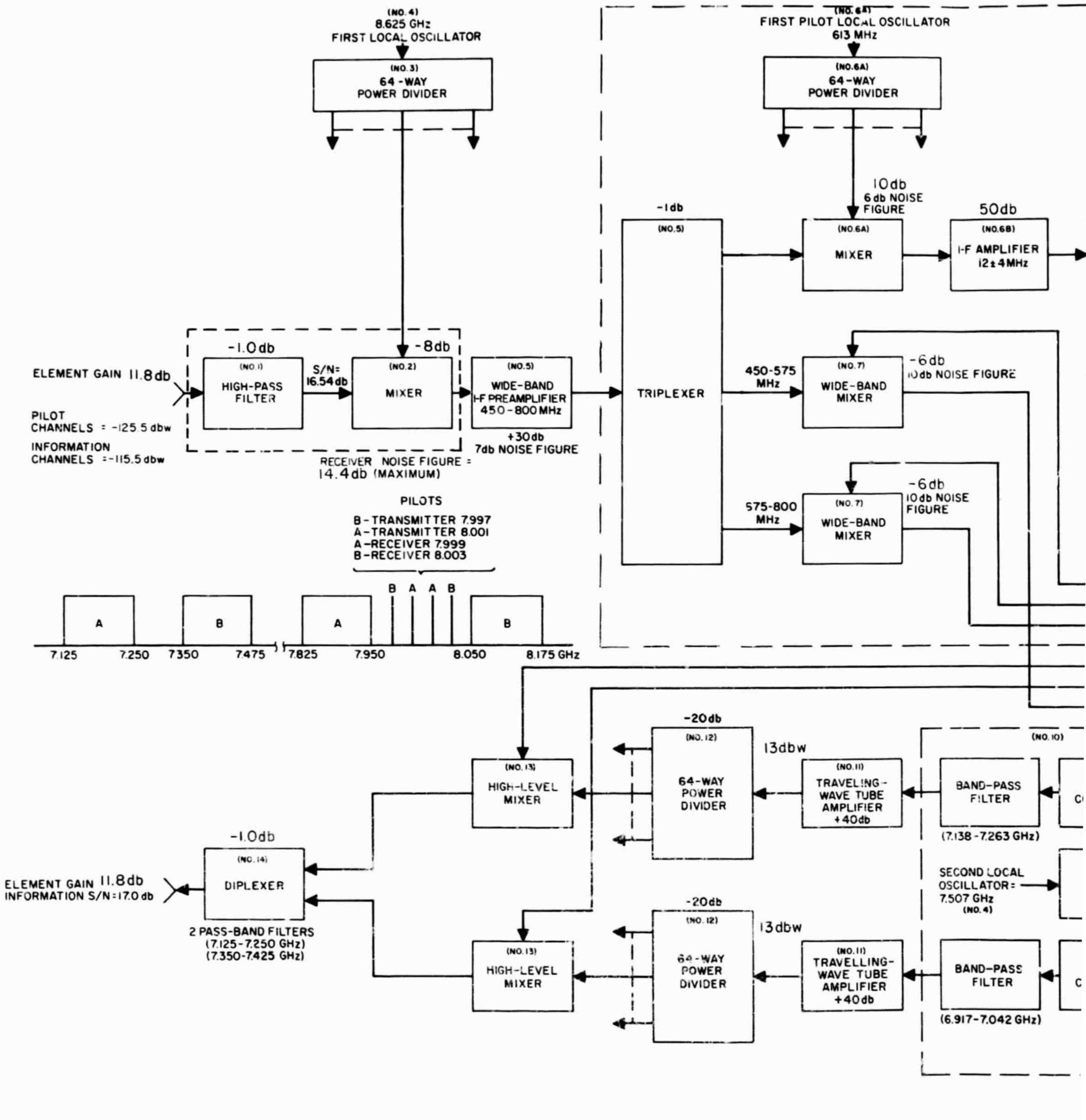

FOLDOUT FRAME 1

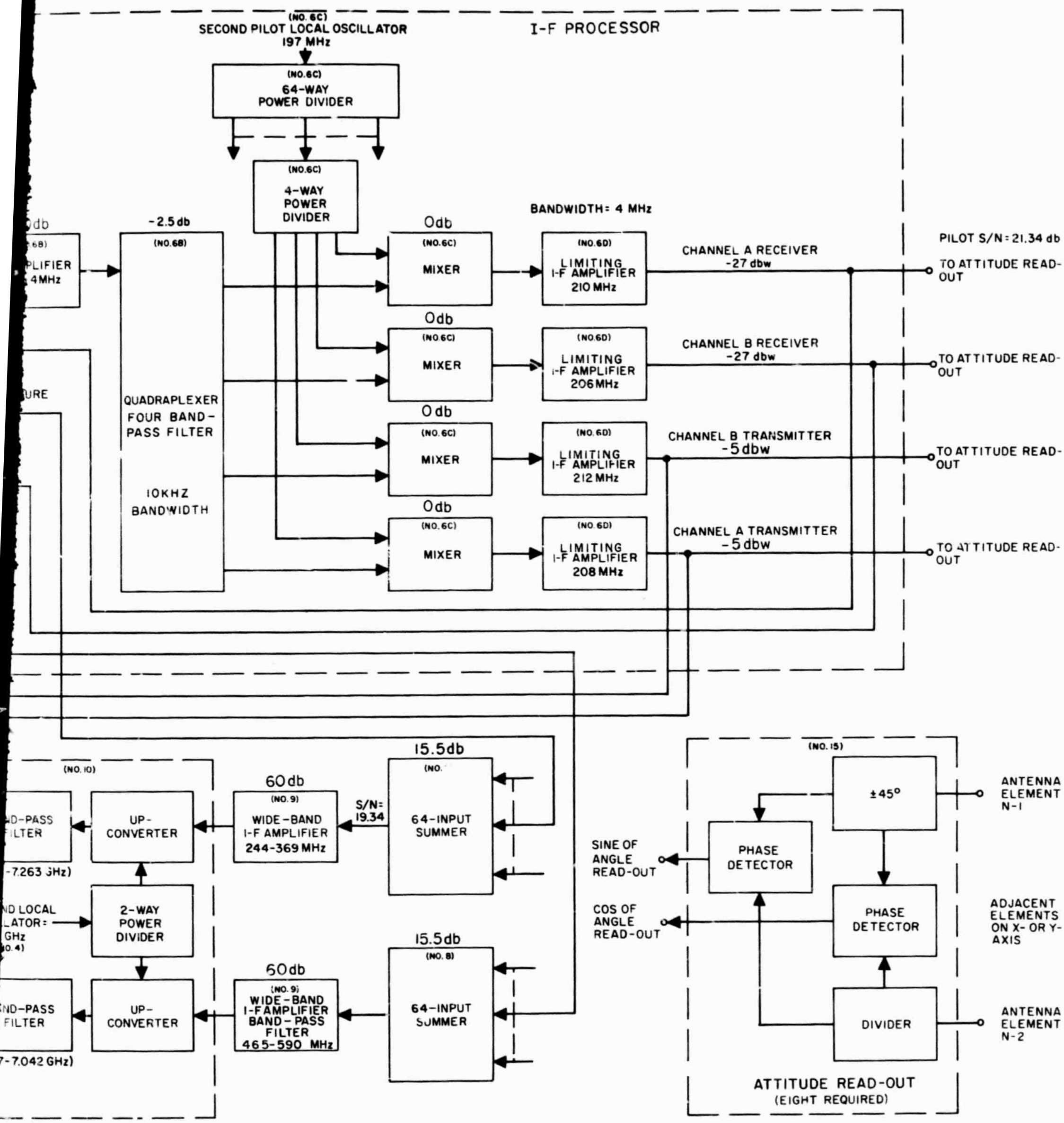

Figure 17. Integrated system block diagram.

required to phase the four beams. For channel A, an information signal with a band of frequencies from 7.825 GHz to 7.950 GHz, a transmitting pilot at 8.001, and a receiving pilot at 7.999 GHz are received by the receiving element and fed through a bandpass filter (No. 1, Figure 17). This filter rejects any signals radiated by the transmitting antenna that may saturate the first mixer (No. 2, Figure 17) or that may appear in the receiver band.

Following the bandpass filter (No. 1), the signal is mixed in the first mixer (No. 2) with a local oscillator (frequency 8.625 GHz) to produce the first i-f frequencies of 675 MHz to 800 MHz for the information signal, 624 MHz for the transmitting pilot, and 626 MHz for the receiving pilot. These signals then pass through a wide-band i-f preamplifier which has 30-db gain. The mixer and amplifier establish the receiver noise figure. Presented in Figure 18 is a picture of the receiver front end which shows the helical receiving element, the bandpass filter and mixer (No. 1 and No. 2) which are the L-shaped units, and the preamplifier. The local oscillator power for the mixers is fed by way of a 64-way power divider which is shown in Figure 19.

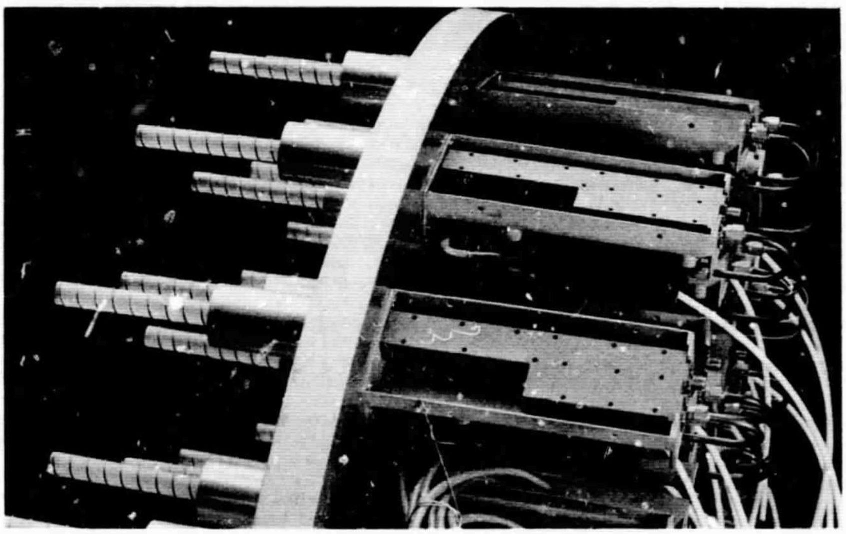

Figure 18. Receiving front end of the self-steering transponder.

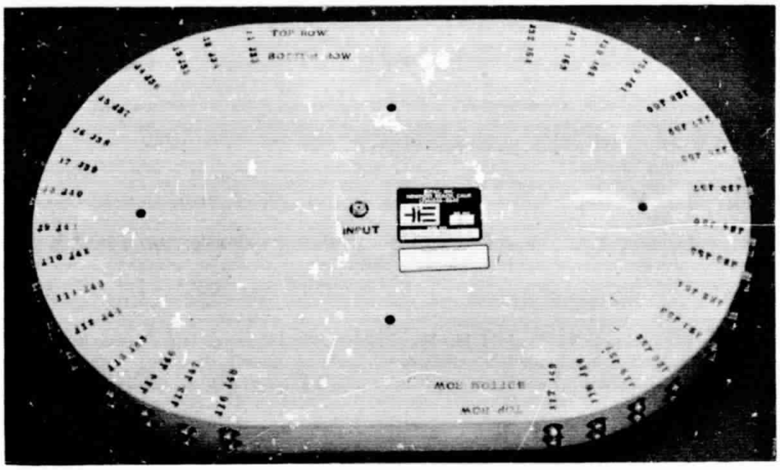

Figure 19. 64-way power divider.

3.1.2 I-f Signal Processing

After preamplification, the i-f signals are fed to the i-f processor which is shown blocked off by a dashed line in Figure 17. The first component encountered by the signal in the i-f processor is a triplexer which separates the two information channels (A and B) and the pilot signals. Each of these signals is then fed to a mixer. The signal flow of the pilot signals will now be considered.

At the first pilot mixer (No. 6A), the pilot signals are mixed with a local oscillator signal of frequency 613 MHz to produce the second pilot i-f frequencies (for channel A) of 11 MHz for the transmitting pilot and 13 MHz for the receiving pilot. The pilot signal frequencies are decreased to these relatively low values to permit the use of narrow-band crystal filters with a noise bandwidth of about 20 kHz. With this pilot bandwidth, the required pilot power can be made a small fractional part of the total power transmitted to the satellite.

After the first pilot i-f mixer, all the pilot signals are amplified by a common pilot i-f amplifier (No. 6B) which consists of four narrow-band bandpass filters. These separate the four pilot signals and establish the noise bandwidth of the pilot channels. These filters also serve to reject the local oscillator and image frequencies that are present at the output of the first pilot mixer.

Following the output of the quadruplexer (No. 6B), the pilot signals are converted to a third pilot i-f frequency, limited in amplitude, and then further amplified by the third pilot i-f amplifier. The last conversion is required because it is necessary to increase the frequencies of these signals to values at least as great as the bandwidth of the information signals to prevent overlap of the information power spectrum when the pilot and information signals are mixed. For channel A the third i-f frequencies are 208 MHz for the transmitting pilot and 210 MHz for the receiving pilot. The third receiving pilot is fed to a wide-band mixer (No. 7) to serve as a local oscillator signal for this mixer. The input to this mixer is the information signal that is present at one of the outputs of the triplexer as was mentioned previously. In the wide-band mixer the interelement phase terms are removed from the received information signals. The third transmitting pilot is used as the local oscillator signal for a mixer that feeds the transmitting element. By mixing this pilot signal with the information signal, the appropriate phase angle is introduced to the transmitted signal again.

A module of the i-f processing unit is pictured in Figure 20 and shows the circuitry that completely accommodates one element of the system. An identical module is contained on the bottom side of the unit shown. The total i-f processor is composed of 32 of these units which are housed by a pigeon-hole assembly in the system.

3.1.3 Information Signal Summer and Transmitter

At the receiver front end, all the incoming signals are mixed with a local oscillator at a frequency above that of the incoming signals; therefore, the spectrum at the input to the i-f processor is the conjugate

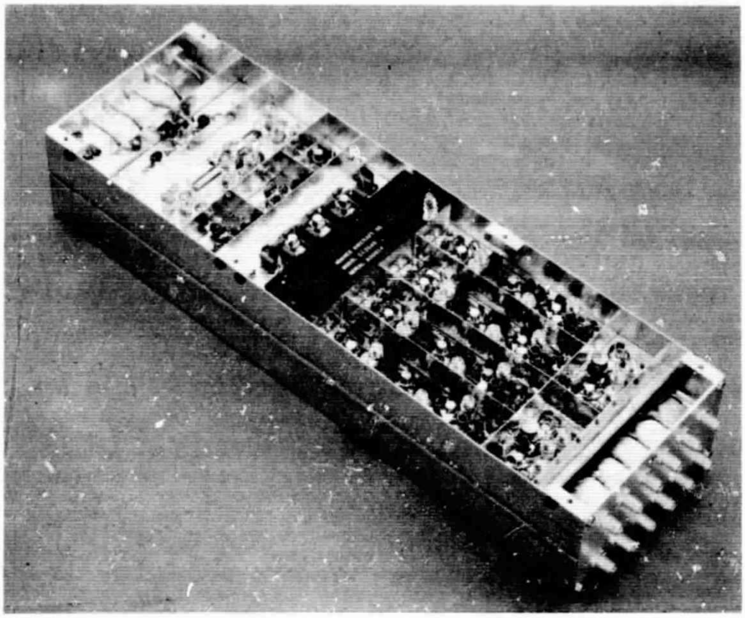

Figure 20. I-f processing module.

of that transmitted by the earth station. The frequency of the first pilot local oscillator is below the frequency of the pilot i-f signals with which it mixes, and the second pilot local oscillator serves to upconvert the pilot i-f frequencies. Therefore, the sense of the phase angles of all the pilot signals at the output of the final pilot i-f amplifiers of a particular element referenced to an arbitrary element is the negative of the sense of these signals as received by the corresponding antenna element. Thus, the receiving pilot has the same phase angle as the information signal at the wide-band mixer (No. 7); phase shifts common for all elements are neglected. The information signal and receiving pilot are mixed by the wide-band mixer, and the difference frequency is selected so that the phase angle of the resulting information signal is independent of the phase angle of the incoming signal. This mixing is performed for each element of the antenna system; therefore, the information signals at the outputs of the 64 wide-band mixers (No. 7, Figure 17) for a channel of the system are in phase. These 64 information signals, which are at frequencies from 465 MHz to 590 MHz, are coherently summed by a 64-input power summer. An improvement by a factor of 64 in signal-to-noise ratio is realized. A single channel can be used for amplification of the received signal beyond the common terminal of the summer.

The output of the 64-input summer is fed to the information i-f amplifier, which has a gain of about 60 db and serves as a bandpass filter, to select the desired part of the power spectrum from the 64-input summer. Following this amplifier, the signal is mixed with a local oscillator frequency of 7.507 GHz (No. 4) and the lower sideband selected by a bandpass filter (No. 10) to up-convert the information signal to a band covering 6.917 GHz to 7.042 GHz. The output of the bandpass filter is then fed to a traveling-wave tube (TWT) amplifier (No. 11) to raise the information signal to a relatively high level before distribution via the 64-way power divider (No. 12) in that channel to the 64 high-level mixers (No. 13) for this one channel of the system.

At the high-level mixers (No. 13) the transmitting pilot is mixed with the information signal and the upper sideband is selected by the diplexer (No. 14). An information signal is produced at a transmitting element with a phase angle that has the opposite sense as the phase angle of the transmitting pilot at the corresponding receiving element. The receiving and transmitting arrays are scaled in wavelength; these conditions are necessary to transmit the information from the antenna system in the direction of the transmit pilot.

3.1.4 Automatic Frequency Control

The crystal filters that pass the pilot r-f signals have a 3-db bandwidth of about 10 kHz. Such a narrow bandwidth causes a relatively steep phase slope in these filters. Thus it is difficult to design the pilot channels for phase tracking across the 10 kHz band. An alternative method is to keep the frequency in the 10-kHz band very constant. To maintain a small frequency excursion in the 10-kHz band requires good stability of the pilot signals. To compensate for frequency variations of the 8.625 GHz local oscillator and to provide a means of monitoring pilot i-f frequencies, an automatic frequency control (AFC)

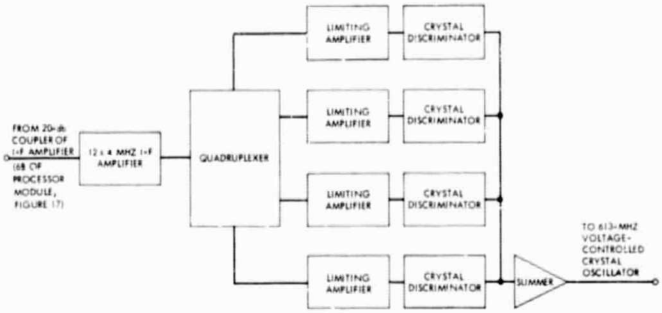

a. block diagram

b. unit

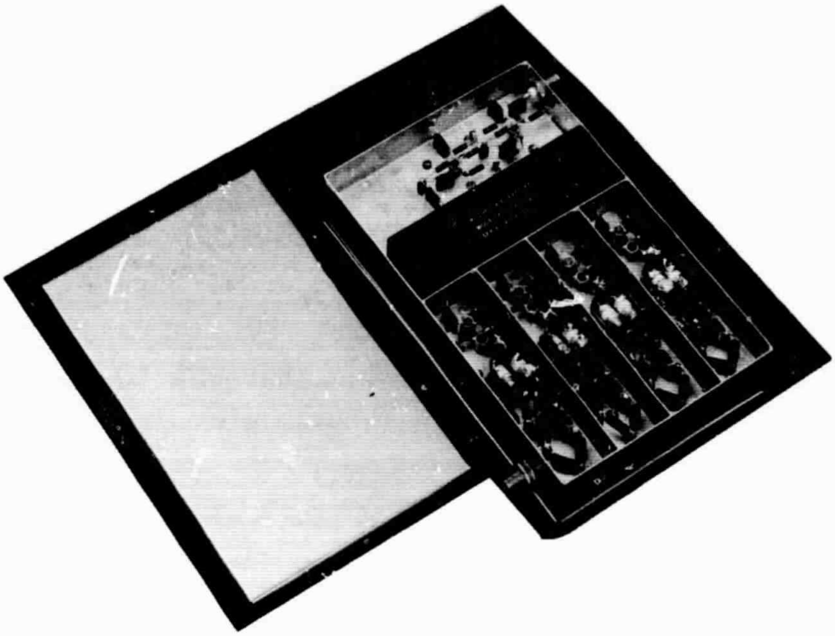

Figure 21. Automatic frequency control.

was incorporated into the system (Figure 21). A block diagram of the AFC is shown in Figure 21a, and a picture of the unit is shown in Figure 21b.

The input to the AFC unit is coupled by way of a 20-db coupler from the output of the 12-MHz i-f amplifier (No. 6B) of one of the i-f processing modules. This signal, which consists of the second i-f pilot signals, is amplified and fed to a quadruplexer which separates the four pilot signals. After the quadruplexer, each of the pilot signals is amplified, limited, and fed to a crystal discriminator. The outputs of the four crystal discriminators are summed and amplified by an operational amplifier. The output of this operational amplifier is then fed to the control input of the 613-MHz voltage-controlled crystal oscillator.

A disadvantage of the type of AFC used is that the average of the pilot signal frequency errors is compensated for rather than individual pilot frequency errors. Therefore, it is possible for an error in one of the pilot frequencies to pull the other pilot signals off frequency. The AFC system proved very useful, however, since it allowed monitoring of the average pilot frequencies and permitted a means of quickly adjusting each pilot signal exactly on frequency. One pilot was transmitted at a time and the pilot frequency was adjusted while the output voltage of the AFC unit was monitored.

For a flight model of the transponder, it might be necessary to compensate for errors of pilot signal frequencies on an individual basis. In this case, a 613-MHz local oscillator would be required for each pilot signal. Each module would have four mixers (No. 6A) and four i-f amplifiers (No. 6B); the quadraplexer would consist of four bandpass filters.

3.1.5 Attitude Readout Considerations

One of the requirements of the engineering model is that it incorporate attitude readout circuits (Figure 22). Mechanization of the attitude readout is discussed in this section.

For attitude information from the satellite to be unambiguous, the angle of incidence of two pilots from two different ground stations must be known. The engineering model has this information for any two of the four pilots. Since any pair can be used to determine the attitude of the spacecraft, the system can be given a redundancy that would greatly increase reliability of the attitude determination.

The signals for the attitude readout are derived from three elements that lie in orthogonal planes at the center of the array. One element lies in the center of the array, one on the x-axis, and the other on the y-axis as shown in Figure 23.

Signals for the angle readout are fed from the final pilot i-f amplifiers to the attitude readout phase detectors. Since the element spacing is on the order of two wavelengths, the output from each phase detector changes by 360 degrees when a pilot position changes by

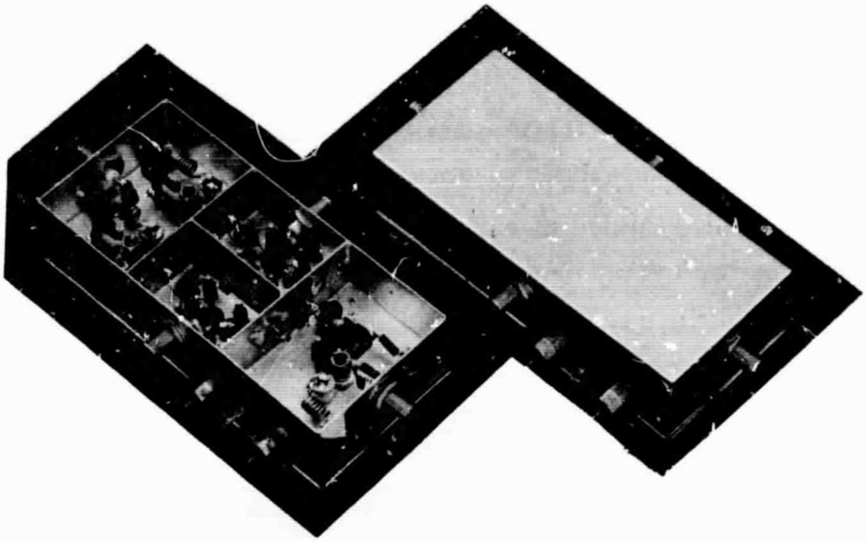

Figure 22. Altitude readout unit.

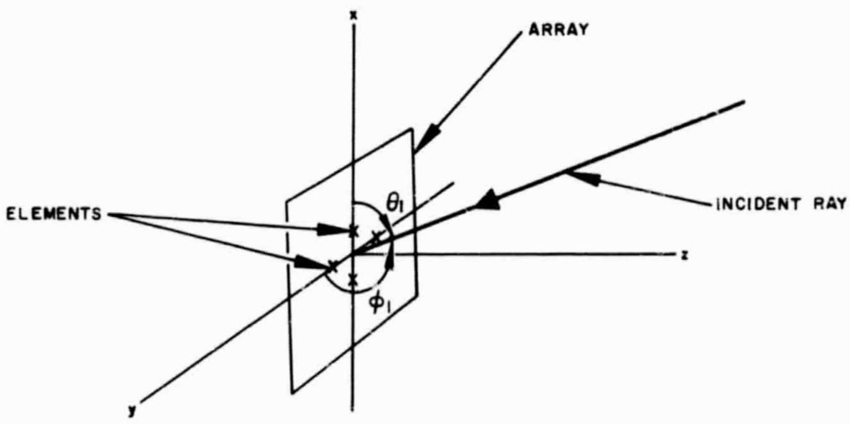

Figure 23. Arrangement of elements and angles determined for attitude readouts.

30 degrees; therefore, unique specification of an angle requires quadrature phase detectors for each angle.

The output voltages from these detectors, which are of the form [cos (Kd cos θ_i)] and [sin (Kd cos θ_i)], provide for a single angle as shown in Figure 24, where K is the propagation constant and is equal to $2 \pi/\lambda$ and d is the interelement spacing. If θ_i varies by 30 degrees, the maximum element separation that can be used with this type of angle readout is $d \equiv 1.9315 \lambda$. The element spacing for the engineering model is $d = 1.75 \lambda$ for which the normalized output voltages from one of the quadrature phase detectors become [cos (3.5π cos θ_i)] and [sin (3.5π cos θ_i)]. The design goal for the accuracy of the attitude readout is ±0.5 degree. This accuracy means that after the attitude readout is calibrated, the relative phase of the signals in the pilot channels used for the attitude readout will not change by more than ±5 degrees. Results of tests of the phase stability of the attitude readout units can be found in the second volume of this Final Report.

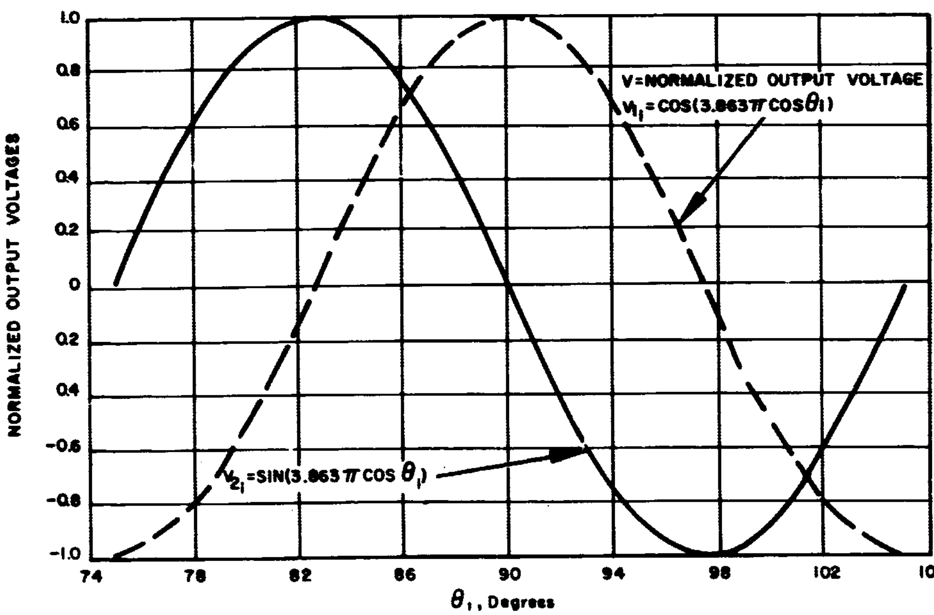

Figure 24. Attitude readout voltages for angle θ_i.

3.1.6 Transmitting Modules

For the transponder, the effective radiated power (ERP) is given by the following formula

$$ERP = N_A^2 \, g_e \, p_e \tag{3-1}$$

where p_e is the power into the radiating element and g_e is the gain per antenna radiator.

In this design, the number of radiating elements was 64, the minimum gain per element was 11.6 db and the minimum ERP was 28 dbw. These values lead to a power per element of -19.6 dbw (11 mw). To allow for a 1-db loss for the diplexers, a minimum power of -18.6 dbw per element was required.

A varactor upconverter (or high-level mixer) was used for the transmitting module. This device is perhaps interim in the state-of-the-art between solid-state r-f amplifiers and traveling-wave-tube (TWT) amplifiers for modular units. The high-level mixer is similar to the low-level mixer except for absolute and relative power levels of the input signals. It has input signals at r-f and i-f and output signals at r-f. Either resistive or reactive mixers may be employed, but the latter were selected for the engineering model since they are capable of outputs of 100 mw at X-band while resistive mixers are limited to low levels on the order of 1 mw.

The efficiences of the high-level mixers are good if the best varactors are employed, but they contribute to the overall system loss since an r-f pump is required. Power for the r-f pump must be generated elsewhere, presently by a traveling-wave tube and in the future perhaps by solid-state oscillators. The overall efficiency of a reactive mixer and pump is perhaps 10 to 15 percent at best.

3.2 ANTENNA ELEMENTS AND ARRAY

Two planar arrays of elements were used for the engineering model, one for transmitting and one for receiving, and each array consisted of 64 12-turn helices arranged in a quasi-random fashion. A picture of a test model of the receiving array is presented in Figure 25.

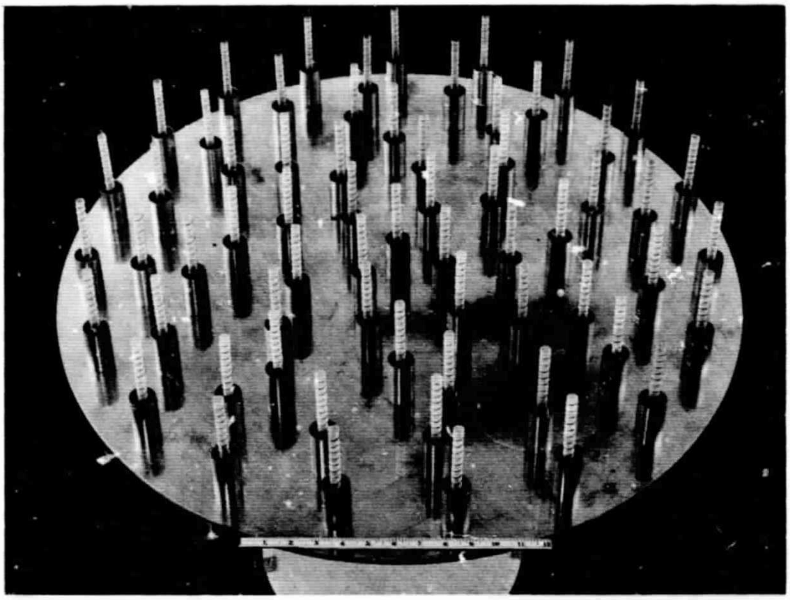

Figure 25. Test model of receiving array (HAC Photo R117465).

Design objectives for the antennas were the achievement of a minimum of 30-db gain over a region subtended by a cone with a half-angle of 15 degrees. The actual measured gain of the receiving array was 30.2 db at the edge of coverage.

3.2.1 Array Design

During the early stages of system design of the engineering model, it was determined that 64 antenna elements would be required to meet the design goals of 30-db minimum gain and a 30-degree coverage angle. This number was determined by assuming that the element pattern was essentially that of a uniformly illuminated segment of the array and to require the directivity of the element to be such that the 3-db point of the element factor falls at ±15 degrees. The element factor was assumed to be of the form

$$\frac{\sin \frac{KL}{2} \sin \theta}{\frac{KL}{2} \sin \theta}$$

where K is the free space propagation constant, L is the edge length of the element area, and θ is the angle off broadside of the principal plane. If the element factor is designed to be down 3 db from its maximum value at $\theta = \theta_o$ θ 15 degrees, then $L/\lambda = 1.714$ which leads to an area gain for an element of

$$g_a = 4\pi\left(\frac{L}{\lambda}\right)^2 = 36.9 \tag{3-2}$$

To account for losses due to spacing, mutual coupling, and other factors, it was assumed that the actual element gain would be 1 db less; that is, that $g_a = 29.2$ at broadside and 1/2 this value at $\theta = 15$ degrees. It was approximated that the minimum element gain over the coverage region would be 14.6 or, in decibels, 11.6 db. For this type of array, with each element connected to an independent generator or load, the total gain, G_A, in the beam-pointing direction is N times the effective gain, g_e, of a typical element. The gain g_e is measured in the presence of all other elements terminated in matched loads and the number of elements, N, is assumed to be sufficiently large so that most elements see similar environments. To determine the number of elements required, the formula

$$N = \frac{G_A}{g_e} = \frac{1000}{14.6} = 68 \tag{3-3}$$

was used. Although the number of elements required to achieve the 30-db minimum was 68, 64 was selected instead for the array design. The choice was based on the nearness of 68 to the binary number 64 and on the greater ease of development of power dividers and summers whose number of inputs or outputs, respectively, is 2^N where N is a positive integer. The predicted gain of 29.8 was achieved at the edges of coverage.

After the number of elements to be used for the antenna array had been determined, the next step in the array design was the selection of an array configuration. The goal was to achieve the maximum-minimum array gain (gain at 15 degrees) with a fixed number of elements (64) and to obtain array patterns that were indicative of a good array design. To achieve the required gain for individual elements, it was necessary for the separation between adjacent elements to be on the order of two wavelengths. If a uniform arrangement of elements were used, then, as the beam was scanned to maximum scan angles, grating lobes would become present very near the cone of coverage of the antenna. Alternatively, if a nonuniform and, more importantly, non-periodic arrangement of elements were used, the occurrence of grating lobes would be minimized. Because of the proximity of the grating lobes to the coverage region, suppression of these lobes by the element pattern would be small. Therefore, a quasi-random arrangement of elements was selected.

To determine the position of quasi-randomly positioned elements, elements were arranged on approximately equally spaced concentric rings. These rings were then rotated with respect to each other until the elements were positioned to produce the desired computed antenna patterns. The position of the elements is listed below in terms of polar coordinates where r_k is the radius of the k^{th} ring of elements, N_k is the number of elements in the k^{th} ring, and φ_i is the polar angular position of the ℓ^{th} element in the k^{th} ring. For this arrangement of elements, the average separation of elements is approximately 2.5 wavelengths.

$r_1 = 0,\ n_1 = 1$

$r_2 = 1.75\ \lambda,\ n_2 = 4,\ \varphi_{21}$ thru φ_{24} = 0, 90°, 180°, 270°

$r_3 = 3.5\ \lambda,\ n_3 = 8,\ \varphi_{31}$ thru φ_{38} = 22°, 67°, 112°, 157°, 202°, 247°, 292°, 337°

$r_4 = 5.0\ \lambda,\ n_4 = 8,\ \varphi_{41}$ thru φ_{48} = 37°, 82°, 127°, 172°, 217°, 262°, 307°, 352°

$r_5 = 6.3\ \lambda,\ n_5 = 3,\ \varphi_{51}$ thru φ_{58} = 4°, 49°, 94°, 139°, 184°, 229°, 274°, 319°

$r_6 = 7.8\ \lambda,\ n_6 = 16,\ \varphi_{61}$ thru φ_{616} = 21°, 43.5°, 66°, 89°, 111°, 133.5°, 156°, 178°, 201°, 223.5°, 246°, 268.5°, 291°, 313.5°, 336°, 358.5°

$r_7 = 9.5\ \lambda,\ n_7 = 19,\ \varphi_{71}$ thru φ_{719} = 2°, 21°, 40°, 59°, 78°, 97°, 116°, 135°, 154°, 173°, 192°, 211°, 230°, 249°, 268°, 287°, 306°, 325°, 344°

3.2.2 Antenna Element Design

A radiating element was required that would have good directivity, reasonably low sidelobes, good efficiency at the receiving and transmitting frequencies, circular polarization, and lightweight. Of the various types of acceptable radiators, the helix was the most suitable.

The goal was the design and development of a helical element that would satisfy the requirement for an 11.6-db gain 15 degrees off-axis. In addition, there were two physical constraints imposed on the design: (1) the element had to be attached directly to its associated microwave filter which was located directly behind a 1-inch honeycomb ground plane with the connector protruding into a hole through the ground plane, and (2) provisions had to be made for rotating the element or for providing a means of adjusting the relative phase of the elements after they were installed in the ground plane.

A computer was used to optimize the gain, number of turns, spacing, and diameter of the element. The computed pattern was close to the design goal; it had a 36-degree half-power beamwidth and 12-db sidelobes. This pattern indicated that the basic element would need only slight modification to fulfill the electrical requirements. The computer design was used as a first approximation for the construction of several hollow dielectric rods, slightly grooved with the desired pitch angle and spacing. A 12-turn, 14-degree helix was wound in the grooves of each rod and secured at both ends.

A test fixture consisting of a ground plane and supporting hardware was used to hold the elements while they were being-tested. The fixture made possible the interchangeability of any part during the empirical optimization of the element.

In addition to the basic helix, a cylindrical cup was fabricated that could be slip-fit over the support of the helix and moved axially to change its depth. These cups have a beam-shaping effect and control the beamwidth, gain, and axial ratio of the elment.

The transformer consists of a three-step coaxial line with impedance values of 50, 75, and 90 ohms. Final matching was accomplished by adjustment of the first quarter turn at the base of the helix.

To satisfy the physical requirements of a given penetration into the ground plane and phase adjustment by rotation, a circularly symmetric structure was used that contained the coaxial transformer and was terminated in an OSM connector. Loosening the two locking screws inside the cup allowed a full 360-degree rotation with a corresponding 360 degree phase shift. A full assembly drawing of the helical radiator is shown in Figure 26.

Each element has essentially two ground planes. One is at the inside base of the cup, and the other is the system ground plane and the supporting structure for all the elements.

The final model of the 7.3 GHz transmitting element produced a rather flat topped beam with 11.8 db gain at the ±15-degree points and an axial ratio of 0.5 db.

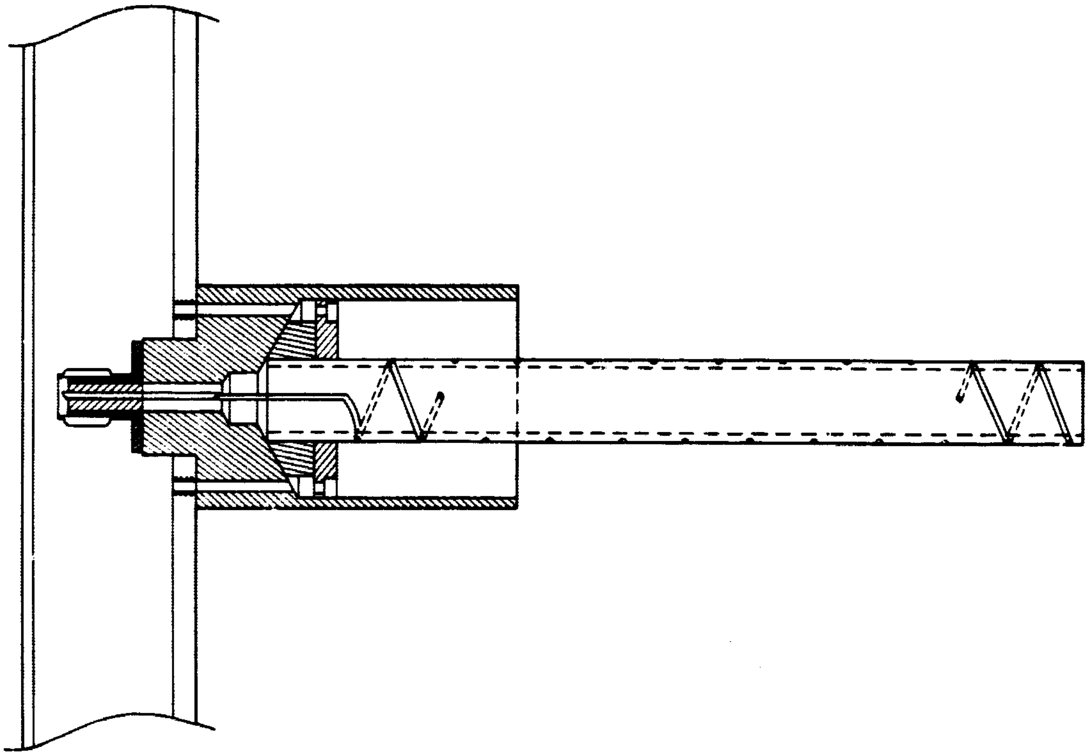

Figure 26. Helical radiator assembly drawing.

An array of 13 elements was built and tested. After satisfactory results were obtained, these elements were used as the first three central rings of the final 64-element array. Measured patterns were in excellent agreement with computer generated patterns using an approximate element expression.

Two 64-element arrays were constructed using this design, one array was at 7.3 GHz ±125 MHz for the transmitter and one was scaled to 8.0 GHz ±125 MHz for the receiver.

3.2.3 Measured Array Patterns

The 8.0-GHz elements were arrayed as shown in the front-end view in Figure 18 and connected to one of the 64-way power dividers to provide a feed structure. These elements were phased to produce a beam, and patterns were taken for several beam-pointing directions. The element pattern with the element in the array and the array patterns for three different beam positions are presented in Figure 27. The element pattern (Figure 27a) shows a broadside gain of 13.9 db with a 3-db beamwidth of 27 degrees. The axial ratio for the elements at broadside was better than 1.0 db. Figure 27b shows an array pattern taken through the $\varphi = 30$ degree plane with the array phased to point the beam to broadside. For this situation, the measured gain was 31.9 db and the measured axial ratio was 0.8 db. As can be seen from the figure, the sidelobe level was more than 18 db below the level of the main beam. Figures 27c and 27d are the array patterns for the beams positioned at $\theta = 15$ degrees, $\varphi = 0$ degrees and $\theta = 15$ degrees, $\varphi = 120$ degrees, respectively. It can be seen from these patterns that no significant grating lobes occurred when the beam was scanned off broadside by 15 degrees, even though the average spacing between adjacent elements was about 2-1/4 wavelengths. This result stemmed from the quasi-random arrangement of elements.

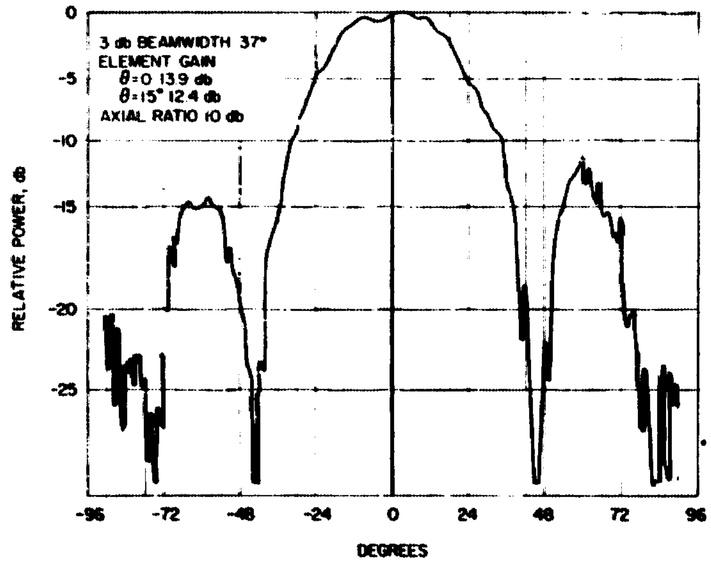

a. Element pattern with element in array

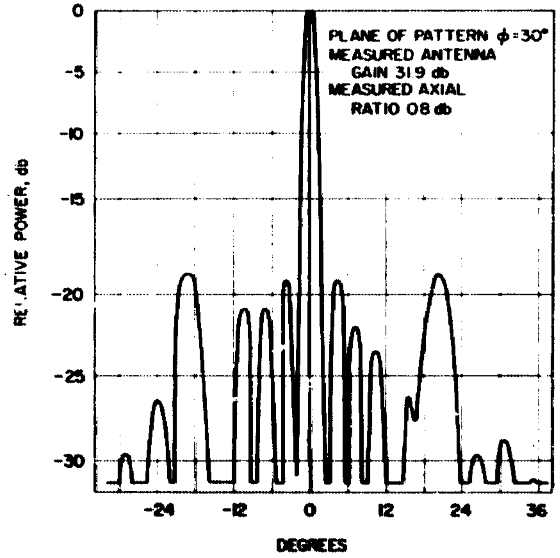

b. Array pattern for beam positioned at $\theta = 150°$, $\varphi = 30°$

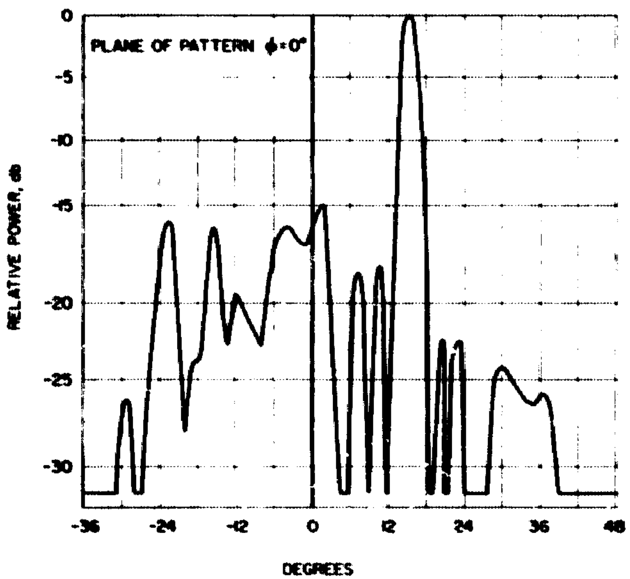

c. Array pattern for beam positioned at $\theta = 15°$, $\varphi = 30°$

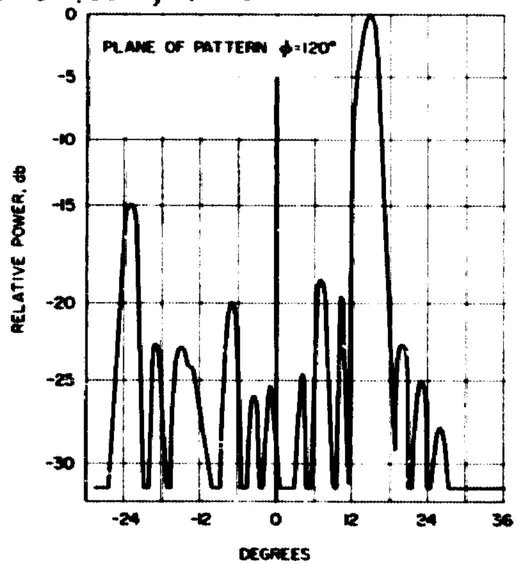

d. Array pattern for beam positioned at $\theta = 15°$, $\varphi = 120°$

Figure 27. Measured patterns of the 8.0-GHz receiving array.

3.3 GAIN AND PHASE ERRORS

Because of errors in phase and amplitude for each of the 64 elements, the average antenna gain will be reduced, and random deviations can be expected. The first step in analyzing such an effect is to calculate the statistics of antenna gain assuming independent phase and amplitude errors at each element. (The independent amplitude error assumption is poor because of the usual definition of antenna gain. However, the difference will be discussed later.) For this model the gain will be defined by the ratio of the power density at broadside in the actual array to the power density at broadside in the error-free array.

From a derivation stemming from probability theory (Howard, 1967), the average power gain of an error-prone antenna can be found to be

$$\bar{G} = \frac{\bar{P}(\theta_o, \varphi_o)}{{}_oP(\theta_o, \varphi_o)} = e^{-\sigma_\delta^2} \left[1 + \frac{\left(\sigma_\delta^2 + \sigma_\epsilon^2\right) \sum_{i=-N}^{N} \left({}_of_i^2\right)}{\left(\sum_{i=N}^{N} {}_of_i\right)^2} \right] \tag{3-4}$$

where

$\bar{P}(\theta_o, \varphi_o)$ = expected power density at broadside

${}_oP(\theta_o, \varphi_o)$ = the error-free power density at broadside

σ_δ = the rms phase error for the signals at the elements

σ_ϵ = the rms amplitude error for the signals at the elements

N = the number of elements

f_i = the excitation coefficient of the i^{th} element

For a 64-element uniformly illuminated array, there results

$$\bar{G} \approx 1 - \sigma_\delta^2$$

$$\sigma_G \approx \frac{\left(256\,\sigma_\epsilon^2 + \sigma_\delta^4\right)^{1/2}}{64} \tag{3-5}$$

where σ_G is the rms error in gain. It can be seen that, unless $\sigma_\epsilon^2 \ll \sigma_\delta^4$,

$$\sigma_G \approx \frac{1}{4}\,\sigma_\epsilon \tag{3-6}$$

The probability distribution of the random gain variability may be approximated by a χ^2 distribution. However for a high number degrees of freedom, the χ^2 distribution approaches a normal distribution. And, at any rate, the normal distribution percentage points will yield the more conservative answers for the gain statistics.

The gain statistics are described by

$$\text{Prob}\left[\text{Gain} > \bar{G} - n\,\sigma_G\right] = P_n \tag{3-7}$$

For the normal distribution,

$P_{1.0}$ = 84.1 percent

$P_{2.0}$ = 97.7 percent

$P_{2.3}$ = 99.0 percent

$P_{2.6}$ = 99.5 percent

where the subscript indicates the multiplier for the standard deviation.

For determination of the gain and phase tolerances to be imposed on the electronics for this system, it was desirable to have a gain degradation as small as was reasonable with a high confidence level. The gain degradation that was allowed for the system was less than 1/2 db with a 99-percent confidence.

The 99-percent gain level is given by

$$1 = \sigma_\delta^2 - 2.3 \left(\frac{\sigma_\epsilon}{4}\right) \tag{3-8}$$

For a total gain degradation less than 1/2 db from the no-error gain (with 99-percent confidence),

$$\frac{1}{2}\text{ db} > 10 \log_{10} \left(1 - \sigma_\delta^2 - 0.575\ \sigma_\epsilon\right) \tag{3-9}$$

is required. This requirement means that any of the following combinations of rms errors would be permissible;

$$\begin{aligned}
&\sigma_\delta < 5^\circ, \quad \sigma_\epsilon = 0.192\ (1.7\text{ db}) \\
&\sigma_\delta = 10^\circ, \quad \sigma_\epsilon = 0.139\ (1.2\text{ db}) \\
&\sigma_\delta = 15^\circ, \quad \sigma_\epsilon = 0.0695\ (0.6\text{ db}) \\
&\sigma_\delta = 19^\circ, \quad \sigma_\epsilon = 0
\end{aligned} \tag{3-10}$$

It is assumed that these results are the main beam peak levels for independent errors that directly describe antenna gain. However, as used here, true antenna gain must be defined in terms of a constant input power to the antenna. In terms of this definition, the main beam peak levels will describe the antenna gain when errors are assumed that are correlated so that total power input is constant. This special type of correlation restricts the antenna gain variations so that larger errors than those quoted previously are permissible. In view of these considerations, the stated phase and amplitude error specification for the system electronics seemed conservative.

The critical design problem was to insure that reasonable phase and gain tracking was maintained between channels, starting from the receiving element and going through the system to the corresponding transmitting element. The critical area was to insure that the tracking was maintained over each 125-MHz channel. Thus every component, whether passive or active, had to track over this band. The overall budget shown in Equation (3-10) was divided on an rms basis among all components. The allocation for each component was based on practical realizability. Only the high-level mixers exceeded their budget and only at the edges of the 125-MHz band. Before assembly, every component was tested individually for the design specifications. After assembly the receiving portion and the transmitting portions were tested separately as discussed below.

3.4 ELECTRICAL AND PHYSICAL CHARACTERISTICS OF THE ENGINEERING MODEL

In this section the results of the final system tests are tabulated and discussed. The test results presented here are only those which are related to overall system performance. During development, considerable test data for individual components of the engineering model were obtained that are not included here. The more pertinent of these data have been delivered to NASA Goddard separately from the Final Report.

Included in the final system tests were (1) receiver front-end noise figure, (2) receiving and transmitting array tracking patterns, (3) two-way tracking patterns, (4) antenna gain and polarization circularity, (5) television pictures as a function of pilot signal power levels, (6) system power consumption, and (7) system weight.

3.4.1 General Characteristics

The general electrical and physical characteristics of the engineering model are presented in Table 3. Included are the design goals for the engineering model, the measured performance, and the projected characteristics for a flight model of a similar system. The electrical characteristics of the flight model would be similar to those of the engineering model with the exception of effective radiated power (ERP); this characteristic would be raised from 28 dbw to 35 dbw. For the

Parameter	Design Goals for Engineering Model	Measured Performance	Projected Characteristics of Flight Model
Number of elements, each for two arrays	64		64
Number of channels	2		2
R-f bandwidth, each channel	125 MHz		125 MHz
Guard band, between channels	100 MHz		100 MHz
Total cone angle of coverage	30 degrees	30 degrees	30 degrees
Element gain, minimum	11.6 db	12.4 db	11.6 db
Array gain, minimum	29.8 db	30.4 db	29.8 db
Polarization	Circular	Circular axial ratio = 0.8 db	Circular
Average mixer-filter pre-amplifier noise figure	15.2 db (maximum)	14.4 db	7 db
Effective radiated power	28.0 dbw	27.8 dbw	35.0 dbw
Ratio of pilot to modulated signal power when 125-MHz bandwidth is utilized	-10 db	*	-10 db
Power consumption: receiver	32.0 watts excluding local oscillator		21.5 watts including local oscillator
Power consumption: pilot processor	108.7 watts	182.6 watts	108.7 watts
Power consumption: attitude readout	0.9 watt		0.9 watt
Power consumption: total transmitter	201.1 watts excluding local oscillator	87.9 watts** excluding local oscillator	204.5 watts including local oscillator
Prime power (exclusive of power supplies)	342.7 watts	270.5 watts	335.6 watts
Power consumption: power supplies	–	–	73.3 watts
Power consumption: total prime power	–	–	408.9 watts
Total weight		180.0 Kg	79.0 Kg

*Pilot signal ratios much lower than the design values were measured in the television tests (see discussion).

**Power consumption applies to one channel of transmitter. For two-channel operation less than twice this value would be needed.

Table 3. Characteristics of the self-steering transponder.

flight model, the i-f processing modules would be reduced in size and weight, many of the coaxial cables and connectors would be eliminated, and the microwave components would be combined into fewer boxes* that would reduce the weight from 180 kilograms of the engineering model to about 79 kilograms.

3.4.2 Tracking Patterns

The engineering model was designed to form beams in the direction of origin of pilot signals so that, as the position of the pilot signals are changed, the beam-pointing directions should correspondingly change. In other words, the beams of the engineering model automatically track their respective pilot signals. Tracking patterns were taken to measure the changes in the array gain of the receiving array and in the effective radiated power of the transmitting array as a function of beam positions. These patterns are presented in Figure 28.

In Figure 28a, the pattern shows the variation in receiving array gain as a function of scan position for a given elevation angle. This pattern was taken by measuring the signal strength at the summed i-f output as the antenna system was rotated in azimuth relative to the pilot generator. As can be seen, the receiving array gain was relatively constant over the ±15-degree coverage with a decrease of about 2 db in gain at the edges of coverage.

A similar pattern is presented in Figure 28b for the transmitting beam of channel A. This pattern was taken by measuring the effective radiated power at the simulated receiving earth station with a constant transmitted power while the engineering model was rotated in azimuth. Again, it can be seen that the pattern drops about 2 db at ±15 degrees, indicating that the ERP is about 2 db less at the edge of coverage as compared with the figure at broadside. If these patterns are compared with the element pattern of Figure 27a, it can be seen that they are essentially the same except that the tracking patterns have lower

---

*No microminiaturized, integrated, or hybrid circuits are assumed.

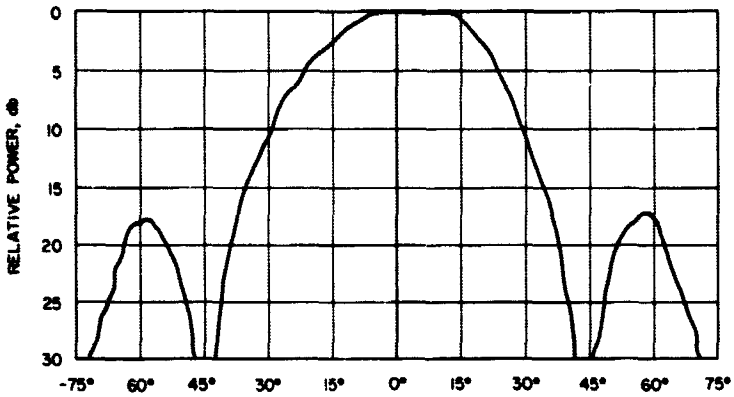

a. receiving pattern

b. transmitting pattern

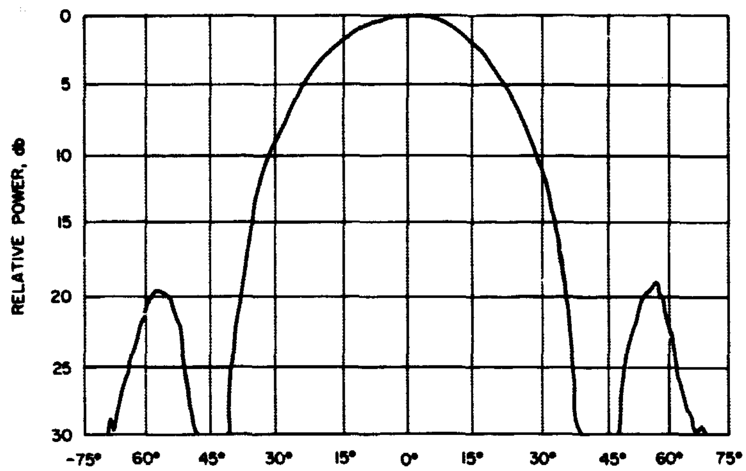

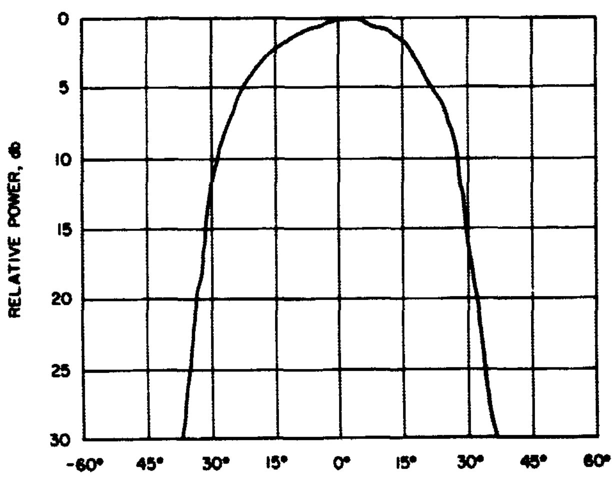

c. two-way pattern

Figure 28. Tracking patterns of the engineering model.

sidelobes. The reason for the apparent lower sidelobes is the fact that the system performance degrades because of the lowered pilot signal levels in the direction of the sidelobes.

The third tracking pattern (Figure 28c) is a composite pattern of the receiving and transmitting beams for Channel A. This pattern was taken by transmitting a pilot and information signal from a simulated earth transmitting station while measuring the power received by a simulated earth receiving station. The two-way patterns would be the superposition of the receiving and transmitting patterns except for the fact that the transmitter is operating in a saturated condition and is thus nonlinear.

3.4.3 The Relaying of Color Television Signals

A test was made to determine the fidelity with which the engineering model could relay color television. Such a test could be used to determine threshold levels and, in addition, to make a meaningful assessment of intermodulation distortion because color television is noticeably degraded by such distortion.

To perform the color television tests, two identical television receivers were used. The first receiver was connected to an antenna to receive locally broadcast signals. The front end, the i-f stages, and the video detector of the first receiver were used. This receiver provided the video signals for both receivers, one in the normal manner through the set and the other by way of an FM modulator, the engineering model acting as a microwave repeater, and an FM demodulator. As shown in the block diagram in Figure 29, the video signal at the simulated earth transmitting station was coupled from TV-1 and used to frequency-modulate a 70-MHz voltage-controlled oscillator with a frequency deviation of 25 MHz. This i-f signal was amplified and then upconverted to 7.925 GHz. The appropriate sideband was selected by a bandpass filter and fed together with a pilot signal to a horn. The resulting signal was sent to the satellite repeater. The signal was then relayed down to a simulated receiving earth station where it was down-converted to 70 MHz and then demodulated by a discriminator to produce the video signal to be fed to TV-2.

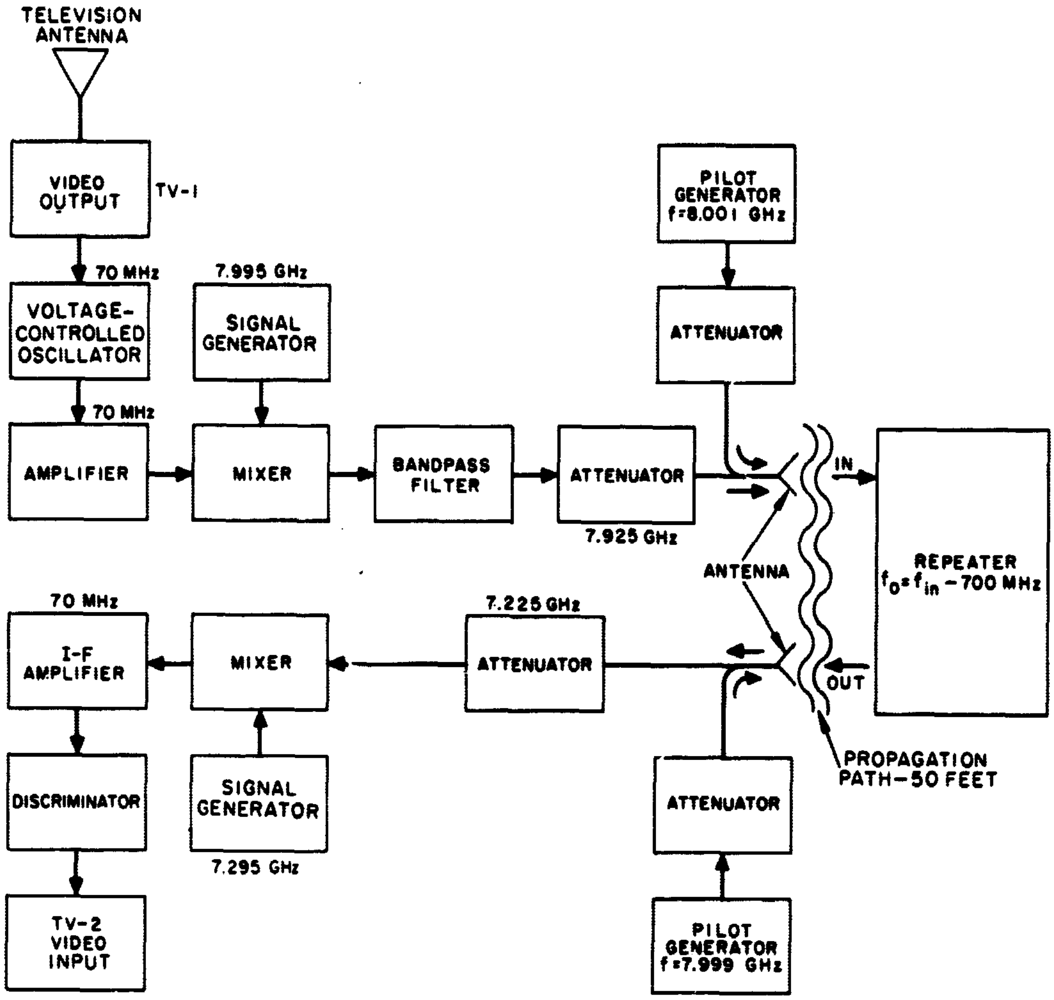

Figure 29. Color television test instrumentation block diagram.

Tests were made by visual comparison of the quality of the pictures displayed by the two television receivers for various conditions of pilot signal levels, information signal levels, and orientation of the transponder with respect to the earth stations. For nominal signal levels, -115 dbw for the information signals and -125 dbw for the pilot signals, the quality of the relayed signal was excellent with no discernible difference in the quality of the pictures displayed by the two receivers.

To record the results of the television tests, photographs were taken of the pictures displayed by the two receivers. Presented in

Figure 30 is a set of photographs that show the variation in quality of the relayed picture as the pilot signals are reduced in level. Both pilot signals were reduced simultaneously in 5-db steps from the nominal level to 20 db below this level while the information signal was held at the nominal level. As can be seen from these pictures, no significant degradation in picture quality was observed until the levels of the pilot signals were reduced 15 db below the nominal levels. At that level, the ratio of pilot signal power to information signal was 25 db.

Presented in Figure 31 is a set of pictures taken for the nominal pilot and information signals levels but with the transponder rotated in azimuth. As can be seen, there was no noticeable degradation of picture quality as the system was rotated to the edge of coverage, ±15 degrees. However, as the system was rotated beyond the coverage region to ±30 degrees, noticeable degradation did occur. This latter situation corresponds to a decrease of about 10 db in transmitting and receiving antenna gain as determined from the tracking pattern. Thus, the degradation in picture quality for the ±30-degree angles corresponds to simultaneously reducing the information signal and pilot signals by 10 db in power. The reduction in ERP from the transponder was not a contributing factor in the degradation of these pictures because the simulated earth receiver was operating well above its threshold.

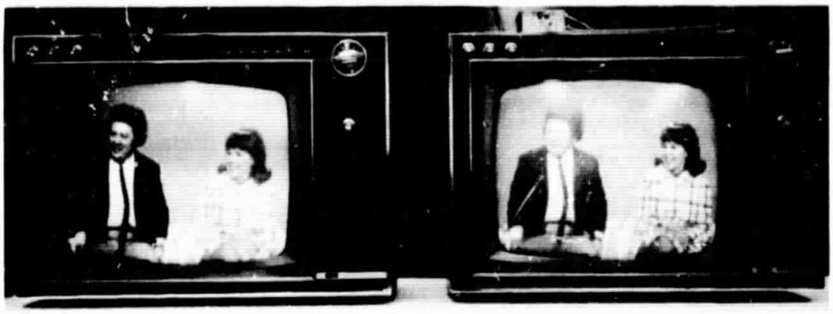

All signals at nominal levels

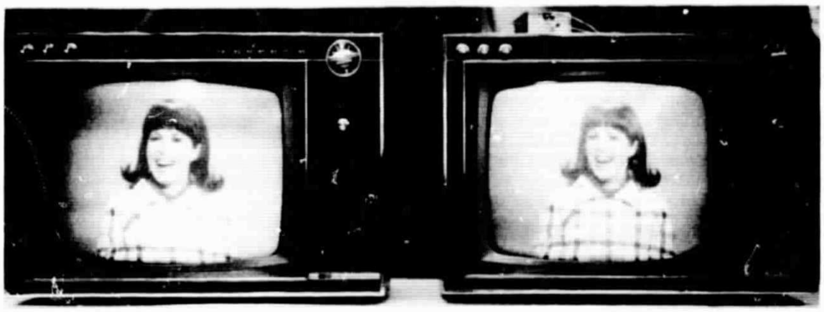

Nominal information, -5 db on pilot signals

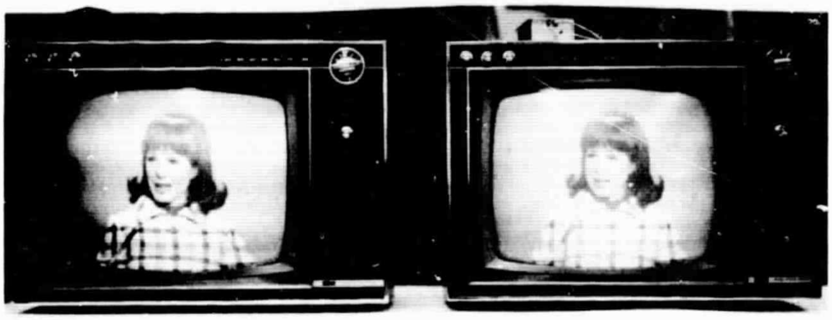

Nominal information, -10 db on pilot signals

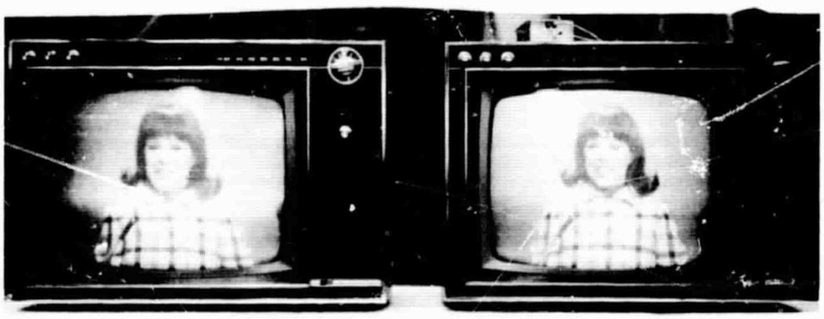

Nominal information, -15 db on pilot signals

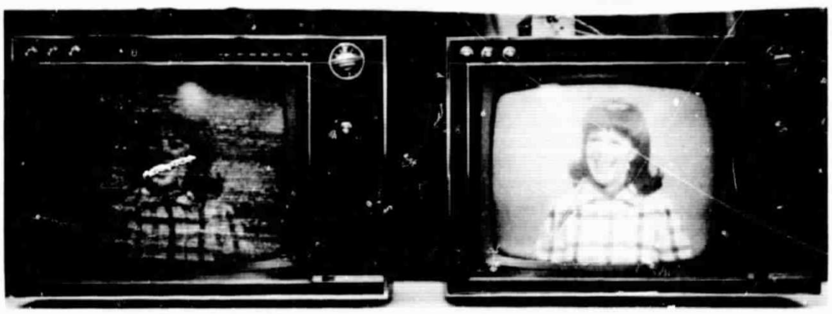

Nominal information, -20 db on pilot signals

Figure 30. Relayed television (left) and normal television (right) pictures for various pilot signal levels.

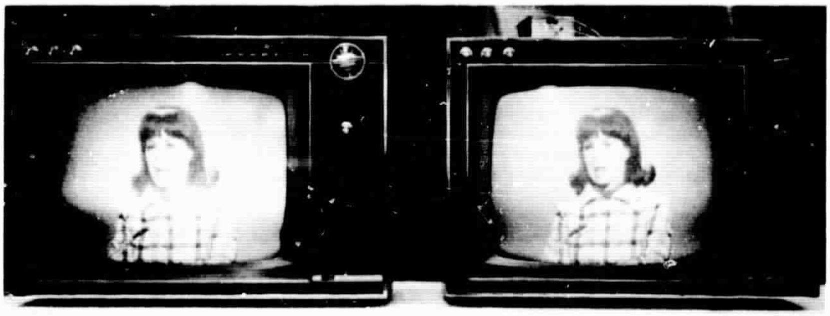

-15 degrees azimuth

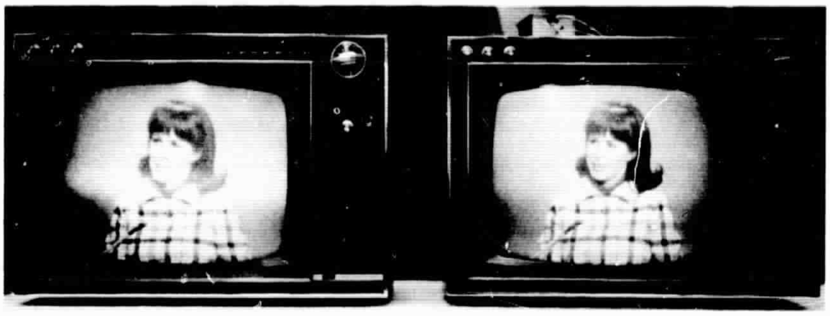

+15 degrees azimuth

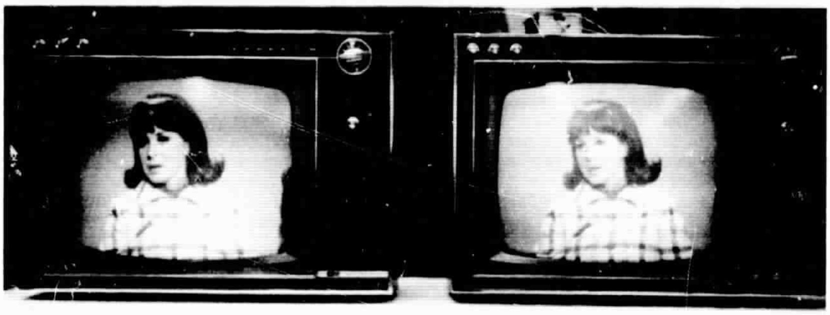

-30 degrees azimuth

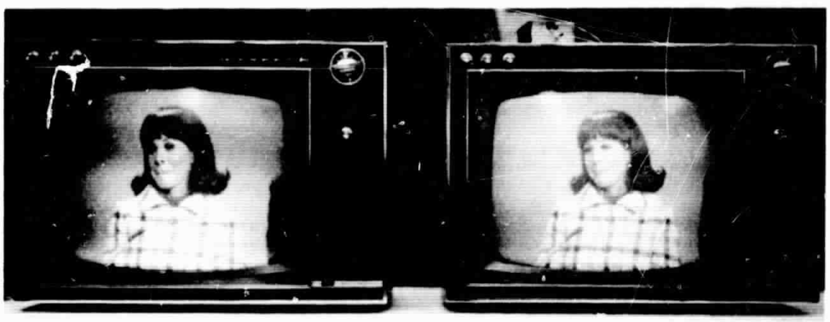

+30 degrees azimuth

Figure 31. Relayed television (left) and normal television (right) pictures for various scan angles.

PRECEDING PAGE BLANK NOT FILMED.

4.0 SELF-STEERING ANTENNA SYSTEM FOR DATA RELAY SATELLITE SYSTEM

Probably the most versatile and efficient satellite transponder is one that can accept multiple, independent signals from a set of arbitrary directions and redirect these signals to another set of arbitrary directions with each signal received and transmitted on an independent high-gain antenna beam. If a high-gain capability is required for each signal, it is most economical to use a common antenna that can form a large number of beams. Since beam direction and satellite orientation are arbitrary, it is necessary to steer these beams. A self-steering antenna appears to be the only practical solution to this problem because it automatically forms beams, requiring only the information obtained from the orientation of the constant phase plane of the incident wave relative to the antenna.

4.1 CHARACTERISTICS OF RELAY REPEATER

A self-steering antenna system that forms multiple, independent beams is very applicable to a communications link such as the Data Relay Satellite System (DRSS). For the antenna system described here, the DRSS is assumed to consist of two low orbiting users that communicate with a ground station(s) via a microwave repeater(s) located at synchronous altitude. This section is concerned with the repeater for the relay station. The system is to accept signals from the two low orbiting users on high-gain antenna beams at S-band and then retransmit these signals on a lower gain antenna to a central earth station at X-band. The system is also to receive signals that have been sent up at X-band and retransmit these on high-gain antenna beams to the appropriate user.

Since the antenna beams for both transmission and reception are coincident for each user vehicle, one pilot signal can be used for each pair of beams. This arrangement yields a considerably simplified system over that in which all the antenna beams are independently steered. To further reduce the system complexity, many of the components of the system are common to all the channels. However, the common use imposes a severe linearity requirement on the components (especially on the up-converters and the r-f amplifiers in the transmitting section) if intermodulation distortion is to be kept at a low level. Fairly high intermodulation levels can be tolerated, though, since the DRSS system is to serve as an emergency voice communications system. For this system with two-channel operation, the r-f amplifiers will be operated very near saturation to enable efficient operation and should yield intermodulation distortion levels of -10 db or less depending on the saturation characteristics of the transmitter.

Before a detailed discussion of the specific system configuration is given, the general characteristics of the DRSS will be established (Table 4). A minimum reasonable antenna gain of 0 db and transmitting power of 20-watts were assumed for the low-altitude users. The noise figure of the users' receivers, exclusive of diplexer and cable loss, was assumed to be 6 db. To determine the number of elements required in the repeater, both the up-link and the down-link must be considered. From the familiar path loss equation

$$\text{path loss (db)} = 20 \log_{10} \left(\frac{4 \pi R}{\lambda}\right) \qquad (4\text{-}1)$$

the path loss for the S-band frequencies is found to be equal to 191 db. The isotropic power level at the repeater is 13 dbw minus the path loss, or -178 dbw. Since the signal level required at inputs of the repeater receiver (see Table 4) is -147 db, the receiving array must have a minimum gain of 31 db. Based on a cone of coverage with a total angle of 24 degrees, a minimum element gain of 13 db is obtained. The number of elements required for the receiving array is then obtained by noting that

$$G = g_e N \qquad (4\text{-}2)$$

Up-Link (2.3 GHz)		Down-Link (2.1 GHz)	
User's transmitting power	20 watts or 13 dbw	Audio signal-to-noise ratio	13 db
User's antenna gain (including losses)	0 db minimum	Carrier-to-noise ratio required	10 db minimum
User's effective radiated power	13 dbw	R-f bandwidth	10 KHz
Path loss (25,900 miles)	191 db	Noise figure of user receiver	6 db
Power level at satellite (isotropic)	-178 dbw	Equivalent noise level	-158 dbw
Noise figure of repeater receiver	7 db	Array gain of user (including losses)	0 db minimum
Equivalent noise level (10 kHz r-f bandwidth)	-157 dbw	Power level required at user (isotropic)	-148 dbw
Audio signal-to-noise ratio	13 db	Path loss	191 db
Carrier-to-noise ratio required	10 db	Effective radiated power (per channel) required from repeater	43 dbw
Signal level required at input of receiver	-147 dbw	Gain fall-off due to beam-pointing error	2 db
Gain required of array	31 db minimum	Minimum gain per element	13 db
Coverage angle	24 degrees	Number of elements	100 (20 db)
Gain per element	13 db	Array gain (Minimum, including fall-off due to beam-pointing error)	31 db
Array gain	33 db minimum for 100 elements	Power into array (for two channels)	15 dbw
		Power per module (for two channels)	-5 dbw

Table 4. Data Relay Satellite System general characteristics.

where g_e is the gain of a single element when measured in the presence of its neighbors and N is the number of elements. From Equation (4-2) it follows that the minimum number of elements required is 64. For the transmitting portion of the system, the number of elements is obtained by using the equation for effective radiated power (ERP):

$$ERP = g_e N^2 \cdot p_e \qquad (4\text{-}3)$$

where p_e is the power for each element. Since the isotropic signal level required at the user satellite is -148 dbw (see Table 4) and the path loss is again 191 db, the ERP required from the synchronous satellite is 43 dbw for each channel. The ERP for two channels would be 46 dbw. Since a fall-off of about 3 db will occur because of a beam-pointing error, g_e will be taken equal to 10 db.

The remaining quantity to specify is the power per module (p_e) which is based on the availability of solid-state r-f amplifiers. At present, 500 milliwatts, including losses, is a reasonable power level for p_e. Using these values in Equation (4-3), the value for N is found to be equal to 90 elements. It is seen that for this system the critical link is the down-link, but only because the output power per module is restricted to 500 milliwatts. A real upper bound does not exist on power because r-f amplifiers can be connected in parallel or, if necessary, a traveling-wave-tube amplifier can be used for each module that can deliver up to several hundred watts if necessary. For the receiving array, a lower bound on the number of elements does exist, however, for fixed parameters on the user vehicle. The number of modules can be decreased only by decreasing the noise figure of the receiver which has a theoretical limit of 0 db and practically cannot be reduced significantly from the values given in Table 4. Therefore, the critical parameter for the synchronous satellite repeater system is the array gain. For the parameters given in Table 4 for the user vehicle, it was shown above that 64 elements would be required to obtain the required gain for the synchronous satellite. This number of elements is about the minimum number that could be used for the system unless the user system had increased array gain and transmitting power. For the system described in this section, 100 elements are assumed, a number that allows some margin for the receiver and brings the power level for each module down to a practical level for r-f amplifiers.

4.2 DOPPLER FREQUENCY CONSIDERATIONS

Because the repeater and the user vehicles are in different orbits, there is relative velocity between the vehicles that gives rise to a doppler frequency. If the repeater and user are orbiting in the same plane, which is the situation for maximum doppler frequencies, then the variation in doppler is sinusoidal to a first-order approximation. If a 200-mile orbit is assumed for the low orbiting user, then the period of an orbit is about 90 minutes which will cause a peak doppler frequency of about 54 kHz. This peak will occur when the relative velocity vector is in the direction from the user to the repeater and is equal to zero when the relative velocity vector is perpendicular to this direction. For this situation expressions can easily be obtained for doppler and rate of change of doppler:

$$f_d = 54 \cos \left(\frac{2\pi \times 10^{-3}}{5.4} t \right) \text{ kHz} \tag{4-4}$$

and

$$\frac{d(f_d)}{dt} = -62.8 \sin \left(\frac{2\pi \times 10^{-3}}{5.4} t \right) \text{ Hz/sec} \tag{4-5}$$

where f_d is the doppler frequency. To account for this doppler frequency, the repeater must have a frequency tracking loop with a loop bandwidth sufficient to track rates of change of doppler as given by Equation (4-5). A frequency search loop will also be necessary for initial acquisition of the signal.

4.3 OPERATION OF SELF-STEERING REPEATER

A self-steering, multiple-beam, microwave repeater that will satisfy the requirements of the Data Relay Satellite System is shown schematically in Figure 32. This system is designed to relay communications between two low orbiting users and a fixed ground station, all of which are located anywhere within the region of earth visible from the repeater. Only that part of the repeater that does the beam steering for the users is shown in the schematic. The link from the repeater to the fixed earth terminal is not discussed. The repeater is designed for two-channel operation but only one channel is discussed below.

In operation, a modulated signal is received by the k^{th} element at the repeater. The signal has the form

$$[1 + f(t)] \cos [(\omega_s + \omega_d) t + \alpha_k]$$

where

ω_s = the transmitted carrier angular frequency

ω_d = the doppler angular frequency

$f(t)$ = the modulating signal

α_k = the phase angle of the signal with respect to an arbitrary reference.

An amplitude-modulated signal is assumed to illustrate the system operation. Other, more complicated modulating techniques may be employed as long as one discrete spectral line exists from which the phasing information can be obtained. For some situations, it may be necessary to send a pilot signal along with the modulated signal to the relay satellite. For the Data Relay Satellite System, if a pilot signal is not used, then when a low orbiting vehicle wishes to receive from the repeater while it is not transmitting intelligence to it, the orbiting vehicle must send up a c-w carrier signal.

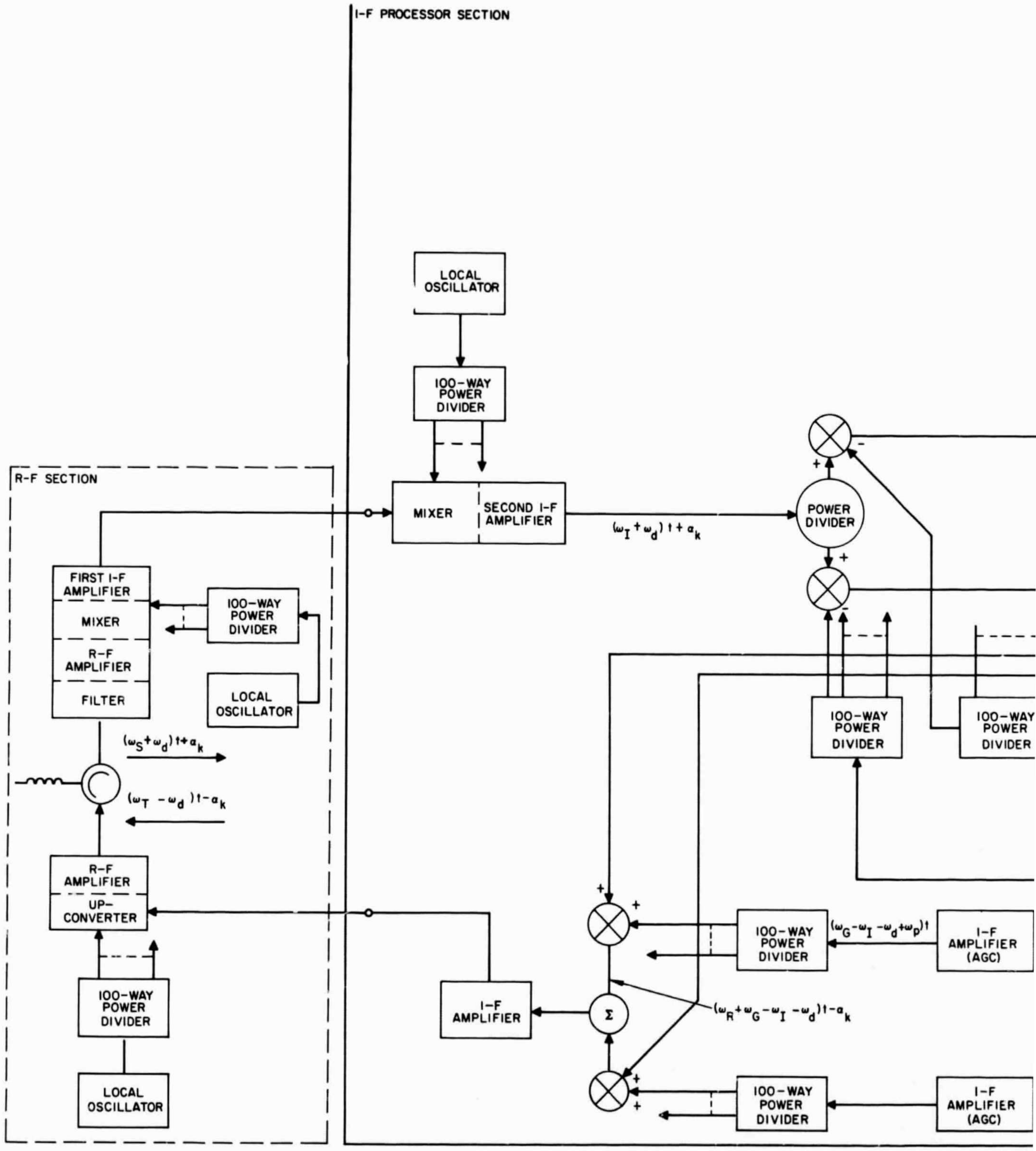

FOLDOUT FRAME 1

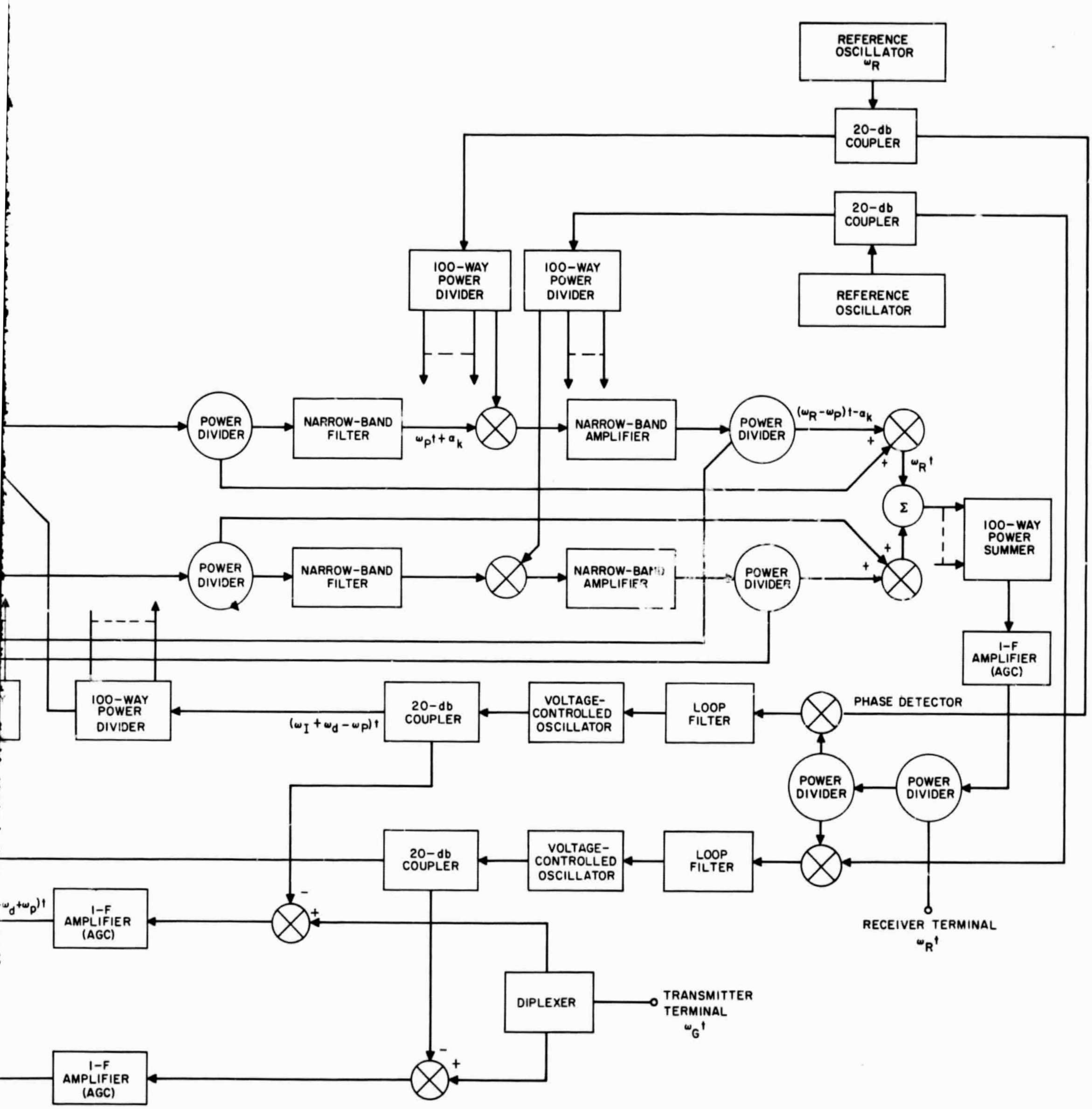

Figure 32. Self-steering repeater for Data Relay Satellite System.

FOLDOUT FRAME 2

PRECEDING PAGE BLANK NOT FILMED.

The signal received by the element is passed to the receiving front-end by a diplexer that consists of a circulator and a filter. The receiving front-end amplifies at r-f, down-converts to a first intermediate frequency and amplifies, further down-converts to a second i-f and further amplifies, so that at the output of the second i-f amplifier, the signal has the form

$$[1 + f(t)] \cos (\omega_I + \omega_d) t + \alpha_k] \tag{4-6}$$

where ω_I = intermediate frequency and, because of the amplification, the signal-to-noise ratio has been established.

Following the second i-f amplifier, the signal is fed to two mixers, one for each channel of the system. Each channel of the system has a voltage-controlled oscillator (VCO) which serves as the local oscillator for these mixers. The frequency range of the VCO's is limited so that the signal at the output of the second i-f amplifier will only pass through the appropriate channel of the system. Since the frequency of the received signal can be anywhere within a 108-kHz band, the doppler frequencies necessitate the incorporation of a frequency search mode into the system. The circuitry for this mode is not shown on the block diagram of Figure 32 but would consist of a sweep generator that would apply a voltage to the control input of the VCO's and an "ON-OFF" gate operated by the received signal at the receiver terminal. For this discussion, it is assumed that frequency locking has already occurred; therefore, for the channel in question, the VCO output voltage is of the form

$$\cos (\omega_I + \omega_d - \omega_p) t \tag{4-7}$$

This voltage is mixed with that represented by Expression (4-6) and the lower sideband is retained to produce at the output of the mixer a voltage of the form

$$[1 + f(t)] \cos (\omega_p t + \alpha_k)] \tag{4-8}$$

Next, the signal, now in the form of Expression (4-8), is fed through a two-way power divider to a narrow-band filter and to another mixer. The path through the narrow-band filter will be considered first.

The voltage represented by Expression (4-8) is an amplitude-modulated signal that is composed of a carrier signal with symmetric sidebands. When this signal is passed through the narrow-band filter, an improvement in signal-to-noise occurs and the sidebands are removed, so that at the output of the narrow-band filter the signal has the form

$$\cos(\omega_p t + \alpha_k) \tag{4-9}$$

This signal is then mixed with another signal obtained from a reference oscillator at angular frequency ω_R and is passed through a narrow-band limiting amplifier to produce a voltage of the form

$$\cos[(\omega_R - \omega_p)t - \alpha_k] \tag{4-10}$$

This voltage is fed via a two-way power divider to a mixer in the transmitting section and a mixer in the receiving section. A voltage of the form of Expression (4-8) is also fed to the mixer in the receiving section so that the output voltage of this mixer is of the form

$$[1 + f(t)]\cos\omega_R t + [1 + f(t)]\cos[2\omega_R - \omega_p)t + \alpha_k] \tag{4-11}$$

The first term of the voltage represented by Expression (4-11) is independent of the phase, α_k, to which it is associated, so the terms of the voltages for all the elements are summed to obtain the gain of the receiving array. The second term of Expression (4-11) is partially suppressed by the 100-input summer, as compared with the first term, and is further removed by the filtering action of the i-f amplifier, so that at the output of the AGC i-f amplifier, the voltage is of the form

$$[1 + f(t)]\cos\omega_R t \tag{4-12}$$

This voltage is then fed to the terminal of the receiver. The voltage in Equation (4-10) from one of the elements also goes to a phase detector at which point it is compared in phased with the output of a mixer that combines the reference oscillator, ω_R, and another oscillator whose frequency ω_{P0}, is the same as that of the first narrow-band filter. The output of the phase detector is fed through a low-pass filter to provide the control voltage required by the VCO to maintain its output voltage as given by Expression (4-7). This frequency-locked VCO provides a common reference for all elements.

Next, the signal to be transmitted from the repeater will be considered. Again, an amplitude-modulated signal is considered of the form

$$[1 + g(t)] \cos(\omega_G t) \tag{4-13}$$

To eliminate the doppler frequency from the signal received by the user, the doppler frequency must be subtracted from the frequency of the signal to be transmitted from the relay system. The voltage given by Expression (4-13) is mixed with the output voltage of the VCO given by Expression (4-7), and the lower sideband is retained. This procedure yields a voltage of the form

$$[1 + g(t)] \cos[(\omega_G - \omega_I - \omega_d + \omega_p) t] \tag{4-14}$$

Thus the doppler frequency is subtracted. The signal now represented by Expression (4-14) is amplified and distributed to a mixer for each of the elements. In the mixer for the k^{th} element, the voltages represented by Expressions (4-10) and (4-14) are mixed, and the output is summed and fed to an i-f amplifier which retains the upper sideband. At the output of this i-f amplifier a voltage is produced of the form

$$[1 + g(t)] \cos[(\omega_R + \omega_G - \omega_I - \omega_d) t - \alpha_k] \tag{4-15}$$

This voltage is then up-converted to the r-f transmitting frequency and further amplified to produce a voltage to be fed to the k^{th} element of the form

$$[1 + g(t)] \cos(\omega_T - \omega_d) t - \alpha_k] \tag{4-16}$$

4.4 OTHER SYSTEM PARAMETERS

4.4.1 Parameters for Satellite-to-satellite Links

For the system that was discussed in detail in Section 4.1, a voice communication link was taken with an audio signal-to-noise ratio of 13 db. The SNR of 13 db makes the intelligibility of a voice marginal. This ratio yields a practical system in terms of the number of modules required and permits the utilization of solid state r-f amplifiers. The system and several alternative links are outlined in Table 5. The first two systems have identical repeaters; the antenna gain of the user and the r-f bandwidth have been increased in the second system to enhance the audio signal-to-noise ratio. The third system presented utilizes vocoded voice for communications with an r-f bandwidth of 3 kHz. These values result in a reduced antenna gain for the repeater which allows a reduction in the number of elements from 100 to 32. The power per module increases to 1 watt. The choice between traveling-wave tubes (TWT) or solid-state amplifiers for the final r-f amplifiers is difficult; TWT's have been chosen for the table, but it is quite possible that transistorized amplifiers would be a better selection.

The fourth system presented is a video link with an r-f bandwidth of 5 MHz. The larger bandwidth would necessitate an increase in the antenna gain and transmitted power of the user satellite. There is no unique solution for any of these systems. For this system the number of modules was decreased to reduce the overall system weight and to allow the utilization of 4-watt TWT amplifiers with the improved efficiency they would give over that of the 1 or 2 watt TWT's.

The final system presented incorporates 10 channels rather than 2. The effective radiated power for this system is very high which results in a fairly high total prime power requirement.

4.4.2 Element Considerations

For the repeater system described for DRSS application, the transmitting and receiving frequencies are at 2 GHz. If a very high antenna gain is required, which is true for the system outlined, the

User Parameters	Link Parameters	Repeater (2 Channels): Number of Modules	ERP Total (dbw)	Weight per Module (power)	Prime Power per Module (watts)	Total Weight (pounds)	Total Prime Power (watts)
Gain: 0 db ERP[(1)]: 13 dbw Noise figure: 6 db	Audio SNR: 13 db Carrier SNR: 10 db R-f bandwidth: 10 kHz	100	46	2.25	2.9	225	290
Gain: 10 db ERP: 23 dbw Noise figure: 6 db	Audio SNR: 27 db Carrier SNR: 14.5 db R-f bandwidth: 36 kHz	100	46	2.25	2.9	225	290
Gain: 0 db ERP: 13 dbw Noise figure: 6 db	Vocoded Voice Carrier SNR: 9 db R-f bandwidth: 3 kHz	32	40[(2)]	3.6	9.8	115	313
Gain: 27 db ERP: 45 dbw Noise figure: 6 db	Video Carrier SNR: 10 db R-f bandwidth: 5 MHz	32	46[(3)]	3.7	21.4	118	686
		(10 Channels)					
Gain: 0 db ERP: 13 dbw Noise figure: 6 db	Audio SNR: 13 db Carrier SNR: 10 db R-f bandwidth: 10 kHz	100	53[(4)]	4.5	14.5	450	1,450

(1) Effective radiated power
(2) Use 1-watt traveling-wave amplifiers: weight — 14 ounces; efficiency — 15 percent
(3) Use 4-watt traveling-wave amplifiers: weight — 16 ounces; efficiency — 25 percent
(4) Use 2-watt traveling-wave amplifiers: weight — 14 ounces; efficiency — 20 percent

Table 5. Links between orbiting users and the repeater.

array size may become very large. Special attention must be given to a design that is reasonably simple and compact and that can also be unfurled in space. Because of the large wavelengths involved, a flush-mounted element seems to be the most desirable radiator in terms of element weight and ease of mechanizing an unfurling technique.

Preliminary work has been performed on an element and array design (Figure 33) specifically to satisfy the requirements as outlined in Table 5. A doubly-wound equiangular spiral such as is shown in Figure 33a was chosen as the basic radiator; seven of these, arranged in a cluster, form the antenna element for a single r-f module of the system (Figure 33b). The amplitude distribution of the 7-element cluster would be tapered to flatten the element pattern in an attempt to raise the gain at the edge of the coverage. Computed gain figures for the 7-element cluster predict a peak gain of 15.3 db and a gain of 13.2 db at 12 degrees from broadside. Four clusters are arranged in a rhomboid (Figure 33c). The entire array is composed of 100 of the 7-element clusters (Figure 34), an arrangement that minimizes the occurrence of second-order beams. Calculated patterns and gain for the 100-module array indicate a peak gain of 35.3 db at broadside and a gain of about 32.2 db when the beam is scanned off broadside by 12 degrees. The 3-db beamwidth is 2.4 degrees.

To keep the weight of the array and the microwave components as low as possible, stripline techniques must be employed, and many of the components will have to be integrated. One arrangement of the antenna and microwave components of the Data Relay Satellite System repeater is suggested in Figure 35, and details of microelectronic construction techniques being studied for self-steering arrays can be found in Section 5.2.

4.4.3 Weight and Power Consumption

Estimates of weight and power consumption made for the system presented in Figure 32 are listed in Table 6. These estimates were based upon utilization of fairly sophisticated techniques such as micro-circuits, miniature hybrid couplers and mixers in the i-f processing

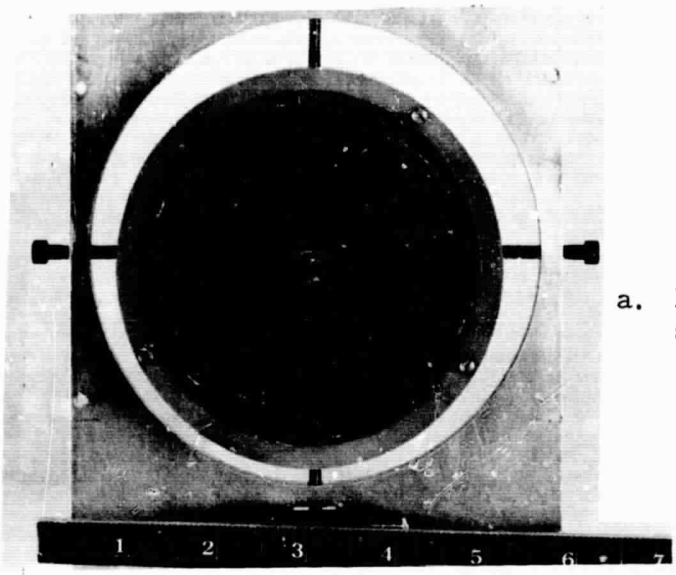

a. Doubly-wound equiangular spiral element

b. 7-element cluster

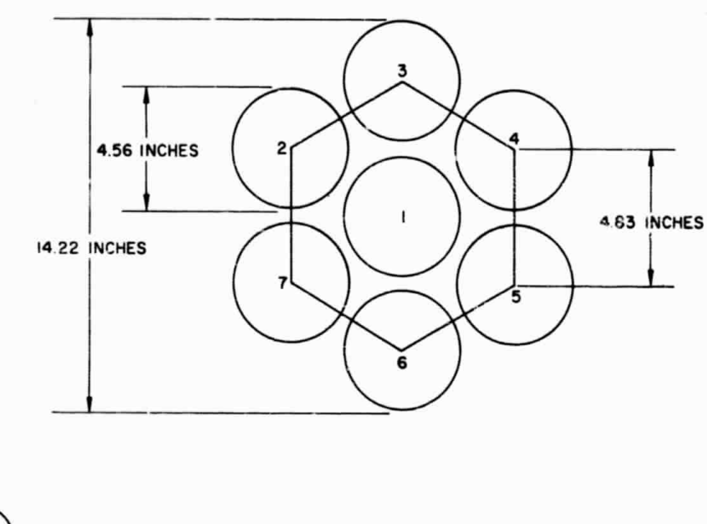

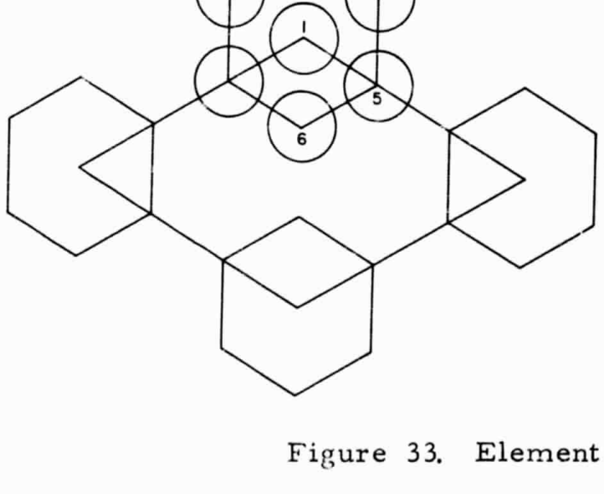

c. Arrangement of array module

Figure 33. Element configuration.

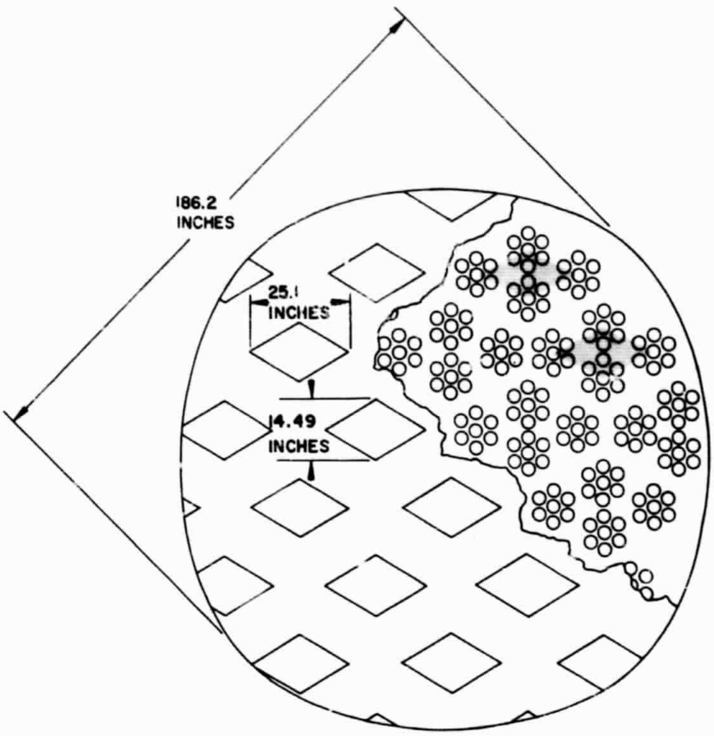

Figure 34. 100-element array.

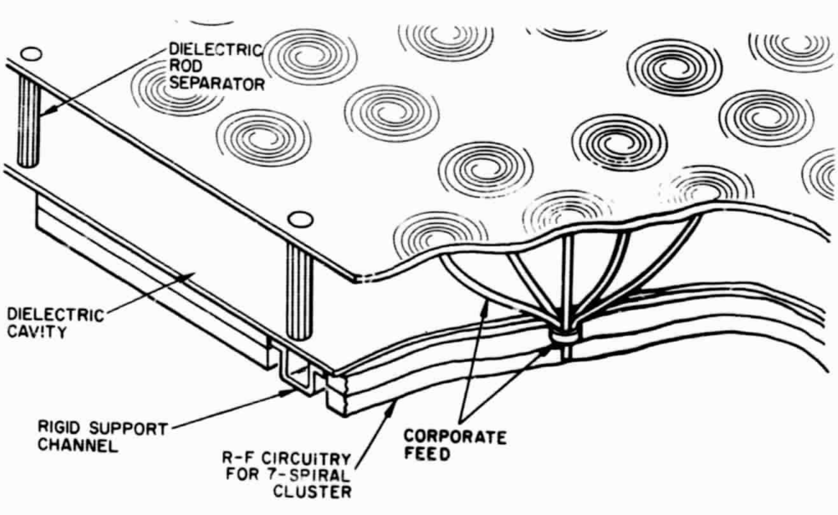

Figure 35. Possible arrangement of self-steering repeater and microwave components.

Item	Quantity	Weight per Unit (ounces)	Total Weight (pounds)	Power per Unit (milli-watts)	Total Power (watts)
R-f Section					
Element—diplexer—receiver module (Element, circulator, filter, r-f amplifier, mixer, i-f amplifier)	100	16.0	100	100	10
Up-converter, r-f amplifier (20 percent efficient)	100	3.0	18.8	1,250	125
R-f power dividers (100-way)	2	40.0	5.0	--	--
Local oscillators	2	15.0	1.9	2,000	4
I-f Processor					
Mixer — i-f amplifier	100	1.6	10.0	188	18.8
I-f power dividers - summers (100-way)	8	14.0	7.0	--	--
I-f local oscillators	3	3.0	0.562	450	1.35
I-f power dividers - summers (3 db)	702	0.15	6.58	--	--
I-f mixers	802	0.3	15.0	--	--
20-db couplers	4	1.0	0.25	--	--
Narrow-band crystal filters	200	0.8	10.0	--	--
Narrow-band i-f amplifier	200	0.5	6.25	100	20.0
AGC i-f amplifiers	3	6.0	1.13	370	1.11
Transmitter i-f amplifiers	100	0.5	3.12	80	8.0
Voltage-controlled oscillator	2	3.0	0.375	450	0.9
Loop filters	2	0.1	0.2	--	--
Diplexer	2	2.0	0.25	--	--
Power supplies (65 percent efficient)			5.0		101.0
Structure			34.0		
TOTAL			225.0 pounds		290.0 watts

Table 6. Weight and power consumption estimate for DRSS repeater (100 modules, 2 channels).

sections, and microstrip techniques for the r-f section. All estimates were based on the present state-of-the-art in components so that no extended development period is anticipated for any component. Thirty-four pounds was included for the antenna housing and support structures. The primary system structure is considered part of the satellite structure and is not included in the weight estimates given in Table 6. As shown in the table, the microwave components make up at least half the system weight. To reduce the weight and size of the overall system, a great deal of effort will have to be devoted to a compact design of these microwave components. The exploratory work on techniques that could be employed in the construction of a miniature front-end module for distributed systems is given in Section 5.0.

4.4.4 R-f Amplifiers and R-f High-Level Mixers

There are several r-f amplifiers and high-level mixers that should be considered for the self-steering repeater. The solid-state amplifier and the traveling-wave tube (TWT) constitute two types. The TWT improves in efficiency as the r-f power rating is increased; the filament power remains rather constant irrespective of the r-f power rating and thus accounts for a large part of the loss of efficiency at low levels. TWT's with up to 30-percent efficiency have been space-qualified with operating lives over 10,000 hours. A gradual, though limited, increase in efficiency is anticipated with, perhaps, some decrease in weight as the technology improves. TWT's can be used in three capacities in satellite and aircraft systems: (1) as the final r-f amplifier in the transmitter, (2) as the amplifier in every radiating module (for every module, one TWT), and (3) as a pump for high-level mixers.

The state-of-the-art in solid-state r-f amplifiers is rapidly changing. Below 2 GHz, 5 watts (at 600 MHz) are being obtained. At 2 GHz, the projection is for several watts with a 30-percent efficiency and a gain of about 30 db, if the expectations are realized at this frequency (Eimbinder, 1966; MERA, 1966). As technology improves, this frequency will be increased to perhaps 4 GHz with similar power.

However, the MERA engineers are pessimistic about the higher frequencies, say 7 or 8 GHz. One alternative would be the utilization of a frequency multiplier that is driven by a 2-GHz amplifier. The efficiency is still satisfactory, but phase as well as frequency is multiplied.

The other approach is to use high-level mixers (also called resistive or varactor up-converters). These devices are perhaps interim in the state-of-the-art between solid-state r-f amplifiers and TWT amplifiers for modular units. The high-level mixer is similar to the low-level mixer except for absolute and relative power levels of the input signals. It has input signals at r-f and i-f and output signals at r-f. Either resistive or reactive mixing may be employed. Resistive mixers are limited to low levels on the order of 1 mw, while reactive mixers are capable of 100 mw output per pair at X-band. These devices are being used in the self-steering transponder engineering model described in Section 3.1.

The efficiencies of the high-level mixers are good but they suffer overall system loss since an r-f pump is required. Power for the r-f pump must be generated elsewhere, presently by TWT's and in the future perhaps by solid-state oscillators. The overall efficiency of reactive mixer and pump is perhaps 10 to 15 percent at best. Thus, the most promising devices in the long run seem to be the solid-state r-f amplifiers for distributed amplifications. Table 7 presents a summary of the characteristics of various r-f amplifiers and high-level mixers as available today.

It should be pointed out that phase and gain tracking must be maintained between all modules of the amplifier. The most critical type of amplifier in this regard is the TWT since it has many electrical degrees between input and output. However, excellent gain and phase tracking have been achieved from tube to tube for tubes specifically designed for phase and gain tracking; from 8 to 12 GHz, the deviation of these tubes from true time delays is 15 degrees and 1db rms (Traveling-wave, 1966). Rapid development in solid-state components suitable as r-f amplifiers is taking place. Among these the promising ones are transistorized amplifiers, Gunn oscillators, and LSA amplifiers.

Type	Frequency Range (GHz)	Power Output	Power Input	Efficiency	Weight	Comments
Traveling-wave Tube	2-10 at a selected frequency	200 mw 1 watt	gain 40 db	8 percent 10-15 percent	12 ounces 14 ounces	Efficiency limited by heater power; use as module amplifier.
Traveling-wave Tube	4-8 at a selected frequency	10 watts	gain 30 db	30 percent	40 ounces 2-1/2 pounds	HAC Syncom tubes, space qualified.
Traveling-wave Tube	2-10 at a selected frequency	35 watts	gain 40 db	28 percent	42 ounces 2-1/2 pounds	Example chosen Watkins-Johnson tube wj-231-6 at 7 GHz, space qualified.
High-Level Mixer (Resistive)	2-10	10 mw maximum (difficult to achieve)	100 mw r-f 400 mw i-f	10 db minimum conversion loss r-f to r-f	2 ounces	Difficult to go beyond these specifications.
High-Level Mixer (Varactor)	2-10	100 mw (achieved)	300 mw r-f 100 mw i-f	6 db maximum conversion loss r-f to r-f	2 ounces	The power output of these devices will increase as the state-of-the-art advances.
R-f Amplifier	2-4	2 watts at 2 GHz projected	gain 30 db	30 percent	< 2 ounces	

Table 7. R-f power amplifiers and high-level mixers.

5.0 NEW TECHNOLOGY SECTION

5.1 BEAM-POINTING ERROR AND SOLUTION

For the synchronous satellite repeater presented in Figure 32, a single array is used for both transmission and reception. The received signal frequency is $\omega_s + \omega_d \approx \omega_s$ and the phase angle of this signal at the k^{th} element relative to an arbitrary reference is α_k. These values correspond to a time lead of $\frac{\alpha_k}{\omega_s}$. If transmission of a beam is required in the direction of the pilot generator, the time lag of the transmitted signal for the k^{th} element must be equal to $\frac{\alpha_K}{\omega_s}$. Since the transmitting frequency of the satellite is equal to ω_T, it is necessary that the phase angle of the signal of the k^{th} element relative to the reference be equal to $-\frac{\omega_T}{\omega_s}\alpha_K$ for the beam to be directed properly. In other words, the phase terms of the received and transmitted signals must be such that

$$\frac{\varphi_T}{\varphi_p} = \frac{\omega_T}{\omega_p} \qquad (5\text{-}1)$$

where φ_T and φ_p are relative phases of the transmitted and received signals at a particular element, referenced to the signals at an arbitrary element. The frequencies ω_T and ω_p are the angular frequencies of the transmitted and received signals, respectively. If the conditions of Equation (5-1) are not satisfied, a beam-pointing error results. For example, for the system presented in Figure 32, $\varphi_T = \varphi_p$. This relationship results in a beam-pointing error that will cause a fall-off in gain of 2 db when the beam is scanned off broadside by 12 degrees. This gain fall-off was considered in preparation of the system parameters listed in Table 4.

The relationships of Equation (5-1) can be obtained by multiplying the phase of the received pilot signal, φ_p, by the ratio of $\frac{\omega_T}{\omega_p}$;

however, phase ambiguities may result if the absolute value of φ_p is greater than π radians. Adjacent modules of the pilot processor can be coupled to eliminate phase ambiguities.* Such a circuit can be used with a c-w pilot signal and a simple antenna array for both transmission and reception. Pilot-coupled modules are illustrated in Figure 36 which shows two i-f modules for adjacent elements. The signals into this processor are denoted by $S_k(t, \tau_k)$ which has the form

$$S_k(t, \tau_k) = \cos(\omega_I t - \omega_p \tau_k) + \cos\left[\omega_s t - \omega_p \tau_k + \varphi(t - \tau_k)\right] \quad (5\text{-}2)$$

where the first term represents the pilot signal and the second term represents the information carrying signal for which phase modulation has been assumed. The r-f pilot frequency is ω_p, the i-f information carrier is ω_I, the phase modulating signal is $\varphi(t)$, and τ_k is the time delay of the signal received by the k^{th} element referred to the signal of an arbitrary element. While phase modulation has been assumed for this discussion, other types of modulation could be employed. The operation of a single module is described first, followed by a discussion of the components that couple adjacent elements.

The incoming signal to the pilot processor module is fed to a mixer. The second input signal to this mixer, which serves as the local oscillator, is obtained from the output of a times-m multiplier and has the form

$$V_k(t, \tau_k) = \cos\left[(\omega_R - \omega_I)t + \omega_p \tau_k\right] \quad (5\text{-}3)$$

where ω_R is the frequency of the signal generated by the reference oscillator.

---

*Coupling modules is a new technique for the elimination of beam-point errors.

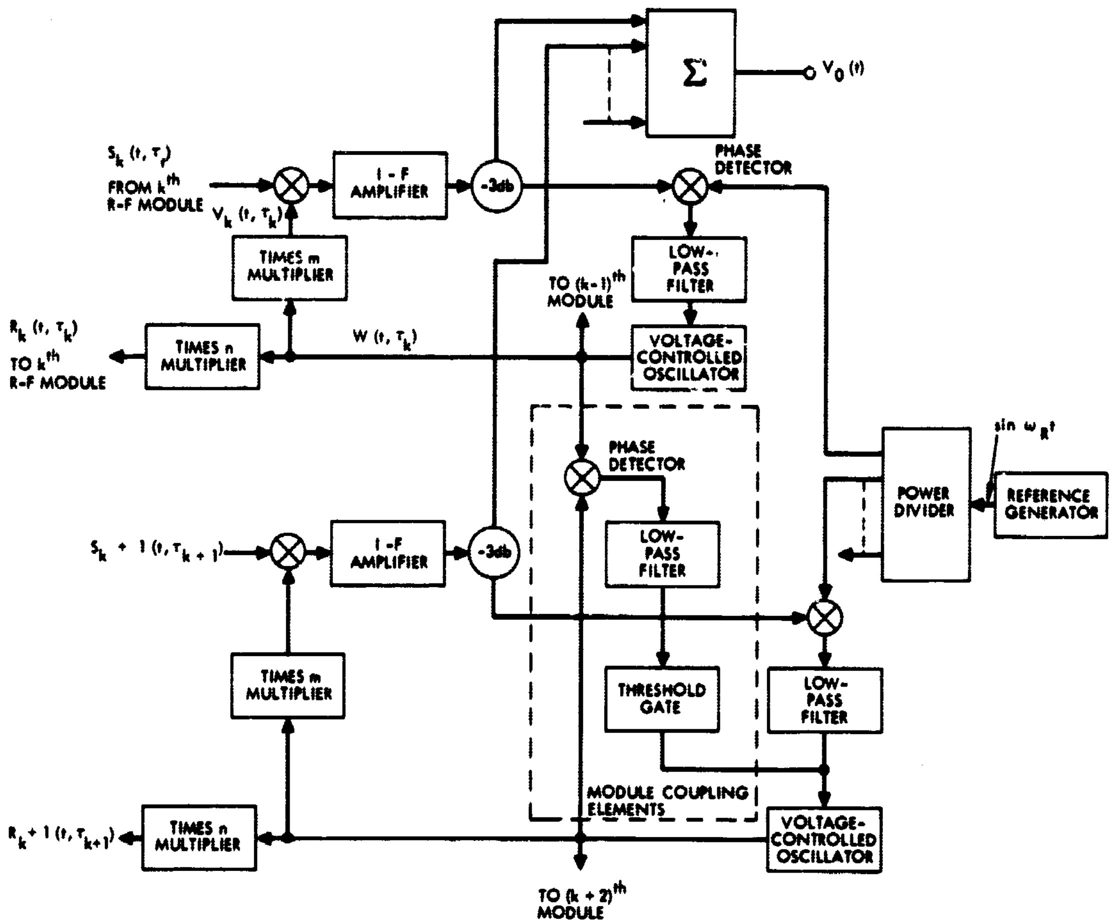

Figure 36. I-f processor for c-w pilot-coupled modules.

The voltages given by Equations (5-2) and (5-3) are mixed and the upper sideband retained to produce at the output of the i-f amplifier a signal of the form

$$V_0(t) = \cos(\omega_{Rt}) + \cos\left[(\omega_s + \omega_R)\,t + \varphi(t - \tau_k)\right] \qquad (5\text{-}4)$$

It can be seen that the time delay, τ_k, has been removed from the carrier but is still present in the modulating signal $\varphi(t - \tau_k)$. However, $(1/\tau_k)$ is much greater than any frequency components of $\varphi(t)$, unless the modulated signal is an extremely wideband signal; consequently, $\varphi(t - \tau_k) \approx \phi(t)$. With this approximation, Equation (5-4) is independent of τ_k; thus, the voltages from the outputs of the i-f amplifiers are in phase and can be summed to realize the receiving antenna gain.

The voltage represented by Equation (5-4) is fed to a phase detector, and the first term is compared in phase with the reference signal, $\sin \omega_R t$, to obtain the control voltage for the voltage-controlled oscillator (VCO). This control voltage, or error voltage, maintains the voltage at the output of the times-m multiplier as given in Equation (5-3).

To generate the signal required to phase the transmitting element and to couple adjacent modules, a signal must be obtained that contains a time lead τ_k, where τ_k is the time lag of the signal received by the k^{th} element. Therefore, the output of the transmitter for the k^{th} module is a voltage of the form

$$R_k (t, \tau_k) = \cos (\omega_L t + \omega_T \tau_k) \tag{5-5}$$

where ω_L is the i-f output frequency of the times-n multiplier (see Figure 36) and ω_T is the r-f carrier frequency of the signal transmitted from the array.

To obtain the voltage given by Equation (5-5), the output voltage of the VCO is considered. This output voltage must be in a form that will result in the voltage represented by Equation (5-3) when its frequency and phase are multiplied by m. To have this result, the output voltage of the VCO must have the form

$$W_k (t, \tau_k) = \cos \left[\left(\frac{\omega_R - \omega_I}{m} \right) t + \frac{\omega_p \tau_k}{m} + \frac{2\pi i}{m} \right] \tag{5-6}$$

where $i = 1, 2, \ldots m$. Equation (5-6) shows that there are m possible phase angles which the VCO may assume that can effect lock-up for the phase-locked loop.

The output voltage of the times-n multiplier is now considered. This voltage is of the form of Equation (5-6) with the frequency and phase terms multiplied by the factor n. That is, $R_k\,(t, \tau_k)$ is of the form

$$R_k\,(t, \tau_k) = \cos\left[\frac{n}{m}\,(\omega_R - \omega_I)\,t + \frac{n}{m}\,\omega_p\tau_k + \frac{n}{m}\,2\pi i\right] \qquad (5\text{-}7)$$

where i may take on any integral value from one to m. The desired voltage is given by Equation (5-5); therefore, it is seen that the ratio of the multiplier factors must equal the ratio of the received pilot frequency to the transmitted carrier frequency; i.e.,

$$\frac{m}{n} = \frac{\omega_p}{\omega_T} \qquad (5\text{-}8)$$

and the integer i must be equal to m. The purpose of the coupling between elements is to insure that this second condition is satisfied.

From a basic consideration of the pilot signal requirement, it can be established that the maximum permissible relative phase difference for the signals received by adjacent elements must be less than π radians in absolute value (Self-Focusing, 1967). Therefore, the relationship exists that

$$\left|\tau_k - \tau_{k+1}\right| \leq \frac{\pi}{\omega_p} \qquad (5\text{-}9)$$

It can be seen from Equations (5-9) and (5-6) that the relative phase difference of the signals at the output of the VCO's for the k^{th} and $(k+1)^{th}$ elements must be bounded above in absolute value by π/m radians for the correct value of i, and that the absolute value of this relative phase difference is bounded below by π/m for an improper selection of i. That is,

$$|\beta| \le \frac{\pi}{m}, \quad \text{for } i = m \text{ (correct selection of i)}$$

and

$$|\beta| \ge \frac{\pi}{m}, \quad \text{for } i \ne m \text{ (incorrect selection of i)} \qquad (5\text{-}10)$$

where β is the phase difference of the signal from adjacent VCO's. Therefore, there exists a boundary that can be used to determine a correct or incorrect selection of i in Equation (5-6).

To understand the performance of this selection process, the components of Figure 36 that couple the two modules together can be considered. These components consist of a phase detector, a low-pass filter, and a threshold gate; they are shown blocked off by a dotted line in Figure 36. The input to the phase detector is obtained from the VCO outputs from two adjacent modules. The output of this phase detector passes through a low-pass filter to produce a voltage as a function of the relative phase angle β which, statically, is of the form $\sin \beta$. This voltage is then fed to a threshold gate that switches the output of the phase detector to the input of the VCO, as shown in Figure 36, if $|\beta| \ge \pi/m$. When the threshold gate closes, a third phase-locked loop is closed that consists of the coupling elements and the VCO of the $(k + 1)^{th}$ module. The reference for this loop is the VCO output for the k^{th} module; therefore, when the gate closes, this loop tends to pull the two VCO's into phase until $|\beta| \le \pi/m$. When $|\beta| \le \pi/m$, the threshold gate is opened and the loops are allowed to operate with no coupling.

For the case just described, the maximum interelement spacing was assumed that dictated a boundary for $|\beta|$ of π/m. If smaller element spacings are required, the bounds given by Equation (5-10) separate. For example, suppose that the element spacing is reduced so that the maximum absolute value of phase difference of the signals received by two adjacent elements is equal to $(3/4)\pi$ radians. Then Equation (5-10) becomes

$$|\beta| \le (3/4)\,\frac{\pi}{m}, \quad \text{for } i = m$$

and

$$|\beta| \ge (5/4)\,\frac{\pi}{m}, \quad \text{for } i \ne m \tag{5-11}$$

Therefore, for this example, the decision boundary remains $|\beta| = \pi/m$; however, now a margin for error has been provided for the threshold gate which would make mechanization less of a problem.

Some of the attractive features of the i-f processing scheme for coupling adjacent elements are

(1) Elimination of the beam-pointing error.

(2) Addition of only three more relatively simple components for each module to a standard adaptive array, except for one module that has no additional components.

(3) Inactivity of the coupling elements after all modules have phase-locked, so that the processor has all the features of a standard adaptive system.

(4) Nonuniformity of the element spacing so that they may be located on a curved surface.

One of the limitations of the system is that the magnitude of the interelement phase shift must be less than π radians; this condition is the same as that which must be satisfied to prevent grating lobes for an array of uniformly spaced elements.

The pilot-coupled module system has not been implemented in hardware nor has it been analyzed in detail. A breadboard would have to be designed, fabricated, and tested before an engineering model implementing the technique could be proposed.

5.2 FRONT-END MODULES FOR SELF-STEERING ARRAYS

Because of the volume limitations imposed on any antenna system in either a satellite or an aircraft, a very compact front-end for the receiver and transmitter is necessary. One method for reducing the size lies in the application of microelectronic construction techniques. One circuit that lends itself readily to such techniques is a receiving and transmitting circuit common to a variety of self-steering array designs. The circuit, shown in Figure 37, has two primary functions: (1) to receive low-level microwave signals from an antenna element and amplify, convert, and process them and (2) to transmit information through the same antenna element in the direction of a received pilot signal. A diplexer is required between the antenna and the receiving-transmitting circuits to isolate the frequencies of each operation. In the discussion that follows, the application of this front-end module to a synchronous satellite self-steering repeater is explored.

5.2.1 Strip Transmission Line

The size of the front-end module and its compatibility with a synchronous satellite depend basically on the type of transmission line of which it is constructed. On the basis of state-of-the-art microwave component design, the choice of line is between shielded, air-dielectric transmission line, referred to as stripline, and unshielded, dielectric-filled transmission line, referred to as microstrip.

a. Types of Line. —

A particular type of stripline called Triline has been designed and built at Hughes especially for the X-band frequencies (Figure 38). This type of line is suitable for construction at all frequencies from 2 to 10 GHz and offers the advantages of design simplicity, noncoupling to adjacent lines, and relatively low attenuation. Losses can be

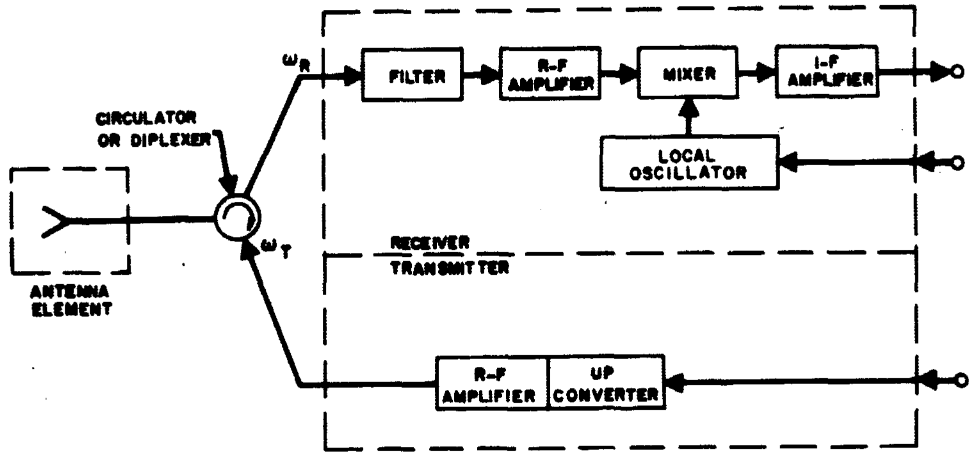

Figure 37. Front-end module circuit for self-steering array.

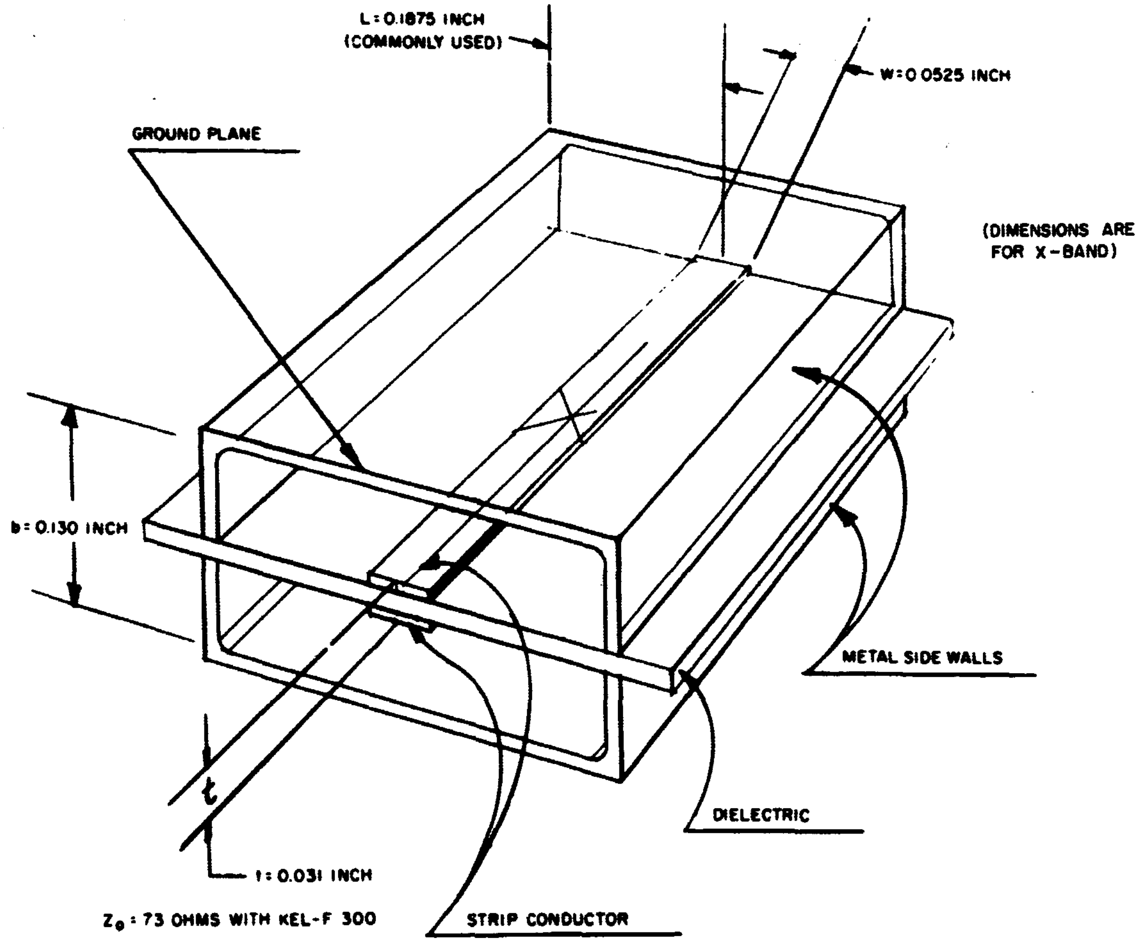

Figure 38. Basic configuration of Hughes Triline.

as low as 0.05 db per waveguide wavelength when Rexolite 2200 is used as the center supporting dielectric.

Microstrip transmission line, in contrast with Triline, concentrates more of the electric field energy in the dielectric so that there is usually more attenuation. As shown in Figure 39, the electromagnetic wave propagates primarily through the dielectric medium bounded by a strip conductor on one side and a ground plane on the other. Microstrip thus has the advantage over Triline of reduced depth and width. In addition, because of its asymmetrical design, microstrip does not have the tight construction tolerances associated with the symmetrical Triline. Microstrip components presently being developed include a circulator, a balanced mixer, a transistor amplifier, an avalanche diode oscillator and multiplier, directional branch line couplers, and transitions to and from OSM coaxial connectors.

A major disadvantage with microstrip is leakage by radiation and coupling to adjacent lines. However, despite this disadvantage, the reduced size and weight and the greater ease of fabrication make microstrip more desirable for satellite system applications. A comparison of the general characteristics of the two kinds of transmission line is given in Table 8.

The front-end module will have to meet certain minimum requirements to be mechanically compatible with the satellite and electrically compatible with the antenna system. Minimum requirements cannot be specified exactly at this time because they depend on a

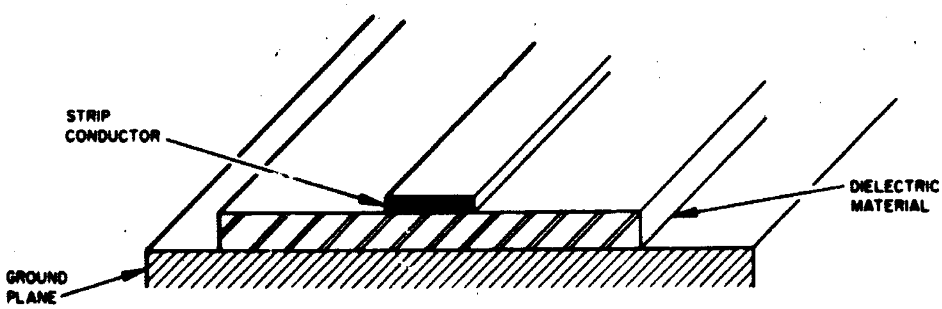

Figure 39. Microstrip transmission line.

Characteristic	Triline	Microstrip
Attenuation	Low	Moderate
Ease of fabrication	Poor	Fair
Difficulty in fabrication	Symmetry of centerstrip	Flatness of substrate and bonding to ground plane
Size (X-band)		
Depth	0.130 inch	<0.1 inch
Ratio of stripline wavelength to free space wavelength	~0.9	~0.3 (alumina substrate)
Width	~0.4 inch	~0.4 inch

Table 8. Characteristics of Triline and Microstrip

number of system parameters that are still being defined. However, some design objectives that should be feasible at any frequency in the 2 to 10-GHz range are listed in Table 9.

b. Comparative Package Size. —

A comparison was made between the package size of the front-end module when made entirely in microstrip and in Triline. It was assumed that the module components were connected as shown in Figure 37 and were laid out so that all the surface area behind the antenna element was utilized. The element size was taken to be a square about $0.7\lambda_0$ on a side where λ_0 is the free-space wavelength of radiation. A tunnel-diode amplifier (TDA) was assumed as the r-f amplifier in the receiver since the design of such a component is presently feasible throughout the frequency range of interest (2 to 10 GHz). For simplicity, only the receiving section of the module was considered.

Parameter	Desired level
Overall noise figure	≤5 db
Transmitter power, module	200 mw c-w
Weight	12 ounces
Size	0.7λ_0 by 0.7λ_0 by 2.5 inches
Antenna element characteristics	Right-hand and left-hand circularly polarized radiation. Gain ≥6 db at -3 db power level Half-power beamwidth ≥25 degrees

Table 9. Typical performance objectives of front-end module.

Size estimates were based on typical stripline dimensions at 8 GHz and extrapolated to the other frequencies. The rule of extrapolation is that length scales inversely with frequency, but width and height need not vary except in circulators, where the radius of the circulator junction varies inversely with the frequency. The approximate dimensions of the various components built in Triline and microstrip at both X-band and at S-band are listed in Table 10.

At X-band the Triline components (Table 10) can be packaged into two sections, one with a width = 0.6 inch, length = 14 inches, and height = 0.2 inch and the other with a width = 0.6 inch, length = 2.4 inches, and height = 0.5 inch. At 8 GHz, the side dimension of the sub-module is $s = 0.7\ \lambda_0 \approx 1$ inch. An equivalent package with a 1-inch cross-section would require a minimum depth of about 2.5 inches.

Component	X-band Triline	X-band microstrip	S-band Triline	S-band microstrip
Circulator	w = 0.6	w = 0.5	w = 2.0	
	l = 0.6	l = 0.5	l = 2.0	
	h = 0.5	h = 0.25	h = 0.5	
Filter	w = 0.6	w = 0.3	w = 0.6	
	l = 1.5	l = 1.0	l = 6.0	
	h = 0.15	h = 0.1	h - 0.15	
Tunnel diode amplifier	w = 0.6	w = 0.5	w = 2.0	
	l = 1.8	l = 0.6	l = 7.0	
	h = 0.5	h - 0.25	h = 0.5	
Balanced mixer	w = 0.6		w = 1.0	
	l = 1.0		l = 3.0	
	h = 0.15	w = 1.0	h = 0.15	
		l = 1.0		
I-f amplifier	w = 0.6	h = 0.1	w = 0.6	
	l = 1.0		l = 1.0	
	h = 0.15		h = 0.15	
Local oscillator multiplier chain (times 8 with filters)	w = 0.6	w = 1.0	w = 0.6	
	l = 10.0	l = 1.0	l = 10.0	
	h = 0.2	h = 0.1	h = 0.2	
Sub-module	9 layers	3 layers	2 layers	1 layer
	w = 0.6	w = 1.0	w = 4.0	w = 4.0
	l = 1.0	l = 1.0	l = 4.0	l = 4.0
	h = 2.5	h = 0.5	h = 0.7	h = 0.1

Table 10. Comparative sizes of component sizes in strip transmission line. (Dimensions are in inches)

In the X-band microstrip package, except at those places at which circulators are employed, the area dimensions of the components will decrease by a factor of about 3. The estimated component sizes might then be built into a package of about three 1-inch square layers with a total height of about 0.5 inch.

As the S-band Triline components are scaled down in frequency to S-band, they increase in size. There are no general rules that govern overall size increase other than the general rules of extrapolation. Triline behaves as does coaxial line so that characteristic line impedances vary little if the same cross-sectional design is used. The lengths of the filters and tuning elements vary inversely with frequency so that length per sub-module component is similarly affected. At 2 GHz, the sub-module in S-band Triline would consist of two layers that would occupy a space about 4 inches by 4 inches by 0.7 inch. In S-band microstrip, all the components above could be integrated onto a single layer sub-module behind the 4-inch square element and have a depth of about 0.1 inch.

These comparisons of package size based on all-Triline or an all-microstrip design at the two extremes of the frequency band, 2 and 10 GHz, indicate that around X-band an all-microstrip design is preferred, while at the lower frequency bands, especially at S-band, a hybrid design with Triline and microstrip components together is recommended.

5.2.2 Microelectronic Components

A two-phase approach to the design and fabrication of the microelectronic front-end module is necessary. In the first phase, each component would be individually developed and evaluated for electrical performance with the receiving and transmitting portions designed separately. The results from this phase of development would permit calculation of the module performance and the layout of the components to determine total weight and size. In the second phase all the components would be fabricated into a modular package and evaluated.

Based on the technology of the near future, an X-band module would be constructed partly in microstrip and partly in stripline. Since microstrip technology has not been evolved at the lower frequencies, an all-stripline component design would apply at S-band.

a. Circulator. —

Ferrite circulators in microstrip have been built with several different substrate materials and thicknesses. A device using 0.025 inch thick alumina substrate was built at Hughes and successfully tested at X-band frequencies (Figure 40). Measured characteristics of this component are, for a bandwidth of 0.5 GHz,

Isolation = 20 db

Insertion loss = 0.4 db

VSWR ≤ 1.2 maximum

According to Hershenov (1967), the ideal approach to circulator design in microstrip is an all-garnet substrate ($\epsilon_r = 16$). Such a substrate combines simplicity of design with ease of fabrication. Hershenov's investigation of this technique led to the successful

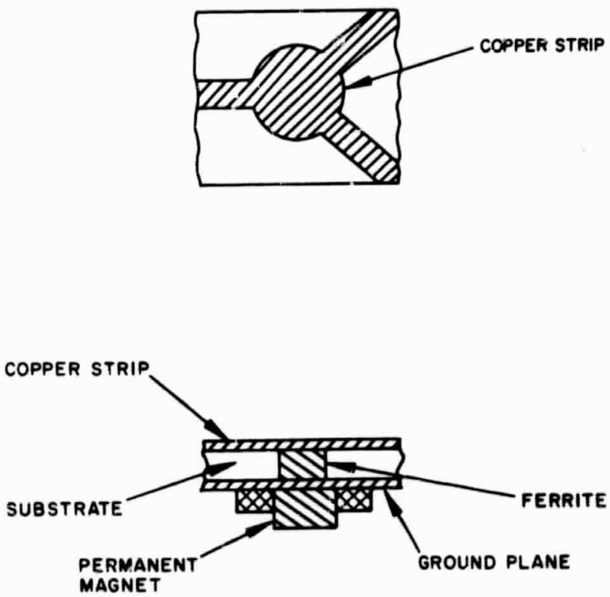

Figure 40. Microstrip circulator.

construction of circulators designed with an electromagnet, a small permanent magnet, and a latching circuit. For substrate thicknesses of approximately 0.025 inch and X-band frequency operation, the garnet circulators provide significantly larger bandwidths than the more conventional ceramic substrates for isolation greater than 20 db. Insertion losses of 0.4 to 0.8 db have been measured; while these figures are slightly higher than those obtained for ceramic substrates, some reduction can be accomplished by more adequate bonding of the evaporated strip conductors to the garnet substrate and the use of proper strip widths. Hershenov also has evidence to indicate the feasibility of applying semiconductor doping techniques to the fabrication of integrated active and passive devices on the substrate. This possibility merits continued attention. The use of garnet in place of alumina for a substrate material would result in about a 3/4 reduction in the waveguide wavelength.

b. Mixer. —

Experimental mixers have been built in microstrip, and models with improved performance are currently being developed. A balanced mixer that employs a branch line coupler and Schottky barrier diodes built on single-crystal sapphire ($\epsilon_r \approx 9$) has been reported by Microwave Associates (Blight, 1967). Used with a preamplifier on the same substrate, the device had a measured noise figure of 7.5 db at 9.375 GHz.

c. I-f Amplifier. —

No microstrip i-f amplifier has been reported, but the design is not expected to present any difficulty. It might consist of a hybrid design of standard integrated circuits. Its gain is necessary within the module because of losses in long cables connecting the module to the i-f circuits.

d. <u>Low-noise R-f Amplifier.</u> —

The use of a self-focusing array to provide a high-gain beam for receiving low-level signals presents a special problem. Because of the losses in the elements and the r-f components and the noise in the mixer, it would be advantageous to include a low-noise amplifier before the mixer. For the lowest noise temperature possible, an amplifier should be used after each element (Advanced Deep Space Study, 1967). Eventually, when ultra-low-noise mixers become available, there will be little advantage in using r-f amplifiers.

At the present time, there are three low-noise microwave amplifiers that may be considered for use in the microelectronic module. These are the transistor amplifier, the tunnel-diode amplifier, and the parametric amplifier. Microwave transistor amplifiers are relatively new devices that have demonstrated moderately low noise performance (Figure 41) and modest gain for single stage designs. Fabrication in microstrip has been accomplished by mounting the transistor chip directly on the strip conductor on the top of the substrate, and bonding leads to the emitter and ground lines. Present transistor amplifiers are operationally limited to frequencies of about 4 to 5 GHz; however, transistor amplifiers at lower frequencies, for example, at S-band or L-band, might be used in an X-band module design if they followed a down-converter after the filter. This possibility may be investigated further if compatible changes in the rest of the system promise improved performance.

A conventional tunnel-diode amplifier (TDA) is a relatively simple device that requires a low driving voltage and has an excellent reliability rating. It has moderate gain and noise figure characteristics that vary with frequency (Figure 41). Single-stage TDA's normally provide a gain of 15 db or more. A microminiaturized TDA has not yet been fabricated in microstrip transmission line. The approach would be to use a five-port circulator (required for stability) built in microstrip with the tunnel diode circuit terminating the third arm as is sketched in Figure 42. In microstrip, the package can be eliminated and more of the electric field can be concentrated at the tunnel diode junction. If

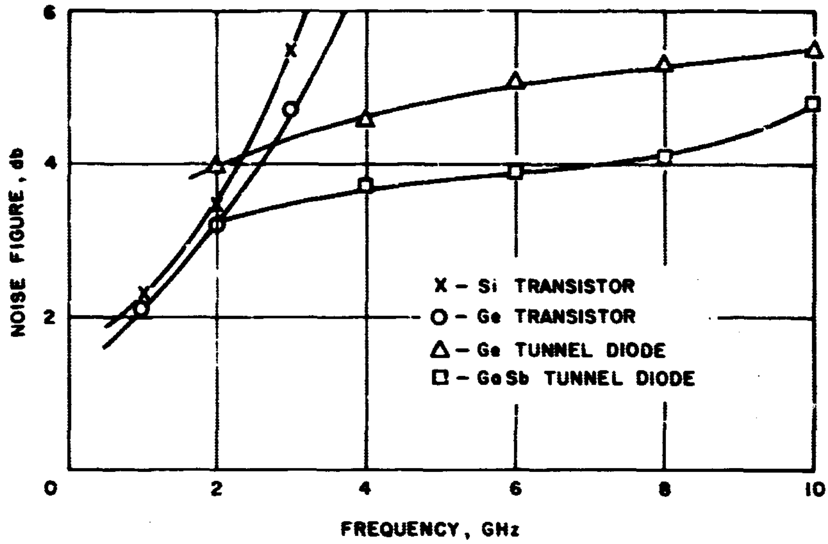

Figure 41. Noise performance of various tunnel diode and transistor amplifiers.

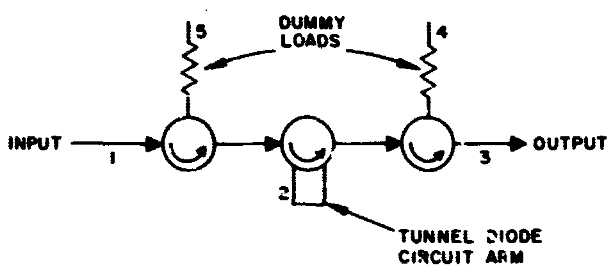

Figure 42. Microstrip stability circuit for a tunnel diode amplifier.

the incorporation of the tunnel diode into microstrip transmission line creates more problems than it solves, however, it can just as easily be used in a miniature coaxial line that connects to the second arm of a microstrip five-port circulator by means of an OSM connector. Low-noise TDA's should have adequate dynamic range for reception, since gain compression occurs at about -40 dbm input. This compression point can be raised, if necessary, by the cascading of units. Noise figures less than 5.5 db and gain on the order of 15 db should be achievable through X-band.

To the knowledge of the present researchers, no reports have been published on the development of parametric amplifiers in microstrip. It has been learned, however,* that International Microwave, a subsidiary of Microwave Associates, is building such a component; the complete design will be done on a single substrate and is expected to exhibit a noise figure on the order of 4 db. This approach will be investigated in more detail for comparison with TDA's.

5.2.3 State-of-the-Art in Module Design

Isolation between the receiving and transmitting sections is of primary concern in the design of a module. A circulator followed by a filter in the receiving arm and another filter in the transmitting arm was suggested as a possible technique for obtaining adequate isolation, say, on the order of 70 db or more. Building the filters in microstrip transmission line would result in high insertion loss and a restriction to wide bandwidths, say >10 percent. Narrow-band filters require a number of high Q elements (Q > 1000); a microstrip element with a Q greater than several hundred is difficult to achieve with current technology.

*Private communication with Dr. Mickey Gilden of Microwave Associates, July 20, 1967, at Microwave Associates' presentation of Microwave Integrated Circuits.

A block diagram of a front-end X-band module that utilizes a stripline diplexer is shown in Figure 43. The mixer and i-f amplifier are shown as a single component. This arrangement anticipates a more advanced microstrip design in which both the mixer diode and the i-f amplifier circuit are integrated onto the same substrate. This design has already been accomplished. The TDA is included in the module because it reduces the receiver noise figure (F_R) by about 2 db, if a noise figure on the order of 8 db is assumed for the mixer-preamplifier.

With reference to Figure 44, it can be seen that the TDA will improve the receiver noise figure by greater than 1 db unless a mixer-preamplifier noise figure of better than 6.6 db can be achieved. A mixer-preamplifier noise figure of about 8 db is foreseen as a reasonable figure that will be state-of-the-art microstrip performance within a year or two. It is therefore reasonable to assume a TDA in the module design unless significant reduction in mixer noise figure is realized on a production basis. A sketch of the module indicating a possible layout of the receiving components is shown in Figure 45.

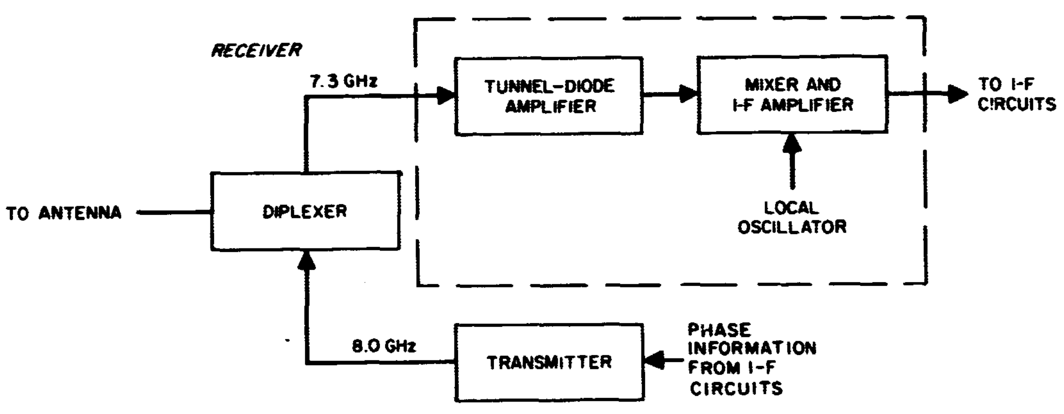

Figure 43. Front-end module block diagram.

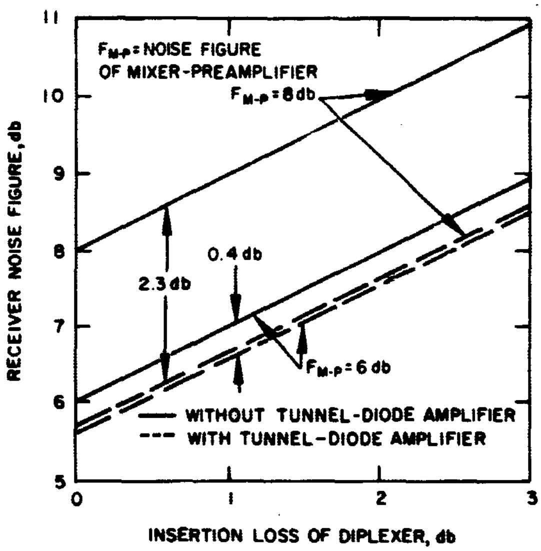

Figure 44. Performance of tunnel-diode amplifier and mixer.

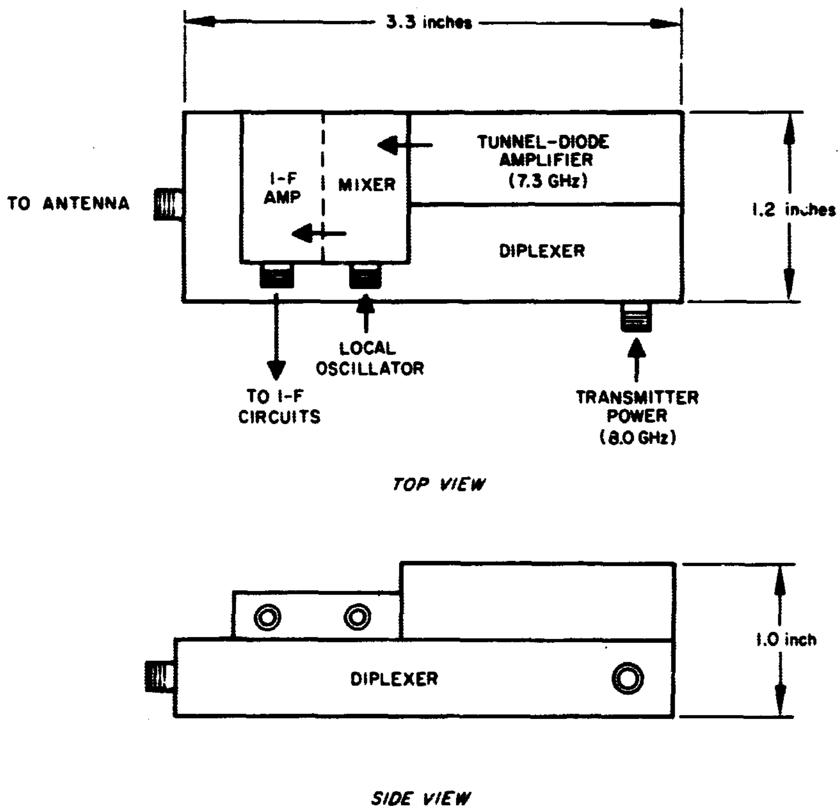

Figure 45. Front-end, X-band module layout with mixer-preamplifier in microstrip and other components in stripline.

REFERENCES

Advanced Deep Space Study (1967). Advanced Deep Space Communication Systems Study, Final Report on Contract NAS 12-81. Hughes Aircraft Company, Report No. P67-15, Culver City, California.

Andre, S. (1963). Satellite Data Transmission System, Final Report on Contract AF33(657)-9043. Technical Document Report No. ASD-TDR-63-759, Sylvania Electronics Systems--Central, Williamsville, New York.

Andre, S. N., and D. J. Leonard (1964). An active retrodirective array for satellite communications. IEEE Trans. AP-12, 181-186.

Belfi, C. A., C. Rothenberg, L. Schwartzman, R. E. Tilley, and A. Willis (1964). A satellite data transmission system. IEEE Trans. AP-12, 200-206.

Blight, R. E. (1967). Microstrip hybrid couplers and their integration into balanced mixers at K- and K -bands. 1967 MTT Symposium Digest, V-4, 136-138, Boston, Mass.

Butler, J. and R. Lowe (1961). Beam-forming matrix simplifies the design of electronically scanned antennas. Electronic Design, April, 170-173.

Cutler, C. C., R. Kompfner, and L. C. Tillotson (1963). A self-steering array repeater. Bell System Tech. J. 42, 2013-2032.

Davenport, W. B., Jr. (1953). Signal-to-noise ratios in bandpass limiters. JAP 24, no. 6, 720-727.

Eimbinder, J. (1966). Microwave IC's: hybrid or monolithic. Electronics 39, 135-142.

Gruenberg, E. L., and C. M. Johnson (1964). Satellite communication relay system using a retrodirective space antenna. IEEE Trans. AP-12, 215-223.

Hansen, R. C. (1961). Communications satellites using arrays. Proc. IRE 49. (a) pp. 1066-1074; (b) "Correction," pp. 1340-1341.

Hershenov, B. (1967). All garnet microstrip circulators for integrated circuits. MTT Symposium Digest, V-6, 142-144, Boston, Mass.

Jaffe, R., and E. Rechtin (1955). Design and performance of phase-lock circuits capable of near-optimum performance over a wide range of input signal and noise levels. IRE Trans. IT-1, 66-76, March.

Kummer, W. H., and R. A. Birgenheier (1966). Spacecraft Antenna Systems, Final Engineering Report on Contract NAS 5-3545. Hughes Aircraft Company, Report No. P66-66, Culver City, California.

Kummer, W. H., and A. T. Villeneuve (1965). Study of Spacecraft Antenna Systems, Interim Engineering Report (Phase 1 - Final Report) on Contract NAS 5-3545. Hughes Aircraft Company, Report No. P65-35, Culver City, California.

MERA (1966). Molecular Electronics for Radar Applications. Contract AF33(615)-1193 with the Air Force Systems Command, Wright-Patterson Air Force Base, Ohio. Texas Instruments, Inc., private communication.

Pon, C. Y. (1964). Retrodirective array using heterodyne technique. IEEE Trans. AP-12, 176-180.

Rutz-Philipp, E. M. (1964). Spherical retrodirective array. IEEE Trans. AP-12, 187-194.

Ryerson, J. L. (1960). Passive satellite communication. Proc. IRE 48, 613-619.

Self-focusing (1967). Self-focusing Antenna Arrays, Interim Technical Report on Contract No. F33615-67-C-1389. Hughes Aircraft Company, Report No. P67-183, Culver City, California.

Sichelstiel, B. A., W. M. Waters, and T. A. Wild (1964). Self-focusing array research model. IEEE Trans. AP-12, 150-154.

Traveling-wave (1966). Traveling-wave Phase Shifter, Phase II, Technical Documentary Report No. RADC-TDR-66- on Contract No. AF30(602)-3532. W. H. Kummer and F. G. Terrio, project engineers. Hughes Aircraft Company, Culver City, California.

Van Atta, L. C. (1959). Electromagnetic Reflector, U. S. Patent No. 2,908,002.

Viterbi, A. J. (1966). Principles of Coherent Communication, chapters 1-4. McGraw-Hill Book Company, Inc., New York.

Weaver, C. S. (1961). Threshold and tracking ranges in phase-locked loops. IEEE Trans. SET-7, 60-70.